

LEBANESE AMERICAN UNIVERSITY

Evaluation of light-activated Ru(II) prodrugs and their photoproducts as potential anti-cancer agents

Maria George Elias

A thesis submitted in partial fulfilment of the requirements for the
degree of Master of Science in Biological Sciences

School of Arts and Sciences
December 2020

© 2020

Maria George Elias

All Rights Reserved

THESIS APPROVAL FORM

Student Name: Maria George Elias I.D. #: 201401502

Thesis Title: Evaluation of light activated Ru(II) prodrugs and their photoproducts as potential anti-cancer agents

Program: Master of Science in Biological Sciences


Department: Natural Sciences

School: Arts & Sciences

The undersigned certify that they have examined the final electronic copy of this thesis and approved it in Partial Fulfillment of the requirements for the degree of:

Master of Science in the major of Biological Sciences

Thesis Advisor's Name: Costantine Daher

Signature:  Date: 22 / 12 / 2020
Day Month Year

Committee Member's Name: Sandra Rizk Jamati

Signature:  Date: 22 / 12 / 2020
Day Month Year

Committee Member's Name: Christian Khalil

Signature:  Date: 22 / 12 / 2020
Day Month Year

THESIS COPYRIGHT RELEASE FORM

LEBANESE AMERICAN UNIVERSITY NON-EXCLUSIVE DISTRIBUTION LICENSE

By signing and submitting this license, you (the author(s) or copyright owner) grants the Lebanese American University (LAU) the non-exclusive right to reproduce, translate (as defined below), and/or distribute your submission (including the abstract) worldwide in print and electronic formats and in any medium, including but not limited to audio or video. You agree that LAU may, without changing the content, translate the submission to any medium or format for the purpose of preservation. You also agree that LAU may keep more than one copy of this submission for purposes of security, backup and preservation. You represent that the submission is your original work, and that you have the right to grant the rights contained in this license. You also represent that your submission does not, to the best of your knowledge, infringe upon anyone's copyright. If the submission contains material for which you do not hold copyright, you represent that you have obtained the unrestricted permission of the copyright owner to grant LAU the rights required by this license, and that such third-party owned material is clearly identified and acknowledged within the text or content of the submission. IF THE SUBMISSION IS BASED UPON WORK THAT HAS BEEN SPONSORED OR SUPPORTED BY AN AGENCY OR ORGANIZATION OTHER THAN LAU, YOU REPRESENT THAT YOU HAVE FULFILLED ANY RIGHT OF REVIEW OR OTHER OBLIGATIONS REQUIRED BY SUCH CONTRACT OR AGREEMENT. LAU will clearly identify your name(s) as the author(s) or owner(s) of the submission, and will not make any alteration, other than as allowed by this license, to your submission.

Name: Maria George Elias

Signature: 

Date: 03/12/20



PLAGIARISM POLICY COMPLIANCE STATEMENT

I certify that:

1. I have read and understood LAU's Plagiarism Policy.
2. I understand that failure to comply with this Policy can lead to academic and disciplinary actions against me.
3. This work is substantially my own, and to the extent that any part of this work is not my own I have indicated that by acknowledging its sources.

Name: Maria George Elias

Signature: 

Date: 03/12/20

Acknowledgment

I would like to send many thanks to my advisor and co-advisor, Dr. Costantine Daher and Dr. Rony Khnayzer, for their advice, guidance, and encouragement, as well as their prompt response to my questions and queries.

Dr. Daher imparted me in becoming an efficacious biologist, particularly in act of sudden hurdles, as he quotes “that is why it is called re-search”.

Dr. Khnayzer guided me through the meticulous chemistry to my thesis and helped make sense of any confusion.

I am extremely thankful to have been a part of a lab full of helping, dedicated, aspiring researchers; Stephanie Mehanna, Najwa Mansour, Petra Kretenova, Christelle Fayad and Elias Elias who were always ready to share new approaches to research, we were a great team. I would also like to mention Dr. Robin Taleb, Dr. Bilal Nehmeh, Dr. Wassim Shebaby, and Dr. Wared Nour El Dine who were always ready to offer any assistance. Special thanks to Jean Karam and Elias Abi Ramia, who were always prepared to help out with all my *in vivo* experiments whether on weekends or during holidays.

I am grateful for the support of my committee members Dr. Sandra Rizk-Jamati and Dr. Christian Khalil, who offered me their guidance and support.

I cannot but express my love and gratitude to my parents for their wholehearted love and support through this entire process. I am grateful for my siblings and friends who were always there for me.

I show appreciation to all Biology faculty affiliates who were great mentors. I thank Ms. Maya Farah, the graduate laboratory supervisor, who was always available, and who taught us to operate certain machines as well as ensuring our safety in the lab

Conclusively, many thanks go to all who contributed to my thesis work directly or indirectly.

Evaluation of light-activated Ru(II) prodrugs and their photoproducts as potential anti-cancer agents

Maria George Elias

ABSTRACT

Photoactivated chemotherapy (PACT) has emerged as a new method for targeted cancer therapy. Strained ruthenium based complexes with octahedral geometry may undergo ligand dissociation once irradiated, forming aquated photoproducts that are greatly cytotoxic compared to their prodrug complex. The current study evaluates light-activated ruthenium prodrugs and their photoproducts as potential anti-cancer agents. The complexes being investigated are: $[\text{Ru}(\text{bpy})_2\text{phen}]\text{Cl}_2$ (unstrained), $[\text{Ru}(\text{bpy})_2\text{BC}]\text{Cl}_2$, $[\text{Ru}(\text{bpy})_2\text{dpphen}]\text{Cl}_2$. Both strained complexes showed a $\lambda_{\text{max}} \cong 450$ nm in the visible range, accordingly, blue LED light (460 nm) was used for their photoactivation. $[\text{Ru}(\text{bpy})_2\text{BC}]\text{Cl}_2$ was synthesized, purified and characterized by NMR and investigated for its mechanistic potential against cancer. The aquated photoproduct of $[\text{Ru}(\text{bpy})_2\text{dpphen}]\text{Cl}_2$ was purified, characterized using ESI/MS and NMR, and shown to be essential for the exhibited toxicity when its prodrug and light irradiated complex were tested on human melanoma (A375) cancer cells. The uptake of $[\text{Ru}(\text{bpy})_2\text{BC}]\text{Cl}_2$, assessed by ICP/MS, started immediately post incubation and plateaued after 24 hours. The uptake was mainly attributed to occur via active transport. Cytotoxicity assays on A375 showed a mean phototoxicity index of 340 at 72 hours, presenting the intracellular aquated photoproducts being effective rather than the dissociating ligands. A significant increase in ROS production and DNA damage was also observed. Flow cytometry results revealed the induction of apoptosis. Western blot analysis of pro- and anti-apoptotic protein revealed apoptosis to be mediated through both intrinsic and extrinsic pathways, as well as via inhibition of the MAPK and PI3K pathways. $[\text{Ru}(\text{bpy})_2\text{BC}]\text{Cl}_2$ (with and without photoactivation), and $[\text{Ru}(\text{bpy})(\text{dpphen})\text{H}_2\text{O}]\text{Cl}_2$ were also investigated for their *in vivo* anticancer activity using a 7,12-Dimethylbenz[*a*] anthracene/12-O-Tetradecanoylphorbol 13-acetate skin carcinogenesis mice model. All complexes reduced significantly tumor growth 3 weeks post treatment when compared to non-treated mice. In conclusion, this study demonstrates that $[\text{Ru}(\text{bpy})_2\text{BC}]\text{Cl}_2$ is a multi-mechanistic PACT drug which exhibits promising *in vitro* and *in vivo* anti-cancer potentials. It also reveals that

[Ru(bpy)(dpphen)H₂O]Cl₂, the aquated form of [Ru(bpy)₂dpphen]Cl₂ photoproduct, has *in vitro* and *in vivo* anticancer activity and could be used as a chemotherapeutic agent.

Keywords: Cancer, Human Melanoma (A375), Photoactivation, Ruthenium, Apoptosis, DNA damage

TABLE OF CONTENTS

Chapter	Page
List of tables.....	xiv
List of figures.....	xvi
List of abbreviations.....	xxi
I- Literature Review.....	1
1.1 Cancer.....	1
1.1.1 Overview.....	1
1.1.2 Normal versus Cancer cells.....	1
1.1.3 Hallmarks of cancer.....	2
1.1.3.1 Continual proliferation.....	3
1.1.3.2 Evading tumor suppressors.....	5
1.1.3.3 Resisting cell death.....	6
1.1.3.4 Enabling replicative immortality.....	7
1.1.3.5 Inducing angiogenesis.....	7
1.1.3.6 Invasion and metastasis.....	8
1.1.4 Causes of cancer.....	8
1.1.4.1 The genetics and the kind of mutations that may trigger.....	8
1.1.4.2 Cell signalling in cancer.....	9
1.1.4.2.i RAS-ERK pathway.....	9
1.1.4.2.ii PI3K-AKT pathway.....	10
1.2 Mechanisms of cell death.....	12
1.2.1 Apoptosis.....	12
1.2.1.1 Intrinsic pathway.....	13
1.2.1.2 Extrinsic pathway.....	14
1.2.1.3 Perforin-Granzyme pathway.....	14
1.2.1.4 Execution pathway.....	14

1.2.2 Necrosis.....	15
1.2.3 Necroptosis.....	16
1.2.4 Autophagy.....	16
1.3 Human Melanoma.....	17
1.3.1 Overview.....	17
1.4 Cancer Therapy.....	18
1.4.1 Surgery, Radiotherapy and Chemotherapy.....	18
1.4.1.1 Platinum based chemotherapy.....	18
1.4.2 Immunotherapy.....	19
1.4.3 Bio-chemotherapy.....	19
1.4.4 Targeted therapy.....	19
1.4.5 Precision Medicine.....	19
1.4.6 Hormonal therapy.....	20
1.4.7 Nanomedicine.....	20
1.4.8 Natural compounds.....	20
1.4.9 Stem cell transplant.....	20
1.5 Ruthenium complexes in cancer treatment.....	20
1.5.1 Light-mediated activation of ruthenium prodrugs.....	21
1.5.1.1 Photodynamic therapy.....	21
1.5.1.2 Photo activated chemotherapy.....	23
1.5.1.2.i Energy transitions of photo excited compounds.....	24
1.5.2 Current Ruthenium compounds under study.....	25
1.6 Ru(bpy) ₂ phen, Ru(bpy) ₂ BC and Ru(bpy) ₂ dpphen: background.....	25
1.7 DMBA/TPA model induces skin carcinogenesis.....	26
1.8 Aim of the study.....	27

II- Materials and Methods.....	28
2.1 Chemicals and Reagents.....	28
2.2 Kits and Solutions.....	29
2.31 Ruthenium Complexes.....	30
2.3.1 [Ru(bpy) ₂ phen]Cl ₂ synthesis.....	30
2.3.2 [Ru(bpy) ₂ BC]Cl ₂ synthesis.....	30
2.3.3 [Ru(bpy) ₂ dpphen]Cl ₂ synthesis.....	31
2.3.3.1 Agua complex.....	32
2.4 Testing the lipophilicity of [Ru(bpy) ₂ phen]Cl ₂ , [Ru(bpy) ₂ BC]Cl ₂ , [Ru(bpy) ₂ dpphen]Cl ₂ and [Ru(bpy)(dpphen)H ₂ O]Cl ₂	33
2.5 Cell line.....	33
2.6 Cellular uptake of [Ru(bpy) ₂ BC]Cl ₂ precursor vs. photoproduct via ICP/MS.....	33
2.7 Mode of uptake of [Ru(bpy) ₂ BC]Cl ₂ precursor.....	34
2.8 Cytotoxicity Assay.....	35
2.8.1 Cytotoxicity of [Ru(bpy) ₂ BC]Cl ₂ (dark vs. light), Ligands and Cisplatin....	35
2.8.2 Cytotoxicity of [Ru(bpy) ₂ BC]Cl ₂ activated intracellularly in a [Ru(bpy) ₂ BC]Cl ₂ free medium.....	35
2.8.3 Cytotoxicity of [Ru(bpy) ₂ BC]Cl ₂ photoproducts on seeded A375.....	36
2.9 ROS detection.....	36
2.10 Western blot.....	36
2.11 Comet assay.....	38
2.12 Cell death analysis.....	39
2.13 <i>In vivo</i> methods.....	40
2.13.1 Estimation of the LD.....	40

2.13.2 Determination of Maximum Tolerated Dose.....	41
2.13.3 Induction of skin carcinogenesis.....	41
2.13.4 Experimental plan.....	41
2.13.4.1 Doses and group divisions.....	42
2.13.4.2 Blue LED light irradiation	42
2.13.4.3 Efficacy.....	43
2.14 Statistical analysis.....	43
III- Results.....	44
3.1 Compound Synthesized.....	44
3.1.1 [Ru(bpy)(dpphen)H ₂ O].Cl ₂	45
3.1.1.1 Generation through blue LED light activation.....	45
3.1.1.1.i Absorption Spectra of [Ru(bpy) ₂ dpphen]Cl ₂ as a function of time..	45
3.1.1.1.ii Photolysis products.....	47
3.1.2 Purification of [Ru(bpy)(dpphen)CH ₃ OH]Cl ₂	49
3.1.2.1 Column 1 fractions.....	40
3.1.2.2 Column 2 fractions.....	52
3.1.2.2.i Absorption Spectra.....	53
3.2 Octanol-water partition coefficient of [Ru(bpy) ₂ phen]Cl ₂ , [Ru(bpy) ₂ BC]Cl ₂ , [Ru(bpy) ₂ dpphen]Cl ₂ and [Ru(bpy)(dpphen)H ₂ O]Cl ₂	54
3.3 Cellular uptake of Ru(II) in A375 cancer cells.....	55
3.4 Mode of uptake of [Ru(bpy) ₂ BC]Cl ₂ precursor.....	57
3.5 The cytotoxic effects of ruthenium complexes on cancer cells survival.....	58
3.5.1 Cytotoxicity of [Ru(bpy) ₂ BC]Cl ₂ (dark vs. light), Ligands and Cisplatin....	58

3.5.2 Cytotoxicity of [Ru(bpy) ₂ BC]Cl ₂ activated intracellularly in a [Ru(bpy) ₂ BC]Cl ₂ free medium and [Ru(bpy) ₂ BC]Cl ₂ photoproducts on seeded A375.....	59
3.5.3 Cytotoxicity of [Ru(bpy) ₂ dpphen]Cl ₂ (dark vs. light)	59
3.5.4 Cytotoxicity of [Ru(bpy)(dpphen)H ₂ O]Cl ₂	60
3.6 ROS production.....	61
3.7 Western blots.....	62
3.7.1 Bcl2-Associated X protein (Bax).....	63
3.7.2 B-cell lymphoma 2 (Bcl-2)	63
3.7.3 Cytochrome c.....	64
3.7.4 Cleaved Caspase 3	65
3.7.5 Cleaved Poly (ADP-ribose) polymerase (Parp).....	65
3.7.6 Procaspase 8.....	66
3.7.7 Cyclin-dependent Kinase inhibitor 1 (P21).....	66
3.7.8 Extracellular signal-regulated kinase (ERK)	67
3.7.9 Protein Kinase B (AKT)	67
3.7.10 Beclin-1.....	68
3.8 Effect of Ru(II) on DNA in A375 cells via the Comet Assay.....	69
3.9 Flow cytometry.....	71
3.10 <i>In Vivo</i>	74
3.10.1 Lethal dose.....	74
3.10.2 Toxicity.....	74
3.10.2.1 Maximum Tolerated dose.....	74
3.10.3 DMBA/TPA model induces skin carcinogenesis.....	75

3.10.4 Efficacy.....	75
IV- Discussion	81
V- Conclusion	92
References.....	93
Appendix.....	115

LIST OF TABLES

Table	Page
Table 1.1. Factors in cell survival and proliferation, which lead to carcinogenesis....3	3
Table 2.1. Conditions and parameters selected on the ICP-MS machine.....34	34
Table 2.2. Treatment conditions used for the evaluation of [Ru(bpy) ₂ BC]Cl ₂ as PACT and [Ru(bpy) ₂ dpphen]H ₂ O]Cl ₂ as a chemotherapeutic in DMBA/TPA-induced skin tumours.....42	42
Table 3.1. The partition coefficient between the hydrophobic octanol phase and the hydrophilic water phase (log P) reported for [Ru(bpy) ₂ phen]Cl ₂ , [Ru(bpy) ₂ BC]Cl ₂ , [Ru(bpy) ₂ BC]Cl ₂ photoproducts, [Ru(bpy) ₂ dpphen]Cl ₂ , [Ru(bpy) ₂ (dpphen)H ₂ O]Cl ₂ , cisplatin, BC and bpy.....54	54
Table 3.2. Concentration of precursor vs. photoproduct.....116	116
Table 3.3. Intracellular concentration of [Ru(bpy) ₂ BC]Cl ₂ precursor vs. photoproducts (μM/10 ⁵ cells) along with the ratio of intracellular/extracellular compound concentration in A375 cell line.....56	56
Table 3.4. Intracellular concentration of [Ru(bpy) ₂ BC]Cl ₂ precursor (μM) along with the ratio of intracellular/extracellular compound concentration in A375 cell line, identifying the mode of uptake.....57	57
Table 3.5. IC ₅₀ values (μM) of [Ru(bpy) ₂ BC]Cl ₂ , Ru(bpy) ₂ Phen.Cl ₂ , BC and BPY ligands along with IC ₅₀ of the positive control cisplatin.....58	58
Table 3.6. IC ₅₀ values (μM) of [Ru(bpy) ₂ BC]Cl ₂ , light irradiated, light – Intracellular and photoproducts.....59	59
Table 3.7. IC ₅₀ values (μM) of [Ru(bpy) ₂ dpphen]Cl ₂ . The IC ₅₀ values were measured on A375 cell line in both dark and light conditions.....60	60
Table 3.8. IC ₅₀ values (μM) of [Ru(bpy) ₂ (dpphen)H ₂ O]Cl ₂ . The IC ₅₀ values were measured on A375 cell line.....60	60

Table 3.9. Effect of Ru(II) treatment on DNA in A375 cells.....70

Table 3.10. Lethal dose and effect observed.....117

LIST OF FIGURES

Figures	Page
Figure 1.1. The development of cancer.....	2
Figure 1.2. Hallmarks of cancer.....	3
Figure 1.3. Cell proliferation and growth pathways.....	11
Figure 1.4. Programmed cell death.....	12
Figure 1.5. Apoptotic pathways.....	15
Figure 1.6 Autophagy and Apoptotic crosstalk.....	17
Figure 1.7 Jablonski Diagram.....	22
Figure 2.1. Calibration curve generated by plotting the peak areas against known concentrations.....	34
Figure 2.2. Comet Assay demonstration.....	39
Figure 2.3. Cell death analysis demonstration.....	40
Figure 2.4. LD demonstration.....	40
Figure 2.5. MTD demonstration.....	41
Figure 2.6. Blue LED light irradiation demonstration.....	43
Figure 3.1. Chemical structure of the compounds synthesized.....	44
Figure 3.2. ¹ H NMR spectra of [Ru(bpy) ₂ phen](PF ₆) ₂	115
Figure 3.3. ¹ H NMR spectra of [Ru(bpy) ₂ BC](PF ₆) ₂	116
Figure 3.4. Blue LED light setup.....	45
Figure 3.5. Absorption spectrum of [Ru(bpy) ₂ dpphen]Cl ₂ in water as a function of time	

in the dark.....	45
Figure 3.6. Absorption spectrum of [Ru(bpy) ₂ dpphen]Cl ₂ in water as a function of time upon exposure to blue light (100 mWcm ² , 448nm)	46
Figure 3.7. Closer picture at the absorption spectrum of [Ru(bpy) ₂ dpphen]Cl ₂ in water as a function of time upon exposure to blue light (100 mWcm ² , 448nm). Arrows indicate the spectral changes trend throughout light exposure.....	46
Figure 3.8. ESI-MS/MS spectrum [Ru(bpy) ₂ dpphen]Cl ₂ before irradiation.....	47
Figure 3.9. ESI-MS/MS spectrum [Ru(bpy) ₂ dpphen]Cl ₂ after irradiation.....	48
Figure 3.10. Column Chromatography elution of irradiated [Ru(bpy) ₂ dpphen]Cl ₂	49
Figure 3.11. [Ru(bpy) ₂ dpphen]Cl ₂ photoproducts fractions eluted.....	49
Figure 3.12. Absorption spectrum of eluted fractions of [Ru(bpy) ₂ dpphen]Cl ₂ photoproducts.....	49
Figure 3.13. ESI-MS/MS spectrum for column 1 fraction characterization.....	51
Figure 3.14. ESI-MS/MS spectrum for column 2 fraction characterization.....	52
Figure 3.15. ESI-MS/MS spectrum for column 2 fraction characterization in 10% methanol.....	52
Figure 3.16. ESI-MS/MS spectrum for column 2 fraction characterization in miliQ water.....	53
Figure 3.17. Absorption spectrum of [Ru(bpy)(dpphen)H ₂ O]Cl ₂	53
Figure 3.18. UV-vis absorbance spectrum of [Ru(bpy) ₂ BC]Cl ₂ precursor vs. photoproduct.....	55
Figure 3.19. ICP-MS analysis for the uptake of Ru(II) in A375 cells.....	56
Figure 3.20. ICP-MS analysis for the mode of uptake of Ru(II) in A375 cells.....	57
Figure 3.21. Cytotoxic effect of [Ru(bpy) ₂ BC]Cl ₂ dark, [Ru(bpy) ₂ BC]Cl ₂ light,	

cisplatin, Phen, BC, and BPY on A375.....	58
Figure 3.22. Cytotoxic effect of [Ru(bpy) ₂ BC]Cl ₂ photoactivated using blue LED light on A375.....	59
Figure 3.23. Cytotoxic effect of [Ru(bpy) ₂ dpphen]Cl ₂ dark and light activated on A375.....	60
Figure 3.24. Cytotoxic effect of [Ru(bpy)(dpphen)H ₂ O]Cl ₂ photoproducts on A375.....	60
Figure 3.25. ROS production upon treatment with [Ru(bpy) ₂ BC]Cl ₂ compounds with or without light irradiation in A375.....	61
Figure 3.26. A375 cells treated with a concentration of double IC ₅₀ of the Light activated prodrug at 24,48 and 72 hours.....	62
Figure 3.27. The western blot images of Bax and actin along with the ratios of the different samples normalized to CD at 24, 48 and 72 hours.....	63
Figure 3.28. The western blot images of Bcl2 and actin along with the ratios of the different samples normalized to CD at 24, 48 and 72 hours.....	63
Figure 3.29. The ratio of Bax/Bcl2 at 24, 48 and 72h.....	64
Figure 3.30. The western blot images of Cytochrome C and actin along with the ratios of the different samples normalized to CD at 24, 48 and 72 hours.....	64
Figure 3.31. The western blot images of cleaved caspase-3 and actin along with the ratios of the different samples normalized to CD at 24, 48 and 72 hours.....	65
Figure 3.32. The western blot images of Cleaved PARP-1 and actin along with the ratios of the different samples normalized to CD at 24, 48 and 72 hours.....	65
Figure 3.33. The western blot image of Procasp8 and actin along with the ratios of the different samples normalized to CD at 24, 48 and 72 hours.....	66
Figure 3.34. The western blot image of P21 and actin along with the ratios of the different samples normalized to CD at 72 hours.....	66

Figure 3.35. The western blot image of p-ERK and ERK along with the ratios of the different samples normalized to CD at 72 hours.....	67
Figure 3.36. The western blot image of p-AKT and AKT along with the ratios of the different samples normalized to CD at 72 hours.....	67
Figure 3.37. The western blot image of Beclin-1 and actin along with the ratios of the different samples normalized to CD at 24, 48 and 72 hours.....	68
Figure 3.38. Microscopic images of the comet formations in comparison to controls.....	69
Figure 3.39. Tail moment index as calculated from the comet assay data.....	70
Figure 3.40. Cell death analysis at 24 and 48 hours.....	72
Figure 3.41. Bar graph representing percent viable, apoptotic and necrotic cells at 24 hours.....	73
Figure 3.42. Bar graph representing percent viable, apoptotic and necrotic cells at 48 hours.....	73
Figure 3.43. Lethal dose obtained via the up and down procedure.....	74
Figure 3.44. Body weight (g) of each mouse measured weekly.....	75
Figure 3.45. Percent survival per MTD group.....	75
Figure 3.46. Random five of thirty-two mice represented, twelve weeks' post DMBA/TPA.....	76
Figure 3.47. Body weight (g) measured weekly per group.....	76
Figure 3.48. Two animals (M1/ M2) represented from each group at day 0 vs. week 4 of treatment.....	78
Figure 3.49. Tumor growth in Balb/c mice bearing DMBA/TPA induced skin tumors treated over 3 weeks as described in Table 2.2.....	79
Figure 3.50. Tumor incidence in Balb/c mice bearing DMBA/TPA induced skin tumors treated over 4 weeks as described in Table 2.2.....	80

LIST OF ABBREVIATIONS

RBF	Round-bottom flask
NMR	Nuclear magnetic resonance
ESI-MS	Electrospray Ionisation-Mass Spectrometry
ICP-MS	Inductively coupled plasma mass spectrometry
DMEM	Dulbecco's Modified Eagle Medium
FBS	Fetal Bovine Serum
EMT	Epithelial-to-mesenchymal transition
ECM	Extracellular Matrix
DMSO	Dimethyl Sulfoxide
$\log P$	Partition coefficient between water and octanol phases
IC ₅₀	Inhibitory Concentration 50
DNA	Deoxyribonucleic acid
RIPA	Radio immunoprecipitation assay
DMBA	7,12-Dimethylbenz(a) anthracene
TPA	12-O-tetradecanoylphorbol-13-acetate
BC	Bathocuproine = 2,9-Dimethyl-4,7-diphenyl-1,10-phenanthroline
Dpphen	2,9-diphenyl-1,10-phenanthroline
BPY	Bipyridine
Phen	[Ru(bpy) ₂ phen]Cl ₂
PBS:	Dulbecco's Phosphate Buffered Saline
SEM	Standard error of the mean
UV-vis	Ultraviolet-visible
Tween 20	Polyoxyethylkene (20) sorbitan monolaurate
SDS	Sodium Dodecyl Sulphate
BSA	Bovine serum albumin
APS	Ammonium persulfate
BAX	Bcl2-Associated X protein
Bcl2	B-cell lymphoma 2
PARP-1	Poly [ADP-ribose] polymerase 1
Casp 3	Caspase 3
ERK	Extracellular Receptor Kinase

P-ERK	Phosphorylated Extracellular Receptor Kinase
AKT	Protein Kinase B
P-AKT	Phosphorylated Protein Kinase B
PI3K	Phosphatidylinositol-4,5-bisphosphate 3-kinase
PIP2	Phosphatidylinositol 4,5-bisphosphate
PIP3	Phosphatidylinositol (3,4,5)-triphosphate
P21	Cyclin-dependent kinase inhibitor 1
Casp8	Caspase 8
Bcl-10	B-cell lymphoma/leukemia 10
Bad	Bcl-2-associated death
Bak	Bcl-2-antagonist/killer 1
Blk	B lymphoid tyrosine kinase
Bim	Bcl-2-like protein 11
Bid	BH3 interacting-domain death agonist
Bik	Bcl-2-interacting killer
Bcl-XS	B-cell lymphoma-extra small
Bcl-XL	B-cell lymphoma-extra large
ROS	Reactive Oxygen Species
IP	Intraperitoneal
ST	Subtumoral
MTD	Maximum tolerated dose
LD	Lethal Dose
PI3K	Phosphatidylinositol-3-kinase
PIP2	Phosphatidylinositol-4,5-bisphosphate
PIP3	Phosphatidylinositol-4,5-trisphosphate
UDP	Up and down procedure
ATC	Acute toxic class

Chapter One

Literature Review

1.1 Cancer

1.1.1 Overview

Cancer develops when the normal cells of the body begin to anomalously replicate and divide as a result of genetic or epigenetic modifications/mutations, which allow the cells to detour the regular homeostatic balance of proliferation (Sever & Brugge, 2015). This irregular propagation may lead to the formation of benign tumors also known as hyperplasia, where a mass of cells hold an abnormal morphology and changes in function (Arvelo, et al., 2015; Baba, et al., 2007). Angiogenesis is triggered by tumour development, namely the establishment of new blood vessels that will supply the oxygen, nutrients and immune cells to the tumor to further progress. (Arvelo, et al., 2015; Nishida et al., 2006). Successively the tumor cells will then endure a plot of events that result in the establishment of a secondary tumor or metastasise. They have the power to invade short distances, yet they obtain their disseminating capabilities by intravasating into confined microvasculature from where they can extravasate, proliferate and develop into secondary tumors, Figure 1.1. (Arvelo, et al., 2015; Katt et al., 2018). Tumors are classified, depending on the kind of tissue it has originated from. Accordingly, cancer can be subdivided into six general categories including solid and non-solid tumors; carcinoma, sarcoma, myeloma, leukaemia, lymphoma and mixed types (National Cancer Institute, 2015).

1.1.2 Normal versus Cancer cells

The major dissimilarity among normal vs. cancer cells is the proliferation abilities (Bajaj et al., 2009). Normal cells divide and multiply in an organized route and are eliminated by the body when damaged. Cancer cells, on the other hand continuously divide in an unorganized manner at which they evade apoptosis via many mechanisms (Li, et al., 2007). Cancer metastasis, is a key reason to cancers disease and mortality, which reports 90% of deaths. Cancer cells are able to separate from the basement membrane via the loss of certain surface proteins at which they can migrate and spread

to metastasize, which is not applicable in healthy cells (Guan, 2015). Additional distinctions, comprise lack of differentiation, accumulation of mutations in various genes, like proto-oncogenes or tumor suppressor genes, as well as disordered cell signalling in cancer cells. (Martin, 2003)

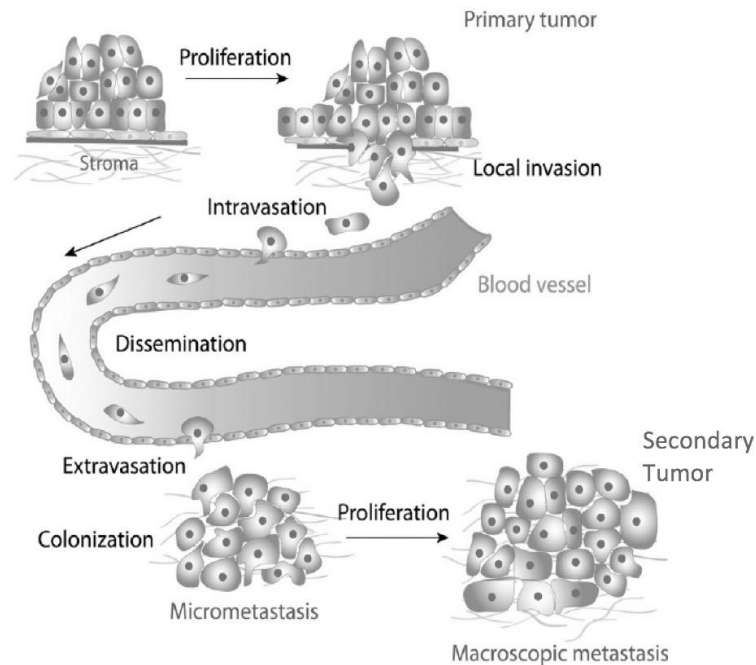


Figure 1.1. The development of cancer. Post angiogenesis, tumor cells intravasate into the local microvasculature from where they can extravasate, develop and grow into a secondary tumor (Saxena et al., 2013). Modified from Saxena, et al. 2013

1.1.3 Hallmarks of cancer

The main triggers of tumorigenesis are the genetic and epigenetic modifications. Yet, cancer development is also associated with other factors comprising, the communication of cancers with the extracellular matrix (ECM) together with nearby non-neoplastic cells and the attainment of distinct traits that modify their normal physiology (Hanahan & Weinberg, 2000). Six hallmarks of cancer were identified to be crucial for pathogenesis. They comprise, sustained proliferation signalling, replicative immortality, evading growth suppressors, resisting cell death, inducing angiogenesis, and activating invasion and metastasis (El-Tanani, et al., 2016; Hanahan & Weinberg, 2000). Hanahan and Weinberg, later showed two added hallmarks which may greatly add to the pathogenesis of cancers: evading anti-tumor immunity that is mediated by natural killer cells, macrophages, B and T lymphocytes

and the disruption of the normal cell metabolism in order to encourage neoplastic proliferation (Hanahan & Weinberg, 2011). The hallmarks of cancer are supported by two essential characteristics. The first comprises genomic instability and amplified mutability driving tumor development, and the second, being inflammation that arranges the tumor microenvironment, which stimulates survival, proliferation as well as invasion (Duijf et al., 2019) Figure 1.2.

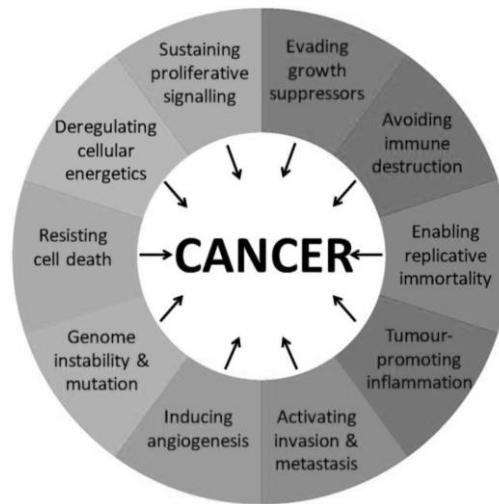


Figure 1.2. Hallmarks of cancer. The six crucial hallmarks of cancer are sustained proliferation, limitless replicative potential, evading tumour suppressors, resisting cell death, stimulating angiogenesis and triggering invasion and metastasis. Additional hallmarks, that may greatly add to pathogenic capabilities of most cancers are, avoiding immune destruction and interrupting the normal cell metabolism to encourage neoplastic propagation (El-Tanani, et al., 2016). Modified from (El-Tanani, et al., 2016).

1.1.3.1 Continual proliferation

The cell's capability in sustaining proliferation, alias, uncontrollable cell division, with no control signal is a key trait of a cancer cell identifying key factors in table 1.1 (Gillet & Barnes, 2000). Carcinogenesis is a multiple event process where changes in tissue architecture and the development of pre-neoplastic nodules head the appearance of cancer, which are due to changes in cell phenotype (Harris, 2002). Epithelial to mesenchymal transition (EMT) is a result of damage or tumorigenesis or it may occur prior to it, and develop hypoxia in local regions, where it encourages the survival and development of tissue stem cells. Epithelial cells change structure from an ordered apical and basal polarity into a fewer well-ordered, migratory fibroblastic

morphology (Wang, et al., 2010; Harris, 2002). Autophagy is also a promoter of preneoplastic and tumor cell survival under demanding conditions (table 1.1). In healthy cells, basal autophagy is a mean, which controls cellular homeostasis by eliminating protein aggregates and any damaged organelles (Feitelson, et al., 2015). On the other hand, starvation stimulated autophagy extends cell survival by reutilizing amino acids and energy, that are essential for cellular health and viability preservation. The reason for the upturn of basal autophagy in cancer cells is to endure stress which is because of non-regulated signalling refereed by proliferation, improved glycolysis, hypoxia and to preserve cancer cells in a state of dormancy (Feitelson, et al., 2015; Harris, 2002). Hormonal signalling and transduction pathways dysregulation can initiate sustained proliferation; they can make growth factors on their own, initiating autocrine proliferating loops, in addition to signaling adjacent normal cells to supply required growth factors (Cheng, et al., 2008). Dysregulation may also be due to over expressed receptors or mechanical modifications in the receptor which prime ligand independent activation (Hanahan & Weinberg, 2011). Each of these may be subjugated therapeutically (Feitelson, et al., 2015).

Table 1.1. Factors in cell survival and proliferation, which lead to carcinogenesis.
Modified from (Feitelson, et al., 2015).

Factor	Contribution to carcinogenesis
<i>EMT</i>	Asissts stem cell growth, and metastasis
<i>Hypoxia</i>	Hypoxia inducible factors (HIF) encourage growth of Cancer Stem Cells as well as angiogenesis. HIF alters metabolism; establishes activation of signaling pathways (Qiang, et al. 2012)
<i>Autophagy</i>	Supports cell survival in result of dysregulated signalling-mediated proliferation, increased glycolysis, and hypoxia
<i>Cancer Stem Cells</i>	Disruptive regulation in “stemness,” dormancy, self-renewal, the potential to make differentiated progeny, resist apoptosis, and chemo-resistance, effectively transformed cell fate and uncontrolled cell growth
<i>Cell cycle proteins</i>	Disruptive expression of cell cycle proteins (Rb, CDKs, cdk inhibitors) lead to dysregulated cell propagation
<i>Signal transduction</i>	Hardwired stimulation of many signaling pathways lead to uncontrolled proliferation (such as, Wnt, Notch, IGF,

<i>pathways</i>	PI3K/Akt, NF- B)
<i>Altered cell metabolism</i>	Initiated transformed survival and development in the counter conditions (e.g., hypoxia) in the beginning stages of carcinogenesis (e.g., altered glycolysis and arginine metabolism) (Kus, et al., 2018)
<i>Hormone signalling</i>	Allow the development of hormone responsive cancers via continuous activation of estrogen and androgen signalling pathways.
<i>Tumor microenvironment</i>	Crosstalk of stromal-tumor cell allows for the development and metastasis of cancer stem cells

1.1.3.2 Evading tumor suppressors

Evasion of tumor suppressors is a vital characteristic of cancer cells. Tumor cells can escape tumor suppressors via genetic and epigenetic means. Genetic mechanisms comprise chromosomal modifications like mutations, deletions, loss of upstream or downstream effectors or inactivation of essential proteins. Epigenetic escape comprises DNA or histone methylation and acetylation. Tumor suppressors like the classical gene encoding p53 and retinoblastoma associated (Rb) proteins, regulate proliferation and cell senescence (Ruhul, et al., 2015). Inhibitory growth factor signals, received from the exterior of the cell act on Rb protein to drive cell cycle progression, as well as being a key regulator of DNA replication, differentiation as well as apoptosis. To move into the cell cycle, the p16 protein must adjust Rb by inhibiting the cyclin depending kinases which phosphorylate Rb, thus permitting the E2f family of transcription elements in order to recruit the expression of the associated genes (Ruhul, et al., 2015; Sage & Burkhardt 2008; Sherr & McCormick, 2002). Protein 53 (p53), has anti- tumor growth functions, like DNA repair, cell cycle arrest and apoptosis. It transduces stressful conditions like low oxygen or glucose, also, cell damage, which the cell system faces, into molecular downstream signals which initiate p53 to stop proliferation and begin apoptosis. So, the loss of p53 can lead to genetic instability and accumulation of mutations driving cancer initiation (Ruhul, et al., 2015). Phosphatase and tensin homolog (PTEN), also a tumor suppressor and metabolic regulator, may drive tumor growth if its functional activity is lost. A phosphatase, PTEN protein, which dephosphorylates phosphatidylinositol (3,4,5) – triphosphate (PIP3), primes the unrestricted activity of phosphoinositide 3 kinase

(PI3K) and protein kinase B (AKT) signalling, that drives tumor growth. (Chen, et al., 2018). The transforming growth factor-beta (TGF-beta), also acts as an anti-proliferative agent, yet, in later stages of cancer, its communication is disrupted and may move from suppressing growth to triggering epithelial-to-mesenchymal transition (EMT), which activates malignancy and invasion (Pickup, Novitskiy, & Moses, 2013).

1.1.3.3 Resisting cell death

The natural barrier of protection against cancer is apoptosis. When DNA damage is increased by hyperproliferation as well as increase in oncogenic signals, apoptosis is stimulated. The regulators of the apoptotic pathway are received either extrinsically or intrinsically. Upon activation, the regulators act on the inactive caspases 8 and 9 to initiate a cascade of protein cleavage that will destroy the cell and be consumed by adjacent cells or phagocytes (Sharma, et al., 2019). The communication of regulator and effectors is organized by pro-apoptotic and anti-apoptotic proteins. Pro-apoptotic proteins, like Bax translocate to the outer membrane of the mitochondria in which, the membrane becomes permeable releasing other pro-apoptotic proteins like the essential Cytochrome c, which, results in the activation of a cascade of caspase proteins (Sharma, et al., 2019; Willis & Adams, 2005). The model anti-apoptotic protein Bcl-2 (as well as, Bcl-xL, A1, Mcl-1 and Bcl-w) obstruct apoptosis by seizing the pro-apoptotic proteins like Bax and Bak at their BH3 domain, which render the mitochondrial membrane proteins inactive (Sharma, et al., 2019). Protein 53, also induce apoptosis due to DNA damage like strand breaks and chromosomal anomalies as previously described, yet p53 acts by increasing PUMA (subgroup of the Bcl-2 family) BH3 and Noxa (pro-apoptotic member of the Bcl-2 family) levels only (Junttila & Evan, 2009; Ruhul, et al., 2015). Another path to apoptosis is the increased activity of oncoproteins like Myc (Junttila & Evan, 2009). Cancerous cells can escape the apoptotic paths by mechanisms like the disturbance of the extrinsic ligand-induced programmed cell death and loss of utility of tumor suppressors. Cancer cells may also escape by increasing the expression of anti-apoptotic proteins or decreasing expression of pro-apoptotic proteins (Lowe, Cepero, & Evan, 2004; Sharma, et al., 2019). Autophagy on the other hand, works on the basal levels in healthy cells and is greatly expressed in conditions of cellular stress like glucose deficiency, similar to apoptosis. Autophagy breaks the cells' machinery for adjacent cells to make use of in storing energy (Himuro, et al., 2019). Beclin-1 is a

characteristic protein of autophagy, in which it holds a BH3 domain, which permits it to bind Bcl-2, allowing autophagy and apoptosis to communicate together or act independently against carcinogenesis (Himuro, et al., 2019; Sharma, et al., 2019). Necrosis is another form of cell death that can occur in cancer cells. Necrosis swells the cells till they burst to discharge their cellular constituents into their surrounding microenvironment. Remarkably, necrotic cells, discharge pro inflammatory signals to the immediate environment where they recruit immune cells to the necrotic medium (Karsch-Bluman, et al., 2019). Captivating evidence has shown that immune cells can help cancer cells stimulate angiogenesis and invasiveness, as well as secrete reactive oxygen species (ROS) that are mutagens. Necrotic cells may also make bioactive regulatory elements like, interleukin-1 alpha that can trigger adjacent cells to grow, thus tumor cells may tolerate some form of necrosis so as to stimulate inflammation and tumor growth (Grivennikov, Greten, & Karin, 2010).

1.1.3.4 Enabling replicative immortality

Cells' ability to continuously divide and grow without cell senescence is known as immortality. Compelling evidence has shown the role of telomeres in the continuous proliferation of cancer cells, as well as the ability to return to a pre-differentiated state in the form of a stem cell phenotype that will allow continuous cellular division (Hanahan & Weinberg, 2011). In healthy cells, telomeres regularly shorten until losing the capability to safeguard the edges of chromosomes that would fuse together resulting in unstable DNA that pressures cell viability. The job of the telomerases is to polymerize and add repeats to the telomeres ends, which are in fact greatly expressed in immortalized cells like cancer cells (Blasco, 2005).

1.1.3.5 Inducing angiogenesis

The process of angiogenesis is regulated by many signals comprising growth factors as well as angiopoietin and interleukin 8. Endothelial cells will proliferate and accumulate to enhance blood supply to the tumors (angiogenesis) (Saman, et al., 2020) Angiogenesis is moderated by the PI3K-AKT pathway via the upregulation of HIF which directs the formation and secretion of the vascular endothelial growth factor (VEGF). (Zhang et al., 2018). Angiogenesis is also aroused by stopping inhibitors like thrombospondin 1 (Tsp1), which may cease angiogenesis in healthy cells by initiating FasL, which induces programmed cell death of endothelial cells (Lawler & Lawler,

2012; Mirochnik et al., 2008). Tsp1 in cancerous cells is repressed by hypermethylation. *Tsp1* and oncogenes like c-Myc, Src and Ras, ensure that the deregulation of Ras-ERK path is a regulator of angiogenesis (Linhao, et al., 2020)

1.1.3.6 Invasion and metastasis

Metastasis originates via the invasion of tumor cells through the stroma allowing them to move to the blood stream. Its onset is connected to the changes in polarity, morphology, adhesion, and cytoskeleton property which are activated via many factors like the chemokines, growth factor and adhesion receptors (Zijl, et al., 2011). Many cancerous cells obtain their obstructive and migration abilities via the loss of their cell to cell adhesion factor E-cadherin, which is a process known as EMT. Invasion starts through the bounding of the ECM by exact receptors such as the integrin, forming actin rich invadopodia, degrading the ECM via matrix proteases, and migrating through the matrix. A signal ends in cell polarization and development of migrating protrusions as lamellipodia, trailed by the adhesion to ECM and decrement of the cell body enforcing the drive away from the migrating front (Bozzuto et al., 2010; Wang, et al., 2010). Protuberances comprising lamellipodia as well as invadopodia are made via actin polymerizing process that can be triggered via actin-related proteins 2/3 (Arp 2/3). Arp2/3 are part of actin nucleation and are controlled via Wilscott-Aldrich syndrome protein (WASP) and WASP-family verprolin-homologous protein (WAVE) (Frugtniet, et al., 2015). After breaking into the basement membrane, the cancerous cells may enter the blood stream and lymphatic vessels; intravasate, then extravasate from the vessels and form novel tumors, a means renowned as colonization (Hanahan & Weinberg, 2000). The PI3K-Akt plus the Ras-ERK paths control invasion and migration through several factors. The Ras-ERK path may additionally encourage EMT via its downstream goal, the activator protein-1 (AP-1), which activates the manifestation of EMT-promoting transcription elements (Liu et al., 2020). AP-1 is moreover involved in invasion and migration via the high expression of matrix metalloproteases (Ji et al., 2015).

1.1.4 Causes of cancer

Cancer is not the result of a single factor but an accumulation of genetic and environmental factors (Anand, et al., 2008).

1.1.4.1 The genetics and the kind of mutations that may trigger cancer

Cancer forms due to genetic mutations which may be inherited or acquired extemporaneously because of replicative errors or due to contact with certain carcinogens that can provoke DNA damage (Anand, et al., 2008). Such genetic modifications may comprise the silencing, deletion or loss of function mutations in tumor suppressor genes and gain of function in proto-oncogenes that may form fundamental oncogenes, driving malignant neoplasms (Croce, 2009). Epigenetic modification like the methylation of cytosine may change the communication of regulators like histone-modifying enzymes or elements which are a part of DNA methylation (Anand, et al., 2008; Suva, et al., 2013). Certain cancer may be initiated via viral infectious agents: like Epstein Bar virus, hepatitis B virus, or human papilloma virus (HPV) (Stanley, 2017).

1.1.4.2 Cell signalling in cancer

1.1.4.2.i RAS-ERK pathway

Mitogen activated protein kinase (MAPK) is a protein modifier via phosphorylation commonly on serine, tyrosine and threonine amino acids, which induces downstream modifications (Meister et al., 2013). These modifications were observed to take part in cell proliferation and migration, thus a key pathway in cancer development and progression (Khavari & Rinn, 2007). Human cells have four main forms of MAPK pathways, namely the c-Jun N-terminal kinase/stress-activated protein kinase (JNK/SAPK) pathway, the p38 kinase pathway, the Big MAP kinase-1 (BMK-1) pathway as well as the classical MAPK/ERK pathway (Baldini et al., 2012). These paths are all elicited via the activation of a cascade of minimum three key kinases: MAPKKK, MAPKK, and MAPK (Zhou, et al., 2017). Once they are activated the mitosis and metabolism as well as gene expression are ordered, thus, cellular survival. The JNK/SAPK pathway works as an apoptotic kinase which responds to stimuli like tumor necrosis factor, cytokines, UV light, heat shocks, chemotherapeutic drug etc. (Stadheim, et al., 2002). These stimuli trigger MAPKKKs that can in order activate MAPKKs via phosphorylation, which in order activates the MAPK, JNK. When activating this flow of events, a succession of caspases as well as apoptotic proteins like Bax and Bcl-2 are controlled accordingly (Qu, et al., 2017). The other

kinase pathway comprises p38 MAPK. This initiates cell growth or death by regulating the cell cycle and altering the cytoskeleton. It is activated greatly by stressful environmental factors such as hypoxia (Lee, et al. 2002). This effectively activates the MAPKKKs that will start MAPKKs which will successively turn on MAPKs, p38 is then activated and a cascade of events triggers downstream effectors and are regulated accordingly (Makeeva, et al., 2006). A third path of these kinases include the extracellular signal regulated kinase 5 (ERK5). This path is also stimulated by stress, growth factors (EGF and VEGF) and cytokines. This Pathway has a role in cell proliferation and cell cycle as well as the pathogenicity of cardiovascular factors (Gomez, Erazo Y Licanzo., 2016). This MAPK member has three signalling cascade which are of, MAPKKK (MEKK2/3) activation which will initiate MAPKK (MEK5) to activate MAPK (ERK5) and trigger a cascade of downstream factors (Gavine, et al.,2015). The last pathway of the kinases is the conventional MAPK/ERK path (Figure 1.3.) that comprises the extracellular signal-regulated kinases (ERK1/2). It was formerly known as the Ras-Raf-MEK-ERK path since it contains a path of protein which transduce signals from the plasma membranes receptors to the nucleus via proteins counting ERK (Wang et al., 2018). Raf and Ras are the MAPKKKs activated via the exterior stimuli that in turn act in MAPKKs (MEK1 and MEK2) via phosphorylation which will activate MAPK (ERK1 and ERK2), triggering downstream activation of around 100 substrates (Stivala, et al., 2019; Wang et al., 2018). Some substrates that are controlled by the activation of ERK are Bid/Bax and p21, and the cell motility inducing MMPs 1, 3 and 9. MAPK can be disabled via MAPK phosphatases (MKP), that remove the phosphate group from ERK and Raf deactivating them. This was associated with cell survival, thus several mutations in these can form cancer (Kondoh, et al., 2007; Sabio & Davis, 2014).

1.1.4.2.ii PI3K-AKT pathway

Phosphatidylinositol 3-kinase (PI3K) is a heterodimer comprised of a catalytic and regulatory subunit, respectively p110 and p85 (Liu, Cheng, et al., 2009). Four classes of PI3K have been identified (classes I, II, III, IV). The first is the major class, subdivided according to which receptor was activated (Jean, et al., 2014). Subclass IA (PI3K α, β, δ) is activated by RTK and subclass IB is activated by (PI3K γ) by G protein coupled receptors (Murthy, et al., 2018). The activation of Ras can activate the

p110 domain of PI3K or the activation of the receptor tyrosine kinase (RTK) can bind along with its adapter proteins and activate the p85 domain of PI3K, thus recruiting PI3K to the plasma membrane (Yu, et al., 1998). This activity will allow the phosphorylation of PIP2 (Phosphatidylinositol-4,5,bisphosphate) via PI3K, converting PIP2 to PIP3 (Phosphatidylinositol-4,5,trisphosphate). Triggering a downstream activation of the serine-threonine AKT (also known as Protein Kinase B, or PKB) (Figure 1.3.) that will trigger the phosphorylation of various proteins leading to a cascade of signals downstream regulating cell survival, one of which include the tuberous sclerosis proteins 1 and 2 (TSC1/2) and glycogen synthase kinase 3 (GSK3) (Liu, Remedi, et al., 2009). PIP3 activation and AKT inhibition overexpression can be prohibited by phosphatase and tensin homologue (PTEN), which degrades PIP3, so, a mutation, or loss of PTEN can constitutively activate PI3K/AKT path, as well as a mutation of *PI3K*, *Ras* and RTK (Castellano, and Downward, 2011; Liu, Remedi, et al., 2009; Georgescu, 2010). The activation of AKT inhibits apoptosis by inhibiting caspase-9 activity and inhibiting MDM2 (Mouse double minute 2 homolog) which down regulates p53 (Shi, et al., 2012), also the inhibition of the pro apoptotic Bcl-2 associated death promoter (BAD), which prevents its binding in order to trigger the anti-apoptotic Bcl-XL protein activity via phosphorylation (Howells, et al., 2011). Furthermore, the mTOR (mammalian target of rapamycin) is an additional substrate that is important for cell survival and is controlled by AKT. It contains mTORC1 and mTORC2 which are two complexes that are constrained by TSC1 and TSC2 correspondingly. Activating of mTORC1 involves several cellular processes like the inhibition of autophagy, protein synthesis and cell growth (Alayev and Holz, 2013). Triggered activation of AKT, will phosphorylate and inhibit TSC1/2 thus, inducing mTOR and cell survival (Huang and Manning, 2008). AKT is also associated with hormonal resistance that may restrict hormonal therapies, and tumorigenesis, as well as drug resistance (McCubrey et al., 2007)

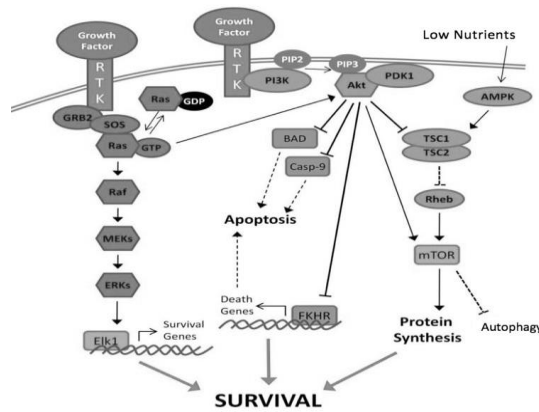


Figure 1.3. Cell proliferation and growth pathways. (Azad, et al., 2010). Modified from (Azad, et al., 2010)

1.2 Mechanisms of cell death

1.2.1 Apoptosis

Programmed cell death, known as apoptosis is a form of defence, which occurs in cells that are distressed intra- or extracellularly by microenvironmental alarms, of DNA damage, replicative stress, etc., to sustain homeostasis, at which it occurs to shield cells of viruses, infections and numerous toxic agents (Flusberg & Sorger, 2015). The characteristics of apoptotic cells are identified via their reduced size, rounded shape, chromatin condensation as well as a dense darkly stained cytoplasm. A process known as budding occurs to form apoptotic bodies, that have a very different shape in contrast to normal cells, these bodies are to be engulfed and phagocytized (Kakarla, et al., 2020). These bodies are phagocytized principally by macrophages, so that they are completely destroyed by the phagolysosomes. While these bodies can be engulfed by various immune cells, apoptosis does not prompt and inflammatory response, majorly due to no production of chemokines and cytokines. (Wallach & Kovalenko, 2014). The two prime apoptotic pathways are the intrinsic/mitochondrial pathways and the extrinsic/death receptor pathway, which meet at the endpoint known as the execution pathway (Elmore, 2007). The cleavage of caspase-3 initiates the execution pathway to the degradation of DNA and cellular proteins, consequently forming the apoptotic bodies (Figure1.4.) (Kakarla, et al., 2020).

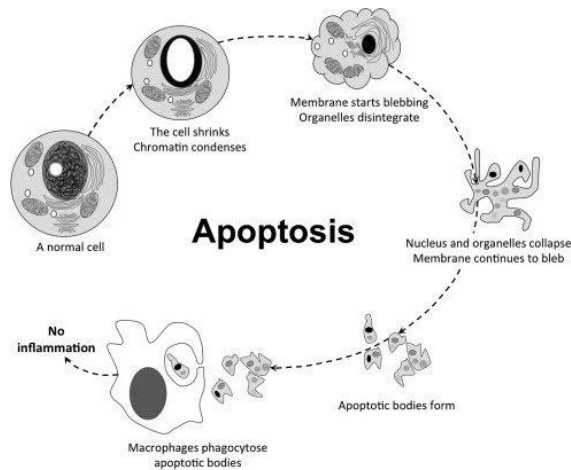


Figure 1.4. Programmed cell death. An apoptotic cells chromatin condenses as it reduces size and forms a rounded shape. The membrane begins to bleb and organelles disintegrate, after which the nucleus and organelles collapse, the apoptotic bodies form, and are recognized by phagocytic cells for ingestion to avoid further progression of the initiator. (Abou-Ghali, et al., 2015). Modified from Abou-Ghali, et al.

1.2.1.1 Intrinsic pathway

Numerous stimuli can act to initiate the intrinsic pathway via intracellular signals such as high cytosolic calcium concentrations, oxidative stress, hypoxia or DNA damage; forms of cellular stress, which prime the pro-apoptotic proteins to the cytoplasm like cytochrome c, due to increased mitochondrial permeability (Harr & Distelhorst, 2010). Cytochrome c binds Apaf-1 and procaspase-9 to initiate the formation of the apoptosomes (Purring-Koch & McLendon, 2000), yet HtrA2/Omi and Smac/DIABLO inhibit inhibitor of apoptosis proteins (IAP) (Corti, et al., 2018). Another group of pro-apoptotic proteins, which are discharged into the cytosol in late apoptosis are the caspase-activated DNase (CAD), apoptosis inducing factor (AIF), and endonuclease G, which move to the nucleus to trigger DNA fragmentation (Schindler, et al., 2006).

The intrinsic pathway is greatly controlled by the proteins of the Bcl-2 family due to the power they have over mitochondrial membrane permeability and thus cytochrome C release (Gupta, et al., 2009). This family of proteins is divided into pro or anti-apoptotic proteins. The pro-apoptotic proteins are Bcl-10, Bax, Bad, Bak, Blk, Bim, Bid, and Bik (Twiddy, et al., 2004). The anti-apoptotic proteins are Bcl-2, Bcl-w, Bcl-x, Bcl-XS, Bcl-XL, Mcl-1 (induced myeloid leukaemia cell differentiation protein) and BAG (Shamas-Din, et al., 2013; Kilbride & Prehn, 2013).

The phosphorylation of serine of the pro-apoptotic protein Bad, occurs in the cytosol unless de-phosphorylation occurs where, it will be translocated to the mitochondria, triggering the release of cytochrome c (Bhakar, et al., 2003). Bad is also capable of separating Bcl-XL and Bcl-2 to neutralize their outcome and induce cell death (Billen, et al., 2008; Zha, et al., 1997). If they are not separated, Bad, Bcl-2 and Bcl-XL will prevent cytochrome c release from the mitochondria (Billen, et al., 2008).

Additional members of the pro-apoptotic Bcl2 family are Noxa and Puma, that are controlled by the tumor suppressor protein p53 (Warren, Wong-Brown, & Bowden, 2019). Anti-apoptotic protein activity is prohibited by the localization of Noxa to the mitochondria, consequently activating caspase-9 (Nakajima, et al., 2014). Yet, the upregulation of Puma will surge the expression of Bax, which will move to the mitochondria inducing the release of cytochrome c (Luo et al., 2005; Lee, et al., 2008).

1.2.1.2 Extrinsic pathway

The death receptor pathway, commonly known as the extrinsic pathway, includes a whole set of interactions between receptors and ligands, that transduce cellular signals leading to their death (Khosravi-Far & Esposti, 2004). The main ligands of this path are TNF (tumor necrosis factor) and Fas (FasL), which bind their corresponding death receptors, TNF (type 1 TNF receptor) and CD95 (Fas), which have conforming intracellular domains which recruit the adaptor proteins such as FADD (Fas-associated death domain), TRADD (TNF receptor-associated death domain), as well as caspase 8 (Nguyen, et al., 2000). Subsequently, the complex of death ligands and receptors is renowned as DISC (death-inducing signalling complex) an activator of pro-caspase 8, which eventually activates apoptosis through the downstream activation of caspases and caspase-3, which is a part of the execution pathway that triggers apoptotic bodies (Raychaudhuri, 2014; Park, 2012).

1.2.1.3 Perforin-Granzyme pathway

The release of granzyme A or B through perforin channels, is a part of a minor pathway which is strictly associated with immune cells; cytotoxic T and natural killer cells (Shi, et al., 1997). Apoptotic death is induced, either by granzyme A which directs caspase-independent cell death via DNA damage (Martinvalet, Zhu, & Lieberman,

2005), or by granzyme B which triggers the execution pathway via caspase-3 activation by caspase-10 cleavage (Thomas et al., 2000).

1.2.1.4 Execution pathway

The previously discussed pathways meet at one point that is known as the execution pathway, where the executioner caspases, 3, 6, 7 play a central role in cleaving various downstream proteins triggering biochemical and morphological alterations perceived in cells undergoing apoptosis (Walsh, et al., 2008). Initiator caspases 8,9,10 activate caspase-3, which activate CAD to condense chromatin and allow DNA degradation due to the cleavage of proteins like PARP and NumA (Stennicke, et al., 1998). The movement of phosphatidylserine to the outer leaflet of the membrane of apoptotic cells can, which allows their engulfment by immune cells, be caspase dependent or independent, (Segawa, Suzuki & Nagata, 2011). It is noteworthy to mention a caspase-3-independent mechanism of cell death identified by either mitochondrial permeability triggering cell death or the loss of mitochondrial function assisting the caspase-3-independent mode of cell death (Tait, et al., 2014).

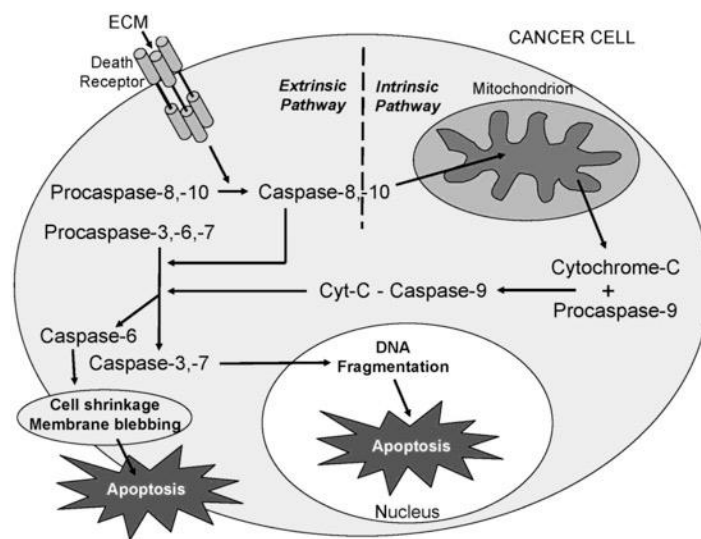


Figure 1.5. Apoptotic pathways. Modified from Walsh, et al., 2013

1.2.2 Necrosis

Necrosis is a cell death process triggered by extracellular injury like hypoxia or inflammation. Necrotic death is associated with activity of various pro-inflammatory proteins like the nuclear factor kappa-light-chain-enhancer of activated B cells (κ B) overexpresses to effectively rupture the cell membrane and thus cell content leakage

(Bharat, 2004; Lenihan & Taylor, 2013). This is why necrosis is characteristic of tissue damage and events of inflammation (Cao, et al., 2015). It is not energy dependent like apoptosis, and sudden damage is what results in the cells death as it loses its functional activity with its surrounding and reacts by oncosis (the cell swelling), which ultimately bursts. It is noteworthy to differentiate between the endpoint of apoptotic cells and necrotic cells, as the apoptotic bodies that form, lose their membrane integrity but are not removed by phagocytosis (Karch & Molkenin, 2015; Cao, et al., 2015; Xu, et al., 2019)

1.2.3 Necroptosis

Necroptosis is a form of programmed necrosis, which is controlled and activated by death receptors like TNFR1 (tumor necrosis factor receptor 1) (Linkerman & Green, 2014). The binding of a ligand to TNFR1, a complex I (pro-survival), loses its ubiquitin group, that produces either complex IIa or IIb. Complex IIa triggers caspase-8 and eventually apoptosis, but, if caspase-8 is constrained complex IIb is employed to trigger the activation of necroptosis (Ikner & Ashkenazi, 2011). RIP1 (receptor interacting protein 1) stimulates RIP3 by provoking auto-phosphorylation as well as trans-phosphorylation, at which RIP3 is oligomerized and a multiprotein complex (necrosome) is moulded (Wu, et al., 2014). Another important protein involved is MLKL (mixed lineage kinase domain-like pseudo kinase), which is phosphorylated by RIP3 to oligomerize and move to the cells membrane to fulfil membrane permeability resulting in necrotic death (Zhao, et al., 2012).

1.2.4 Autophagy

Autophagy is a mechanism at which cellular components like proteins are packed into the lysosomes to be digested, at which its products may be recycled, or used as an energy source (Harr & Distelhorst, 2010). This can be initiated due to cellular stress like the deprivation of nutrients. A protein marker, overexpressed during autophagy is, Beclin-1. It functions to bound numerous cofactor to control the lipid kinase Vps-34 protein and initiate Beclin-1-Vps34-Vps15 complex, thus inducing autophagy (Kang, et al., 2011). Beclin-1 can be inhibited by Bcl-2 or Bcl-XL as they bound its BH3 domain, which can be prevented by the phosphorylation of Bcl-2 and Beclin-1 (Cheng, et al., 2001). Additionally, there is a crosstalk between autophagy and apoptosis through the caspase-mediated cleavage of Beclin-1, generating N and C

terminal fragments at which the C terminal fragment moves to the mitochondria, transducing apoptosis (Kang, et al., 2011).

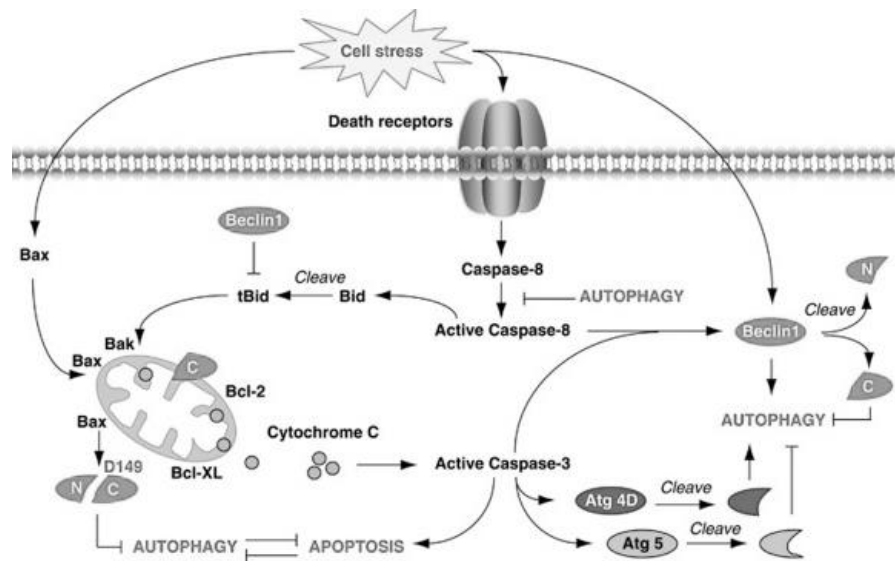


Figure 1.6. Autophagy and Apoptotic crosstalk. Caspase-mediated cleavage of Beclin-1 mediates the crosstalk of apoptosis and autophagy. (Kang, et al., 2011)

1.3 Human Melanoma

1.3.1 Overview

Melanoma, is recorded to be one of the most serious types of skin cancers to develop in melanocytes of which are our cell forming melanin (Mayo Clinic, 2020). In the UK, melanoma skin cancer deaths have been reported to be a little more common in males (56%) than in females (44%) (Cancer Research UK, 2017). Its occurrence has greatly increased in the U.S by 250% below 30 years and a 47% worldwide surge in the past 10 years. (Restrelli, et al., 2014). There are numerous biological and environmental factors that can be a risk to developing melanoma. The nature of hormones and level destabilisation between males and females as well as different oxidative stress between genders can be a stimulator of melanoma, as well as family history (Roh, et al., 2015). The exposure to ultraviolet radiations from sunlight or from tanning lights have been reported to be environmental factor that can increase the risk of emergent melanoma (Restrelli, et al., 2014). Treating melanoma, is via the classical cancer therapeutics, being chemotherapy, immunotherapy and targeted therapy (Commandeur, et al., 2014).

1.4 Cancer Therapy

Many different treatments are being implicated and adopted in cancer therapy. These conventional methods are used depending on tumor location, size, stage, as well as the patients' health (Zhang, et al., 2012).

1.4.1 Surgery, Radiotherapy and Chemotherapy

Surgery can be an efficient treatment in treating primary tumors that are localized and have not metastasized (Tremmel, et al., 2015). In combination to surgery, radiotherapy can be implemented, prior to surgery to rid outer tumor projections, or areas of the tumor that cannot be operated on, as well as be used in post-surgery to destroy any residues of the tumor (Abraha, 2018). Chemotherapy, termed by Paul Ehrlich, to refer to the treatment of cancer using chemicals upon his interest in alkylating agents, can be used together with surgery, or in combination with radiotherapy to enhance its effectiveness at local tumors that are not surgically accessible; yet it is also effective alone (Arruebo, et al., 2011; Lash & Gilman, 2013).

1.4.1.1 Platinum based chemotherapy

Cisplatin was first introduced in the 1960s and is currently used to treat various tumors. In the early twenty-first century, treatments were centered on administering high dosages of cytotoxic chemotherapeutics which, disturbed both malignant and normal cells. This may have attained tumor abolishment, yet it was linked to great systemic toxicity, which is the reason behind today's research for therapies that target only cancer cells more or less (Lippert, 1999; Golubnitschaja, et al., 2016).

Cisplatin, also known as cis-diamminedichloroplatinum (II), has been renowned for its mode of action in crosslinking DNAs purine bases, to interfere with cellular repair mechanisms, thus inducing DNA damage, consequently apoptosis (Tanida, et al., 2012). Despite its great use, Cisplatin has many side effects like neuromuscular hurdles, gastro-intestinal harms, ototoxicity, and renal tube injury (Oun, et al., 2018). Not to mention its primary acquired resistance, at which cancers overcome its mechanistic damage, by inhibiting the drug's uptake or inhibiting its activity by GSH (glutathione) molecules, thus enhancing DNA repair. This is what initiated the design of new metal based drugs, one being ruthenium (Rocha, et al., 2018).

1.4.2 Immunotherapy

This form of therapy unlike those mentioned above, uses the host immune system to rid the cancer rather than directly target it. These natural biological constituents can be made in the laboratories. These include antibodies, interleukins, interferons and cytokines. Advantages of this therapy is its specificity and regulated toxicity in treating cancer (Riley, et al., 2019). There are various forms of immunotherapy, like cytokine therapy, dendritic cell vaccines, but two main ones are: checkpoint inhibitors (CPI) and adoptive cell therapy (ACT) (Yang & Rosenberg, 2016; Darvine, et al., 2018). CPIs work by blocking barrier proteins on the T cells and redevelop immunity against cancers (Darvine, et al., 2018). Adoptive cell therapy comprises of the combination of numerous mature T cell subsets with the aim of ridding a tumor and inhibiting its recurrence. CAR-T (chimeric antigen receptor T cells) cell therapy is a form of ACT, effectively avoiding refractory B-cell malignancies. CAR-T are T cells, that are genetically modified to target specific tumor antigens via surface receptors at which they bind and destroy those expressing the antigen (Schepisi, et al., 2019).

1.4.3 Bio-chemotherapy

Administering both immunotherapy and chemotherapy is known as bio-chemotherapy, and is commonly used in treating metastatic malignant melanoma (Verma, et al., 2008).

1.4.4 Targeted therapy

This therapy practice, aims to treat cancer by targeting characteristic changes in cancer cells which aid their proliferation and propagation, in specific the molecular mechanisms of cancer, thus avoiding toxicity to off-target cells, observed in conventional chemotherapy (Padova, 2015).

1.4.5 Precision Medicine

This treatment allows health carers to specifically treat patients according to the genetic understanding alias the tumor profiling of their disease. This allows the usage of certain treatments upon DNA sequence comparisons (Hodson, 2016). Gene therapy is one approach, at which the addition of the functional copy of a faulty gene can be replaced, or modifying the expression of certain apoptotic coding genes like tumor suppressor genes and oncogene silencing (Kaufmann, et al., 2013).

1.4.6 Hormonal therapy

Hormone therapy is a way to slow or stop the progression of breast and prostate cancers, which are hormone-dependent for growth. Accordingly, nowadays, luteinizing hormone releasing hormone analog and aromatase inhibitors are implemented in breast and prostate cancers (Rauh, et al., 2015; Liu, Sun, et al., 2018).

1.4.7 Nanomedicine

This therapeutic includes nanoparticles used to encapsulate certain drug molecules, to enhance their bioavailability and solubility in tumors. This form of therapy has been considered and improved due to the size of the nano-molecules (1-1000 nm), as well as their high surface-to-volume ratio increasing targeted to combination therapies (Xu, Ho, et al., 2015).

1.4.8 Natural compounds

Natural compounds involve bioactive derivatives from plants, which have been and continue to be studied for their preventive and therapeutic effects against cancer. Most of the natural compounds act by inhibiting DNA replication (Lash & Gilman, 2013).

1.4.9 Stem cell transplant

This form of therapy has been implemented in hope to restore blood-forming stem cells in patients who underwent high doses of radio or chemotherapy and had their bone marrows destroyed. This enhances the bone marrows utility and permits the generation of functional cells as well as destroying malignant cells (Khaddour et al., 2020).

1.5 Ruthenium complexes in cancer treatment

Ruthenium (Ru), a transitional metal, has 3 oxidation states; Ru(II), (III) and (IV), which have a hexa-coordinate ruthenium center with an octahedral geometry, which allows their binding and intercalation with DNA. The oxidation of Ru(IV) has not been studied further since it is very unstable. Ru(III) is inert in normal tissue, thus, it can be used as a prodrug, which will be reduced to Ru(II) upon arrival to hypoxic and acidic

tumor environments putting it in its cytotoxic state, holding many possible mechanisms of action (Guo, et al., 2013; Zeng, et al., 2017). Platinum (Pt) and Ru(II), Ru(III) are similar in that they have a high kinetic stability, at which the kinetics of ligand exchange is imperative of minutes to days, yet, ruthenium has many advantages over platinum (Groessel, et al., 2010). Due to the fact that cancer cells are promptly dividing, they must have more iron, which is why cancer cells upregulate the expression/formation of transferrin receptors, to obtain more iron bound transferrin (Wessling-Resnick, 2018). Ruthenium has the ability to bind the transferrin receptor the way iron does, which is of advantage, to normal cells since ruthenium would bind cancerous cells 2 to 10 folds more. This backs to ruthenium's selective toxicity, targeting cancerous cells, thus limiting systemic toxicity, and its advantage over platinum based drugs (Daniels, et al., 2012; Guo et al., 2013). The mechanism of cytotoxicity of ruthenium complexes are many. It can hinder the replication and transcript of telomere DNA by directly binding, thus prompt apoptosis, or by inhibiting associated enzymes, therefore, inhibiting cell proliferation (Zeng, et al., 2017). Ruthenium has been shown to accumulate in cellular organelles like the endoplasmic reticulum (ER), mitochondria, and the lysosomes (Côte-Real, et al., 2013; Bravo-Sagua, et al., 2013; Puckett & Barton, 2007). Of the ruthenium complexes that target the ER, cause oxidative stress, inducing apoptosis. As for those, which, brought to the mitochondria, can cause the loss of membrane potential, its degradation and thus the activation of the intrinsic apoptotic path via the overexpression of pro-apoptotic protein such as Bax and the consecutive release of cytochrome c to the cytoplasm, activating the following caspases, thus apoptosis (Fulda & Debatin, 2006). Also, the ruthenium complexes which target lysosomes stimulate apoptosis as well as autophagy by facilitating the formation of the autolysosome (Lin, et al., 2018; Yuan, et al., 2015)

1.5.1 Light-mediated activation of ruthenium prodrugs

1.5.1.1 Photodynamic therapy

Photodynamic therapy (PDT) is constituted of a photosensitizer (PS) activated by a non-toxic light source, in the presence of tissue oxygen. Most PS in their ground state (S_0) have two relaxed electrons of opposite spins (Kaspler et al., 2016). As seen in figure 1.7; Jablonskis diagram explains after the PS is administered topically, locally, or systemically, the PS is irradiated with light of a wavelength in its absorption range, triggering the excitation of the PS to the excited single state (S_1), an unstable

and short lived process (Plaetzer, et al., 2009). In the S_1 phase energy can be released in the form of heat/fluorescence and either return to the relaxed state: S_0 or undergo an intersystem crossing (ISC) to a less excited state that is long-lived in triple state (T_1), which can undergo a type I or II reaction. Type I includes electron and proton exchange between cell substrates consequently forming free radicals that can form ROS by reacting with molecular oxygen forming hydrogen peroxide and hydroxyl radicals which are greatly toxic. Type II; T_1 can transfer its excited state energy to the triplet ground (stable) state oxygen (3O_2), to form a 1O_2 singlet oxygen, which is extremely reactive, forming prompt communications with cell substrates mediating damage and thus cell death (Mari, et al., 2015).

This therapeutic approach is alluring to cancer therapy because of its selectivity to the tumor and irradiated region mediating toxicity, accordingly limiting systemic toxicity. This characterizes PS design. The PS should be built to confine to the tumor, be inert in the dark and toxic upon irradiation, interpreted as having a high phototoxicity index (PI); the ratio of light to dark, obtained via IC50s. (Kaspler, et al., 2016; Kim, et al., 2018).

Ruthenium complexes, are considerate for PDT due to their octahedral geometry which allows the insertion of many ligands to characterize their photo physical assets and 1O_2 production which arbitrates DNA damage when exposed to blue light (Maytin, et al., 2018). What may interfere with the success of PDT is the amount of oxygen in the tumor, so this prevents its activity in an environment of no oxygen (Korbelik, 2006).

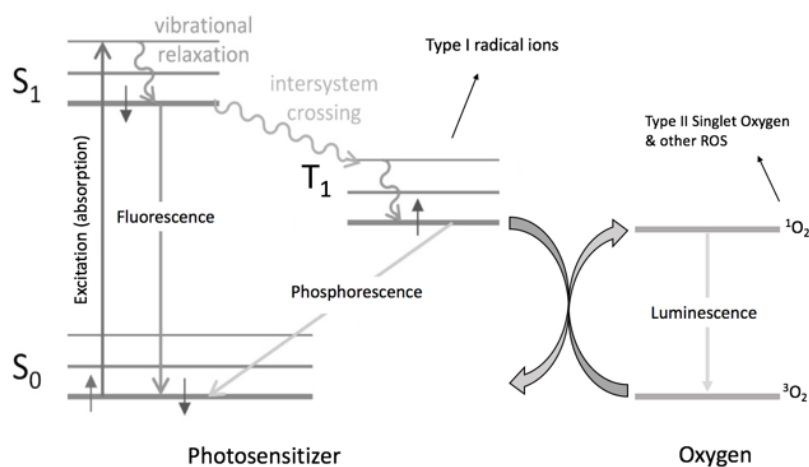


Figure 1.7 Jablonski Diagram. Activating a photosensitizer by light irradiation,

moves it from its relaxed state S_0 to its excited state, S_1 . The unstable S_1 can undertake an intersystem crossing to which an excited triple state T_1 is yielded, which can liberate radicals and radical ions or transfer energy to 3O_2 to emit phosphorescence thus forming singlet oxygen and ROS (Caspar & Meyer, 1983). Modified from Caspar & Meyer, 1983

1.5.1.2 Photo activated chemotherapy

Photo activated chemotherapy (PACT) is a therapeutic way to introduce a biologically active compound (prodrug) secured from the interaction with cells and only activated upon light irradiation (photo activation) in certain tumor tissue. This is opportunistic to the use of inorganic compounds against organic compounds, since they can be irradiated for activation over a broad spectrum (Peters, et al., 2001). PACT is advantageous over PDT since it is not dependent on oxygen and can therefore be applicable to hypoxic tissues. It might also be less photosensitive than PDT because many compounds are positively charged, that are greatly water soluble when allied with counter anions, hence aiming for cellular components instead of collecting in fat tissues. PACT targets cell death primarily by ejecting the ligand, crosslinking to DNA, which can trigger apoptosis, autophagy or necrosis (Lee, Hur, et al., 2006; Mari, et al., 2015). Upon PACT, the dissociated active species can target various cellular molecules and stimulate cell death, making it potentially more advantageous to PDT, which is reliant on ROS production, which forms an evitable immune response that causes painful necrotic incidents. PACT targets distinctive organelles or cytoskeletal constituents which induce cell death due to photo damage. PACT triggers programmed cell death if death receptors were targeted or mitochondrial membranes deciding the extrinsic or intrinsic path of apoptosis respectively. Photo toxicity affects specifically Bcl-2 and Bax (Marques, et al., 2008, Koval, et al., 2010; Kessel, et al., 2012). Necrosis occurs when the photosensitizer (PS) aim for the plasma membrane, allowing the intracellular leaks to the environment. Necrosis can be controlled by the dose of light used and locality of the PS. If high doses are implicated and the PS targets the membrane, necrosis is expected, while low doses contribute to apoptotic events (Marques, et al., 2008; Dahle, Steen & Moan, 1999). Autophagy can also be triggered by PACT, when too much light induced damage ensues, cells can no longer repair themselves (Kessel, et al., 2012, Kew, et al., 2013). A study observed the ability of PACT targeting organelles associated with autophagy, like the lysosome, before the

membrane was lysed, suggesting a therapeutic selectivity to organelles without completely damaging the cell (Berg & Moan, 1994; Zhou, et al., 2020).

Strained polypyridyl ruthenium complexes, are suited for PDT and PACT. They have been shown to be best suited for PACT as they are kinetically inert and easily changed photo chemically absorbing in the visible range. Though most of the polypyridyl Ru(II) complexes are stable upon activation, those with an octahedral geometry will efficiently photo dissociate due to a break in the Ru-N bond and ligand ejection because of a decreased ligand field splitting; a result of excited triple metal-centred state. This is obtained through the excited $^3\text{MLCT}$ state. The ejection of the ligand allows the aquating of the complex and binding DNA, or the dissociation of active bits caged by a metal center, generating its active cytotoxicity (Mansour, et al., 2018, Mehanna, et al., 2019; Campagna, et al., 2007). Khanyzer and team, have been working on compounds of such, where they built $[\text{Ru}(\text{Bpy})_2(\text{Me}_2\text{phen})]^{2+}$ ($\text{Me}_2\text{phen} = 2,9\text{-dimethyl-1,10-phenanthroline}$), Me_2phen being the dissociative ligand upon irradiation forming the aqua complex chemically or intracellularly and the freeing of Me_2phen was successive (Al-Hageh, et al., 2018).

1.5.1.2.i Energy transitions of photo excited compounds

The photo excited state (visible range) of a compound to $^1\text{MLCT}$ (metal- to-ligand charge transfer) state triggers prompt intersystem crossing to a less excited $^3\text{MLCT}$ (triplet) state/ ^3IL (triplet intra-ligand) state. Those of the $^3\text{MLCT}$ form resilient luminescence of the compound most prominently bound cellular component or DNA. Yet, those of the ^3IL (longer lived) state are reliable on the phototoxic effect of the compound. They can have two conformations. One being a non-polar form of ^3IL with a principal $\pi \rightarrow \pi^*$ eccentric which supports the formation of $^1\text{O}_2$ and $^3\text{ILCT}$ (triplet intra-ligand charge transfer) formal which secures electron transfer effect with oxygen or the targeting of biological components and reactions which will trigger ROS (Zerdane, et al., 2017).

1.5.2 Current Ruthenium compounds under study

Several ruthenium complexes have made it to clinical trial, like NAMI-A and KP109 (Meng, et al., 2009). Both these compounds are Ru(III) prodrugs which are activated upon the exposure to hypoxic physiological states of cancerous cells, yet they have

different mechanistic actions against cancer, which both offer selectivity to tumors, accordingly reducing the treatments side effects (Meng, et al., 2009; Alessio & Messori, 2019). NAMI-A is functional against only secondary tumors. Clinical trials have shown its anti-metastatic activity in lung cancers, it only passed phase 1 clinical trials, after which it showed a stark side effect in phase II trials and was not further studied (Rademaker, et al., 2004). KP109 has been shown to be effective on various cell lines. It has also been shown effective on primary tumors. KP109 reached phase II clinical trials but was withdrawn due to its poor efficacy and little solubility options. (Bergamo et al., 2009). A different form of KP109 is currently under study *in vitro*, KP1339, which is the sodium salt form of KP109 (Heffeter, et al., 2013; Wernitznig et al., 2019). Both compounds have proven to be effective against tumors that are cisplatin resistant (Golla, Swagatika, Chauhan & Tomar, 2017)

1.6 Ru(bpy)₂Phen, Ru(bpy)₂BC and Ru(bpy)₂Dpphen: background

Ruthenium holds many imperative properties that errand the synthesis of complexes with hypothetical use in PACT. This study looks into ruthenium bipyridyl complex, which all have octahedral geometry. The unstrained control; [Ru(bpy)₂phen]²⁺ (bpy = 2,2'-bipyridine and phen = 1,10-phenanthroline), and the sterically strained complexes [Ru(bpy)₂dpphen]²⁺ (dpphen = 2,9-diphenyl-1,10-phenanthroline) and [Ru(bpy)₂BC]²⁺ (BC = Bathocuproine = 2,9-Dimethyl-4,7-diphenyl-1,10-phenanthroline) by methyl or phenyl groups on 2,9- positions of the ligand, phenanthroline, respectively. The photochemistry of [Ru(bpy)₂dpphen]PF₆ was previously characterized in acetonitrile and showed the dissociation of the ligand, bpy rather than the strained dpphen ligand, forming [Ru(bpy)(dpphen)(CH₃CN)₂]²⁺ photoproduct (Laemmel, Collin & Sauvage, 1999). The Khnayer team re-established this and showed comparable substitution of the chloride complex in water, generating its aqua complex, at which they investigated its cytotoxic effects on various cancer cell lines for possible use in photo activated chemotherapy, as it was selectively phototoxic upon irradiation showing high phototoxicity index. The ligands were biologically ineffective, reinforcing the idea that the cytotoxic effects were facilitated by the ruthenium aqua complex generated once irradiated (Mansour et al., 2018). Possible reasons to why dpphen ligand did not dissociate is ascribed to two possibilities. Either π - π assembly of the phenyl groups of dpphen (surge activation energy for photo dissociation) or the firmness of the dpphen compared to bpy, which hold a distorted

conformation because of the rotations of the pyridine ring around C2-C2' ring (Laemmel, Collin & Sauvage, 1999, Mansour et al., 2018). $[\text{Ru}(\text{bpy})_2\text{BC}]^{2+}$ holds a ligand providing great steric hindrance (via methyl groups) and lipophilicity (via phenyl groups), characterising its immediate uptake by cancer cells. $[\text{Ru}(\text{bpy})_2\text{BC}]^{2+}$ photo physical behavior and photochemical substitutions have been propertied but its photochemotherapeutic mechanistic potential is to be further studied as Mehanna and colleagues have briefly demonstrated its apoptotic directory (Yoshikawa et al., 2015, Mehanna, et al., 2019).

1.7 DMBA/TPA model induces skin carcinogenesis

The compound, 7,12-Dimethylbenz(a) anthracene (DMBA) is a polycyclic aromatic hydrocarbon which forms radicals as well as oxygenated metabolites, consequently leading to the oxidative stresses generating damages by initiating lipid peroxidation (Rieder, et al., 2000). Previous studies have demonstrated DMBA topical administration, as a skin carcinogenesis initiator and TPA (12-O-tetradecanoylphorbol-13-acetate) as an enhancer acting as a proinflammator increasing cytokines (Kong & Xu, 2018). The tumors are initiated and promoted further due to DNA damages by DMBA, followed by continuous application of a chronic promoter; TPA, which activate protein kinase C (PKC), via two pathways. One includes the phosphorylation of CREB and the other includes the de-phosphorylation of AKT, increasing proliferation (Chung, et al., 2011; Nasti, et al., 2016).

1.8 Aim of the study

The primary aim of this study, is to synthesize and evaluate polypyridyl ruthenium(II) complexes, $[\text{Ru}(\text{bpy})_2\text{phen}]\text{Cl}_2$, $[\text{Ru}(\text{bpy})_2\text{BC}]\text{Cl}_2$, $[\text{Ru}(\text{bpy})_2\text{dpphen}]\text{Cl}_2$, and generate $[\text{Ru}(\text{bpy})(\text{dpphen})\text{H}_2\text{O}]\text{Cl}_2$ (as a chemotherapeutic) from its prodrug to study the photochemical behaviour and *in vitro* PACT potential, as well as the *in vivo* tolerability, toxicity and efficiency of $[\text{Ru}(\text{bpy})_2\text{BC}]\text{Cl}_2$ and $[\text{Ru}(\text{bpy})(\text{dpphen})\text{H}_2\text{O}]\text{Cl}_2$ as chemotherapeutics, due to the promising therapeutic abilities of $[\text{Ru}(\text{bpy})_2\text{dpphen}]\text{Cl}_2$ *in vivo*.

The objectives implemented for the aims of this study:

- Synthesize and purify $[\text{Ru}(\text{bpy})_2\text{phen}]\text{Cl}_2$, $[\text{Ru}(\text{bpy})_2\text{BC}]\text{Cl}_2$,

[Ru(bpy)₂dpphen]Cl₂ prodrugs by UV/vis spectroscopy, proton nuclear magnetic resonance (¹H NMR), and test the irradiated (photo activated) chemical transformations via ¹H NMR and HR-ESI/MS (high resolution electrospray ionization mass spectrometry)

- Generate [Ru(bpy)(dpphen)H₂O]Cl₂ through the photo-induced transformation of its prodrug [Ru(bpy)₂dpphen]Cl₂
- Cytotoxicity assays, of the compounds on human melanoma cell line (A375) in dark and blue LED light irradiated conditions, for *in vivo* comparisons on a skin carcinogenesis model on balb/c mice.
- Study the cytotoxicity of [Ru(bpy)₂BC]Cl₂ on A375 by quantifying cellular uptake via inductively coupled plasma mass spectrometry (ICP/MS), flow cytometry examination for cell death via annexin/7-AAD staining, clarification of the mechanisms mediating cell death via western-blotting, and ruthenium(II) induced DNA damage assessment via the comet assay, as well as the detection of ROS generation.
- Investigating the safety, toxicity and efficacy of the chemotherapeutic effect of [Ru(bpy)₂BC]Cl₂ and [Ru(bpy)(dpphen)H₂O]Cl₂ in a DMBA/TPA skin carcinogenesis model, whilst the photochemotherapeutic effect of the prodrugs is still under the development of an appropriate model to elicit its PACT potential. Biological mechanisms are to then be studied for those mediating tumor cell death via western blotting.

Chapter Two

Materials and Methods

2.1 Chemicals and Reagents

1,10-Phenanthroline, cis-Dichlorobis(2,2'-bipyridine) ruthenium II, 2,9-Dimethyl-4,7-diphenyl-1,10-phenanthroline, Silica Oxide for Column Chromatography; 60Å, Aluminium Oxide for Column Chromatography, Sephadex LH-20, Hexafluorophosphate, Ethylene glycol, PVDF sterile syringe filters (33 mm, 0.45 µm, Millipore® Millex®), PTFE syringe filters, Dowex-22: Chloride coated beads, Dulbecco's Modified Eagle's Medium (DMEM), (with 4.5 g/L glucose/ L-glutamine/ sodium bicarbonate/ sodium pyruvate, liquid, sterile-filtered), Dulbecco's Phosphate Buffered Saline (PBS) 1X (with MgCl₂ and CaCl₂), Trypsin- EDTA with phenol red 1X, Triton X-100, SDS, Glycine, Polyoxyethylkene (20) sorbitan monolaurate (Tween 20), Bovine serum albumin, 2-mercaptoethanol, glycerol, Trypan blue, DMBA (D3254), TPA (P1585), Tris-HCl and NaOH pellets were purchased from Sigma Aldrich, Missouri, USA and used without any further purification. NaCl was purchased from HiMedia, India. APS and Tris Base were purchased from Fisher Scientific, USA. Penicillin-streptomycin solution for cell culture, 10K/10K stock, 10,000 U/mL Pen/Strep was purchased from Gibco, Germany. Fetal bovine serum (heat inactivated, sterile- filtered) was purchased from Lonza, Germany. LC-MS grade water, Acetonitrile, DMSO, Methanol, Ethanol, Nitric Acid and Acetic Acid, from Fisher Chemical. Cell Proliferation Reagent WST-1 from Roche Diagnostics, Indianapolis, IN, USA. Acrylamide/Bis solution, TEMED, Laemli Buffer Goat Anti-Rabbit secondary antibody (HRP Conjugate), and Goat Anti-Mouse secondary antibody (HRP Conjugate) were purchased from Bio-Rad, Hercules, CA, USA. Spectra Multicolour Broad Range Protein Ladder, from ThermoFisher, UK. Anti-beta actin (ab8227), Anti-Cleaved Caspase-3 (ab49822), Anti-cleaved PARP-1 (ab32064), Anti-Bax (ab32503), Anti-cytochrome C (ab133504), Anti-PERK (ab76299), Anti-ERK (ab184699), Anti-AKT (phospho T308) (ab38449), Anti-pan-AKT (ab8805) Anti-Caspase 8 (ab108333) Anti-Bcl-1 (ab207612) antibodies were purchased from Abcam, Cambridge, USA.

Human melanoma cell line (A375), originated from a 54-year-old female via explant

of her tumor. This cell line is greatly used in research for the understanding of metastasis and tumor growth by studying several pathways. (Imanis Life Sciences, n.d.).

2.2 Kits and Solutions

- Guava[®] Nexin Reagent mix-and-read assay kit (Texas, U.S.A)
- DCFDA/H₂DCFDA Cellular ROS Assay Kit (Abcam, Cambridge, U.S.A)
- Comet assay Kit - R&D Systems Trevigen (Maryland, U.S.A.)

The following solutions and buffers were prepared:

RIPA buffer: 50mM Tris-HCl, pH 8.0, 150mM NaCl, 1% Nonidet P-40 (NP-40) or 0.1% Triton X-100 0.5% sodium deoxycholate, 0.1% sodium dodecyl sulphate (SDS), 1mM sodium orthovanadate.

Resolving gel (10%) (for 2 gels): 8 ml type 2 water, 6,6 ml 30 % acrylamide, 5ml buffer pH=8.8, 100μL 20 % SDS, 200μL 10 % APS, 10μL TEMED

Buffer for separating gel (500 mL): 90.75 g Tris base, 500 mL distilled water, pH=6.8

Stacking gel (10%) (for 2 gels): 4.2 ml type 2 water, 1.275 ml 30 % acrylamide, 1.875 ml buffer pH=6.8, 37.5μL 10 % SDS, 75μL 10 % APS, 7.5μL TEMED

Buffer for stacking gel (200 mL): 12 g Tris base, 200 mL distilled water, pH=8.8

Running buffer 5X (TGS)(1L): 15g Tris Base, 72g glycine, 25 mL 20% SDS, pH=8.3

Transfer buffer 5X (500 mL): 7.6g Tris Base, 37.5g glycine, pH=8.5

Transfer buffer 1X (100 mL): 20 mL Transfer buffer 5X, 60 mL distilled water, 20 mL methanol

TBS 10X: 24.2 g Tris Base, 80 g Glycine, pH=7.6

Tris-buffered saline with Tween 20 (TBST): 40 mL TBS 10X, 360 mL distilled water, 0.1% Tween-20

Blocking buffer: 5% bovine serum albumin (BSA) in TBST

Alkaline Unwinding Solution: pH>13: Per 50 ml of Alkaline Solution: 0.4 g NaOH Pellets, 250μl 200mM EDTA (cat # 4250-050-04), 49.75mL dH₂O

Alkaline Electrophoresis Solution, pH >13: 8 g NaOH pellets, 2 ml 500mM EDTA (pH=8), add to 1L dH₂O

Fixation solution (Per sample): 10µl 10X Fixation Additive (cat# 4254-200-05), 10µl glacial acetic acid, 30µl dH₂O, 50µl methanol

Staining solution (Per sample): 35µl dH₂O, 5µl 20X Staining Reagent #1 (cat#4254-200-01), 5µl 20X Staining Reagent #2 (cat#4254-200-02) 5µl 20X Staining Reagent #3 (cat#4254-200-03). 50µl 2X Staining Reagent #4.

2.3 Ruthenium Complexes

2.3.1 Ru(bpy)₂Phen.Cl₂ synthesis

Ru(bpy)₂Cl₂·2H₂O (100 mg, 0.20 mmol) and 1,10-phenanthroline (39.64 mg, 0.22 mmol) were dissolved in a solution of ethanol to MiliQ water (1:1) (8 mL) in a round-bottomed flask (RBF). The solution was degassed under Argon for 1 hour and then refluxed for 3 hours at 90°C. Once complete, the solution was cooled to room temperature, solvents were evaporated under reduced pressure, and the product was dissolved in enough methanol, at which an aqueous solution of saturated KPF₆ was added to allow precipitation at 4°C. The precipitates were then collected via vacuum filtration and washed thoroughly with ice cold H₂O. The product was dried in the vacuum oven overnight. Next, [Ru(bpy)₂phen]PF₆ was purified by column chromatography on sephadex LH20 using methanol as the eluent, and fractions were collected and joined depending on color intensity, as well as the peaks 448nm detection, and dried under reduced pressure. Yield: 121.4 mg; 91%. ¹H NMR and ESI-MS were used to evaluate their photochemistry and purity. To use the product [Ru(bpy)₂phen]PF₆, biologically, conversion of the complex to chloride salt was achieved, using enough dowex beads washed well in MiliQ water and then the drug added to them in a beaker along with enough MiliQ water to cover the dowex beads and left overnight to allow complete conversion. The solution (orange), was then filtered through micropores (PVDF sterile syringe filters, 33 mm, 0.45 µm, Millipore® Millex®).

2.3.2 Ru(bpy)₂BC.Cl₂ synthesis

Ru(bpy)₂Cl₂·2H₂O (100 mg, 0.19 mmol) and BC (74.25 mg, 0.21 mmol, MW 360.45 g/mol) were mixed in 8 mL ethylene glycol in a RBF and degassed for 1 hour under argon. Next, the solution was refluxed for 6h at 200 °C for 6

hours in the dark (to avoid photo reactivity resulting in photoproducts). The final product was then cooled to room temperature and filtered across micropores (PTFE syringe filters) into a beaker at which it was precipitated by adding a saturated aqueous solution of KPF_6 dropwise. The precipitate was then vacuum filtrated, and moved to the vacuum oven under which it was dried overnight. The precipitate was then dissolved in 1mL methanol, and purified by column chromatography on sephadex LH20 using methanol as the eluent. The purified fractions were then joined intensity color wise, additionally according to UV/vis 454 nm peak detection and dried of methanol under reduced pressure. Yield: 179.7 mg, 89%. To test for the purity and photochemistry of our products, deuterated acetonitrile (500 μL) was used to dissolve 5mg of the product and moved to NMR tubes to be tested. ^1H NMR and ESI-MS were used to evaluate their photochemistry and purity.

To use the product $[\text{Ru}(\text{bpy})_2\text{BC}](\text{PF}_6)_2$, biologically, conversion of the complex to chloride salt was achieved, using enough dowex beads washed well in MiliQ water and then, the drug added to them in a beaker along with enough MiliQ water to cover the dowex beads and left overnight to allow complete counter-ion exchange. The solution (orange), was then filtered through micropores (PVDF sterile syringe filters, 33 mm, 0.45 μm , Millipore® Millex®).

2.3.3 $\text{Ru}(\text{bpy})_2\text{Dpphen}.\text{Cl}_2$ synthesis

2,9-diphenyl-1,10-phenanthroline (Dpphen) was synthesized according to a published procedure (Dietrick-Buchecker, et al. 1982). $\text{Ru}(\text{bpy})_2 \text{Cl}_2 \cdot 2\text{H}_2\text{O}$ (100 mg, 0.2 mmol) and dpphen (69 mg, 0.19 mmol) were mixed with ethylene glycol (8 mL) in a RBF. The solution was degassed for 1 h under argon pressure and then refluxed for 6 hours. After cooling at room temperature, the product was filtered across micropores (PTFE syringe filters) into a beaker at which it was precipitated by adding a saturated aqueous solution of KPF_6 , then vacuum filtrated and washed thoroughly with ice cold H_2O . The product was dried in the vacuum oven overnight. The precipitate was then purified by column chromatography on silica gel and eluted with 92 % acetonitrile, 7 % H_2O and 1 % KNO_3 . Fractions were tested via UV/vis for peak 448nm and combined accordingly noting colour intensity and evaporated under reduced pressure. The solid was re-dissolved in a saturated aqueous solution of KPF_6

to rid NO_3 , then vacuum filtrated and washed thoroughly with ice cold H_2O and dried in the vacuum oven. Yield: 153.5 mg, 72 %. To test for the purity and photochemistry of our products, deuterated acetonitrile (500uL) was used to dissolve 5mg of the product and moved to NMR tubes. ^1H NMR and ESI-MS were used to evaluate their photochemistry and purity. For biological testing the hexafluorophosphate salt was converted to chloride salt using Dowex chloride ion exchange resins to promote the solubility of the complex in water. Using enough dowex beads washed well in MiliQ water and then the drug added to them in a beaker along with enough MiliQ water to cover the dowex beads and left overnight to allow complete conversion. The solution (orange), was then filtered through micropores (PVDF sterile syringe filters, 33 mm, 0.45 μm , Millipore® Millex®).

2.3.3.1 Agua complex

The precursor was exposed to Blue LED light (100 mW/cm^2 , I= 99) for 3 hours in MiliQ water, and directly injected into the ESI-MS to insure the maximal formation of the aqua complex photoproduct. To purify the photoproduct, column chromatography on two sequential columns (40/60) of alumina (20 cm) were performed using DCM: MeOH (99.7: 0.3) to elute the compound required in fractions. Fractions were tested via UV/vis for peak shift from that of the precursors (448 nm) and combined accordingly noting colour intensity and evaporated under reduced pressure. To test for the purity and photochemistry of our products, the compound was dried of eluents and 5mg were weighed and dissolved in deuterated water (500uL) and moved to NMR tubes to be tested on ^1H NMR. To test via ESI-MS, a concentration of 20 μM of the product was prepared in MeOH and directly injected into the ESI-MS.

For biological testing the purified fractions, which contain the photoproduct were dried of DCM and MeOH and dissolved in water at which their concentration was detected using UV-vis to prepare a stock. The stock solution (yellow), was then filtered through micropores (PVDF sterile syringe filters, 33 mm, 0.45 μm , Millipore® Millex®).

2.4 Testing the lipophilicity of $[\text{Ru}(\text{bpy})_2\text{phen}]\text{Cl}_2$, $[\text{Ru}(\text{bpy})_2\text{BC}]\text{Cl}_2$, $[\text{Ru}(\text{bpy})_2\text{dpphen}]\text{Cl}_2$ and $[\text{Ru}(\text{bpy})(\text{dpphen})\text{H}_2\text{O}]\text{Cl}_2$

The lipophilicity of [Ru(bpy)₂phen]Cl₂, [Ru(bpy)₂BC]Cl₂, [Ru(bpy)₂dpphen]Cl₂ and [Ru(bpy)(dpphen)H₂O]Cl₂ was measured by calculating the partition coefficient between water and octanol phases or log*P*, using a modified method (Hageh et al., 2018). The compound in study was weighed (0.5-2 mg), and re-suspended in water saturated with octanol (1 mL). The mixture was placed in a shaker at 230 g for 1 h at room temperature. Complete separation of the aqueous and organic phases was achieved by centrifugation at 1,670 g for 10 min. Using a glass syringe, the lower aqueous phase was aspirated while degassing through the organic (octanol) phase. UV-vis absorption spectra were then acquired for both phases and log*P* values were computed using the formula below:

$$\log P = \log \left(\frac{C_{\text{octanol}}}{C_{\text{water}}} \right) \text{ where } C \text{ is the concentration derived from photometric data.}$$

2.5 Cell line

Human melanoma; A375 cell line was purchased from ATCC (www.atcc.org).

2.6 Cellular uptake of Ru(bpy)₂BC.Cl₂ precursor vs. photoproduct via ICP/MS

A final concentration of 10⁵ human melanoma cells (A375)/mL were seeded in 6-well plates, and adhered overnight at 37°C in an environment of 5% CO₂. The cells were then treated with a final concentration of 3 μM of either [Ru(bpy)₂BC]Cl₂ as a precursor or its photoproduct, which was generated via a blue LED light activator setup for 3 hours and detected via UV-vis (Figure 3.18). After 0, 1, 3, 6, 12 or 24 hours, the media was removed, and the cells were washed three times with cold PBS and left dry. The following day, 400 μL of 68% HNO₃ was added to each well, for an hour and a half, for complete digestion. The digests were moved to 15 mL conical tubes, to which 7 mL milliQ water was then added, followed by the addition of 7 mL of 10 ppb internal standard of indium, which resulted in a final concentration of 2% HNO₃. The cellular uptake of Ru(II) was quantified via ICP-MS based on external standards. The results are averages of three different experiments (± SEM), optimized following the calibration curve and expressed as μM/cell.

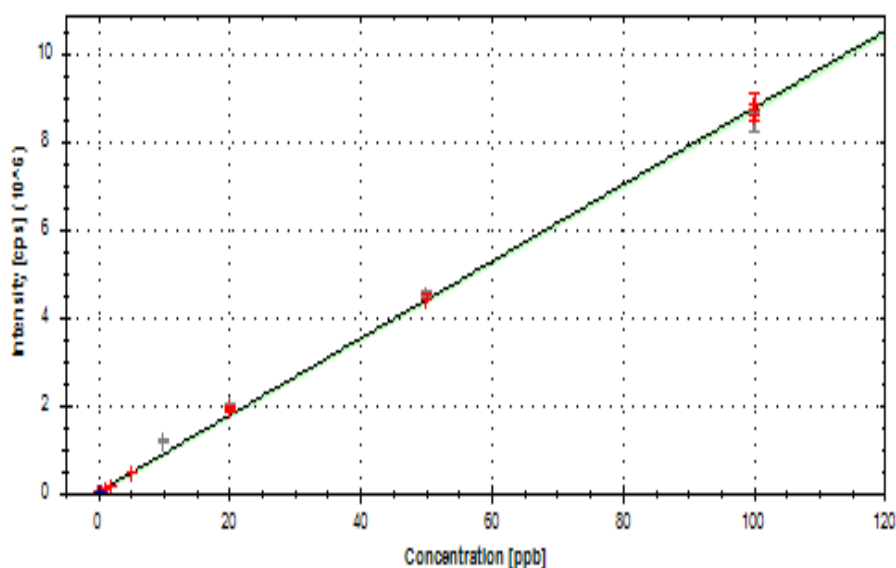


Figure 2.1. Calibration curve generated by plotting the peak areas (measured by the ICP-MS) against known concentrations (102Ru(STD)).

This curve was used to quantify the cellular uptake of both $[\text{Ru}(\text{bpy})_2\text{BC}]\text{Cl}_2$ precursor and its photoproduct; $y = 8.7 \times 10^4 x + 2.1 \times 10^4$ and $R^2 = 0.99938$

Table 2.1. Conditions and parameters selected on the ICP-MS machine.

Parameter	Value
Plasma RF power	1550W
Nebulizer gas flow rate	1.0 L.min ⁻¹
Auxiliary gas flow rate	0.8 L.min ⁻¹
Collision gas flow rate (He)	4.7 L.min ⁻¹
KED voltage	3 V
Extraction lens	-250 V
Isotope monitored	¹⁰² Ru
Dwell times	10ms

RF, radio frequency; He, helium; KED, kinetic energy discrimination

2.7 Mode of uptake of $[\text{Ru}(\text{bpy})_2\text{BC}]\text{Cl}_2$ precursor

A375 (1×10^5 cells/mL) were seeded in 6-well plates (2 ml/well in DMEM) and incubated overnight at 37°C and 5% CO₂. Cells were then treated with 3 μM of $[\text{Ru}(\text{bpy})_2\text{BC}]\text{Cl}_2$ under various conditions, to determine the mechanism of uptake. The incubation periods were determined, based on results from exploratory experiments.

For temperature uptake, cells were cultured in DMEM media and incubated for 2

hours at 4 and 37°C with [Ru(bpy)₂BC]Cl₂ (3 μM).

In order to inhibit transferrin receptor mediated uptake, cells were pre-treated with 1 μg/ml of anti-transferrin antibody (Abcam, Cambridge, USA) for 2 hours, followed by an additional 2-hour incubation at 37 °C and 5% CO₂ with 3 μM of [Ru(bpy)₂BC]Cl₂ in the presence of the antibody.

The medium was then removed precisely as mentioned previously in section 2.6 and analysed via ICP-MS. The results are averages of three different experiments (± SEM), optimized following the calibration curve (Figure. X above.) and expressed as μM/cell.

2.8 Cytotoxicity Assay

2.8.1 Cytotoxicity of [Ru(bpy)₂BC]Cl₂ (dark vs. light), Ligands and Cisplatin

A375 cells were cultured in Dulbecco's Modified Eagle's Medium (DMEM) containing 10% FBS and 1% Penicillin/Streptomycin and incubated in a humidified chamber at 37 °C and 5% CO₂. Cells (10⁴ cells/mL) were then seeded in 96 well culture flat bottom plates. The complexes, whether in the dark or light activated, as well as their ligands and cisplatin were tested for their cytotoxicity, after achieving a concentration of 120 μM in the first well, then a 3-fold serial dilution, pipetted along 50uL from each well to the other, resulting in 8 different final concentrations of the drug (range of 120 μM to 0.006 μM). One of the complex treated plates was exposed, 12 hours after drug addition, to blue LED light (I=50; 100 mW/cm²), for 30 minutes, while a copy of this plate was kept in dark conditions. After 72 hours, the medium was removed and 100 uL DMEM, followed by 10 uL of WST-1 (Roche Diagnostics, Indianapolis, IN, USA), a cell proliferation reagent were added to each well. After an hour, the absorbance was measured at 450nm using the VarioskanTM LUX Multimode microplate reader (ThermoFisher). Three independent experiments were implemented, and each sample was triplicated.

2.8.2 Cytotoxicity of [Ru(bpy)₂BC]Cl₂ activated intracellularly in a [Ru(bpy)₂BC]Cl₂ free medium

Same procedure as 2.8.1 applies, yet the supernatant was removed and 100 uL of DMEM, was added prior to activation, ensuring only the compound taken up by the

cell is activated and the only effective.

2.8.3 Cytotoxicity of [Ru(bpy)₂BC]Cl₂ photoproducts on seeded A375

Same procedure as 2.8.1 applies, yet the 3-fold serial dilution of only the drug was performed on a separate 96-well plate, at which it was activated for 30 minutes and then each well filled drug was transferred to its consecutive position on the 96-well plate, which contained the seeded A375 cells, and incubated for 72 hours, till analysis.

2.9 ROS detection

To investigate, for the presence of reactive oxygen species in treated cells, DCFDA/H₂DCFDA-cellular ROS Assay Kit (Abcam, Cambridge, USA) was used. 25000 cells/mL of A375 cells in DMEM were seeded in two 96-well plate (dark vs light irradiated plate). Cells were treated with IC 50 drug concentration and after 12 hours, were washed with 1X kit buffer, and stained with DCFDA (25 μM) for 45 minutes, then re-washed with 1X kit buffer, after which Phenol red free media was added. One of the plates was irradiated by blue LED light for 15 minutes, whilst the other was in the dark. The plates were then immediately scanned to measure fluorescence, using the Varioskan™ LUX Multimode microplate reader (Thermo Fisher) at an excitation/emission of 485/535 nm. To generate the positive control (20 μM TBHP), cells were washed with 1X kit buffer, and stained with DCFDA (25 μM) for 45 minutes, then removed and TBHP was added in phenol red free media, and incubated for 2 hours and scanned as mentioned above.

2.10 Western blot

A375 cells (10⁵ cells/mL) were plated in 6-well plates and treated with double the IC50 concentration of [Ru(bpy)₂BC]Cl₂ after which one of the plates was irradiated by blue light for 30 minutes, 12 hours after drug addition, and the other kept in the dark. After certain time points (24, 48 and 72 hours), plates were placed on ice and the supernatants were moved into labelled conical tubes, at which they were centrifuged at 1500 rpm for 5 minutes at 4 °C. Only pellets were kept in each tube. Meanwhile, 200 uL of lysis RIPA buffer were added to each well, and cells were scrapped, and moved on top of their corresponding pellet, then put on the shaker for 10 minutes at 4

°C. Samples were, centrifuged at 13000 rpm for 15 minutes at 4 °C, and the supernatants (containing the proteins) were transferred to Eppendorf tubes. Using the Bio-Rad protein assay (Bio-Rad, Hercules, CA, USA), 2 μ L each protein lysate was mixed with 3 μ L RIPA buffer and 200 μ L of diluted Bradford reagent. The mixture of each was moved to a 96-well plate to read its absorbance at 595nm using the Varioskan™ LUX Multimode microplate reader (ThermoFisher). After generating a standard curve using BSA and RIPA buffer, the absorbance results obtained were used to prepare a concentration of 20 μ g of each protein condition in RIPA buffer and 2x Laemli Buffer containing 9% β -mercaptoethanol, to insure equal loading. The samples were then heated at 100°C for 5 minutes.

The resolving and stacking gels were prepared in between a thick and short glass plate clamped to a 1.5mm spacer plate on a casting frame. Once dry the gels were moved to the SDS-page cassettes, and running buffer (TGS1X) was added. Combs were then carefully removed. 20 μ L/well of each protein (20 μ g) were loaded and 5 μ L of ladder was added to the first well. Gel Electrophoresis was set to run at 80V for 30 minutes and then at 120V for 90 minutes. Meanwhile, PVDF membranes (6.5×8.5cm) and filter pads (7×9cm) were cut. PVDF membranes were activated in methanol for 1 minute, then washed in distilled water and moved to transfer buffer till use. Filter pads were soaked in the transfer buffer along with the gels post-run for 15 minutes. A sandwich of pad-membrane-gel-pad was prepared cautiously to prevent bubbles and placed in a cassette in a Semi-dry blotter (Bio-Rad, Hercules, CA, USA) set at 1A for 30 minutes to transfer proteins from the gels to PVDF membranes (Pall Corporation, Ann Arbor, USA). Once complete, membranes were removed and blocked in blocking buffer (1× TBS, 0.1% Tween-20, 5% BSA) for 45 minutes. They were then probed overnight with primary antibodies against several apoptotic and anti-apoptotic protein markers at 4°C overnight. The primary antibody was then removed and membranes were washed thrice with TBS-T for 10 minutes. The membrane was then treated with either rabbit or mouse horseradish peroxidase (HRP)-coupled secondary antibodies (Abcam, Cambridge, UK) for 1 hour and 30 minutes, then washed away with TBS-T; thrice for 10 minutes.

Protein detection was then performed using the chemiluminescence ECL kit (Bio-Rad, Hercules, CA, USA). A 1:1 mix of Clarity Western Peroxide Reagent and Clarity Western Luminol/Enhancer Reagent were added to cover the membranes in the dark for 2 minutes. Blot images were then obtained using the ChemiDoc imaging

instrument (Bio-Rad, Hercules, CA, USA). Lastly, band intensities were quantified and reported as a ratio of protein of interest to actin using the Image Lab software (Bio-Rad, Hercules, CA, USA).

2.11 Comet assay

DNA damage was evaluated using the Comet Assay kit (4251-050-k) purchased from R&D systems (Minneapolis, USA). A375 human melanoma cells were seeded in 6well plates at a concentration of 10^5 cells/ml and either untreated or treated with IC₅₀ drug concentration for 12 hours, after which, one of the plates was irradiated with blue light, while the other was kept in the dark. Incubation of the cells for 24, 48, and 72 hours at 37°C and 5% CO₂ was performed. KMnO₄ and PBS were respectively used to generate positive and negative controls for 25 minutes. Subsequently, cells in the supernatant were collected, the well were washed with PBS and trypsinized for 5 minutes. The collected cells were centrifuged for 10 minutes at 3000 rpm and the pellet was washed with cold PBS. 10^5 cells/ml of the pellet were combined with low melting agarose (LMA) at 37°C at a ratio of 1:10, spread on the total surface of the comet slides and left in the dark at 4°C for 30 minutes for the agarose to solidify. The slides were then immersed in Comet Assay lysis solution overnight at 4°C. Lysis solution was then tipped off the next day, and the slides were flooded with an alkaline unwinding solution (200mM EDTA, 1mM NaOH) for 30 minutes at room temperature in the dark. The slides were then washed in alkaline electrophoresis buffer solution buffer (1X TBE, pH 13) for 5 minutes and then transferred to horizontal electrophoresis apparatus, at which they were placed at an equal distance from the electrodes. Slides immersed in Electrophoresis buffer (1X TBE, pH 13) were subjected to electrophoresis, run at 20 V for 25 minutes. Once completed, slides were tapped off from excess TBE, washed twice with deionized water for 5 minutes then with 70% ethanol for another 5 minutes and left to air-dry. Next, samples were fixed using a fixation solution for 20 minutes at room temperature, immersed in deionized water for 30 minutes and then stained with staining solution for 5-20 minutes at room temperature, until the comet tails acquired the desired intensity under the microscope (10X objective). When observed, the reaction was stopped by adding 5% acetic acid (100uL) for 15 minutes followed by a deionized water wash; slides were then air-dried and stored in the dark until set for analysis. A total of 50 aimlessly selected cells were

assessed and scored for tail intensity using the Comet Analysis Software Package (CASP). DNA damage is imitated by increased tail moment index (TMI), which is the tail DNA content of cells multiplied by the tail length and divided by 1000 (Lu, et al., 2017).

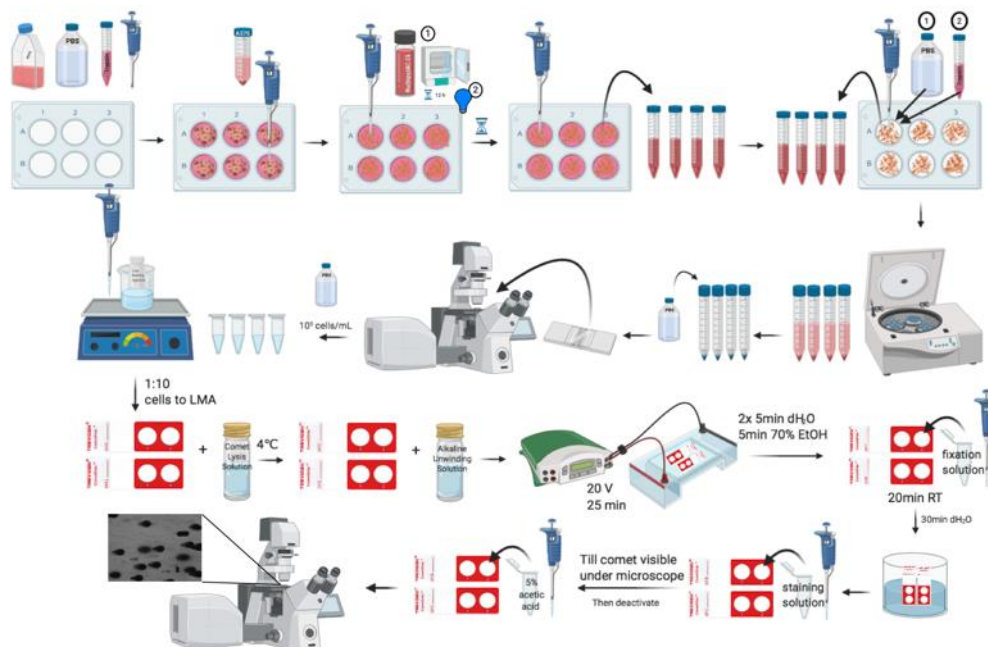


Figure 2.2. Comet Assay demonstration

2.12 Cell death analysis

Annexin V-Phycoerythrin (Annexin V-PE) and 7-AAD (7-amino-actinomycin D) staining (Guava Nexin Reagent Kit, Luminex, Austin, Texas, U.S.A), were used to analyse cell death and the path of death it takes 24, 48 and 72 hours post-treatment. A375 cells were seeded in a 6-well plate (10^5 cells/mL) and treated with IC50 light concentration of $[\text{Ru}(\text{bpy})_2\text{BC}]\text{Cl}_2$. After 12 hours, the plate was irradiated with blue LED light ($I=50, 100 \text{ mW/cm}^2$) and incubated at 37°C and $5\% \text{ CO}_2$. After 24, 48 and 72 hours, supernatant/medium was moved from each well into respectively labelled conical tubes onto ice. The cells were trypsinized with $200 \mu\text{L}$ trypsin /well, and the detached cells were moved on top of the previously collected media respectively /labelled conical tube. Then, $10\mu\text{L}$ of this mix was added to $10\mu\text{L}$ Trypan blue to count the cells under the inverted microscope (Nikon Eclipse TE300). A final concentration of 500 cells/ μL was obtained and adjusted per condition into Eppendorf tubes on which, centrifugation at 1500 rpm for 5 minutes at 4°C , was performed. The supernatant was dissolved, and the pellet was suspended in $100 \mu\text{L}$ Guava Nexin

Reagent buffer, provided by the kit. Each sample was pipetted onto a 96-well plate, and incubated in the dark for 10 minutes. Cells were then analyzed using the Guava® easyCyte 8HT Benchtop Flow Cytometer (Millipore, Luminex, USA). AnnexinV/7-AAD data was measured on FL1-H versus FL2-H scatter plot.

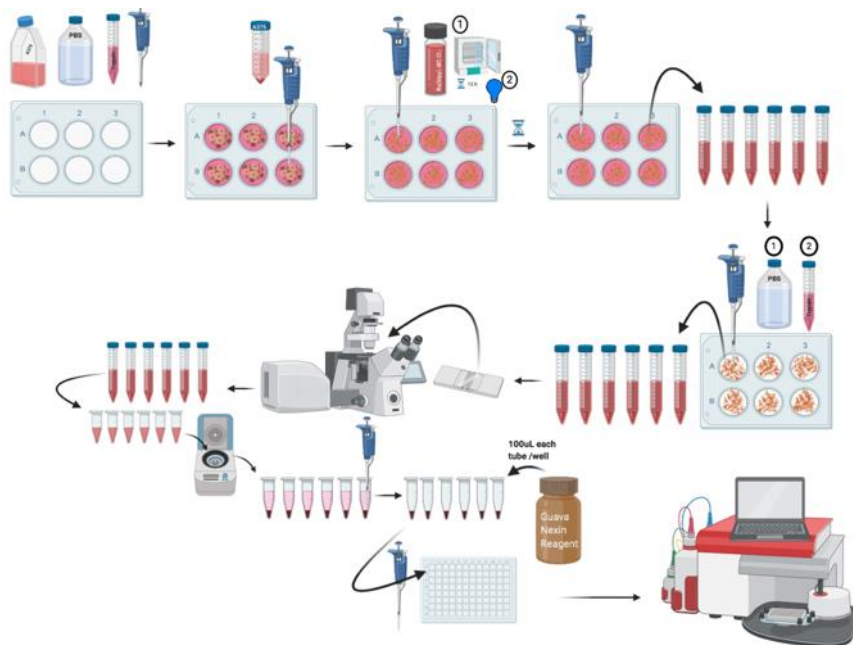


Figure 2.3. Cell death analysis demonstration

2.13 *In vivo* methods

2.13.1 Estimation of the LD

Using a modified acute toxic class (ATC) method (Erhirhie, et al., 2018), one BALB/c female mouse of 6-weeks-old, was administered one dose of $[\text{Ru}(\text{bpy})_2\text{BC}]\text{Cl}_2$ IP, sequentially based on the record of death, recording it as the lethal dose (LD). Knowing the LD; another mouse was used, to test another dose by reducing the dose previously reported as LD, if death was not observed the dose would be increased subsequently on another, leading to the determination of our lethal dose range.

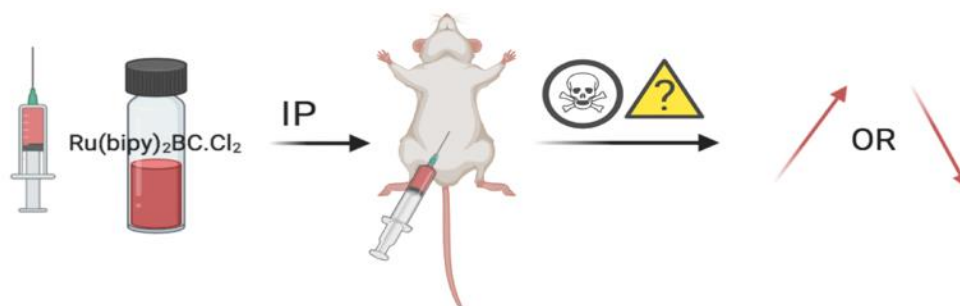


Figure 2.4. LD demonstration

2.13.2 Determination of Maximum Tolerated Dose

Once LD was detected, MTD (Maximum Tolerated Dose), (Wu, et al., 2016) was tested over a 28-day period of weekly IP injections of $[\text{Ru}(\text{bpy})_2\text{BC}]\text{Cl}_2$, which accordingly will decide the dose used for treatment, to test its efficacy. Mice (four groups of three) were monitored over the 28 days for changes in body weight, physical or behavioral signs of discomfort and contra indication effects of the treatment. Groups are demonstrated in figure 2.5. A group receiving weekly injections of saline was added for comparison.

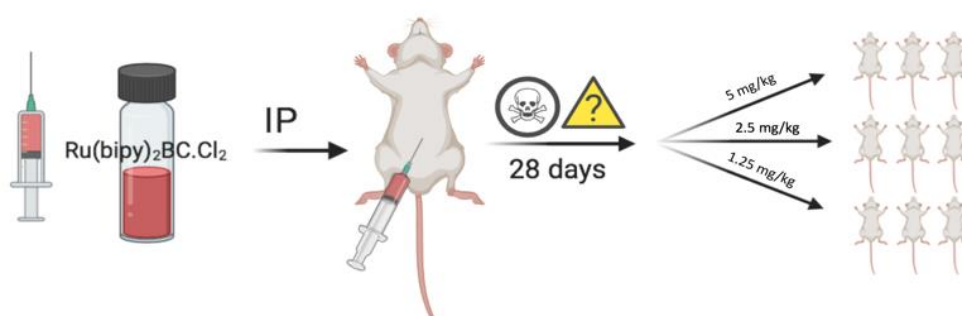


Figure 2.5. MTD demonstration

2.13.3 Induction of skin carcinogenesis

A BALB/c mouse, skin cancer model was induced by multi-stage DMBA/TPA chemical carcinogenesis following a modified protocol (Kwitniewski, et al., 2009). Briefly, 6-week-old mice were treated with a topical application of DMBA (200 nmol in 0.2 mL acetone) on their shaved dorsal skin. One week later, 8 nmol of TPA (in 0.2 mL acetone) were applied twice a week on the same area for a total of 6 weeks. The application was interrupted for a week, after which, another DMBA application was performed as above. Following a one-week lapse, TPA-treatment was resumed till the end of the study.

2.13.4 Experimental plan

After 12 weeks (2 rounds of DMBA and continual TPA), multiple tumours had developed and mice were divided homogeneously into groups, at which treatment was started on week 13.

2.14.4.1 Doses and group divisions

Animals were subdivided as shown in Table 2.2. After 12 hours of fasting, all animals were weighed and treated twice a week, unless specified otherwise.

Table 2.2 Treatment conditions used for the evaluation of [Ru(bpy)₂BC]Cl₂ as PACT and [Ru(bpy)(dpphen)H₂O]Cl₂ as a chemotherapeutic in DMBA/TPA-induced skin tumours.

Groups (G)	Treatment	Dose	Route	Irradiation	Frequency
G0	Saline	Physiological	IP	No	BIW
G1	[Ru(bpy) ₂ BC]Cl ₂	1mg/kg	IP	No	BIW
G2	[Ru(bpy) ₂ BC]Cl ₂	1mg/kg	IP	Yes	BIW
G3	[Ru(bpy)(dpphen)H ₂ O]]Cl ₂	2.5 mg/kg	ST	No	BIW
G4	Cisplatin	2.5 mg/kg	IP	No	QW

IP, intraperitoneal; ST, subtumoral; QW, once per week; BIW, twice a week.

2.13.4.2 Blue LED light irradiation

LC-MS/MS preliminary studies have shown that the drug used, must be activated for a minimum of 90 minutes for penetration *in vivo*, to achieve the desired concentration of the active molecule. Groups requiring blue LED light (LED zoomable flashlight operated in blue range at maximal intensity; 1500 Lumens) (ROKKES, China) (G2) irradiation were irradiated for 90 minutes using a restrainer. Restraining is necessary to guarantee photo activation of the drug selectively in the dorsal tumors, which will be exposed to a focused type of light. To minimize the distress due to restraining, the animals were exposed intermittently (45 minutes exposure within the restrainer followed by 10 minutes resting period and another 45 minutes in the restrainer). Additionally, to escape overheating caused by light exposure, the back of

the mice was cooled with water running (to filter out high wavelength, mainly infrared (IR) (Hoffman, 2007)) through a plexiglass container built to separate the light source from the skin. Skin temperature was also measured using a laser thermometer.

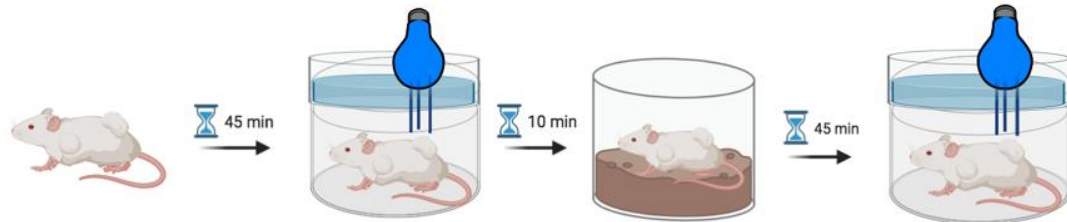


Figure 2.6. Blue LED light irradiation demonstration

2.13.4.3 Efficacy

Tumor volumes were measured weekly using a Vernier calliper and the treatment was conducted for a period of 4 weeks. To end the study, mice were euthanized and tissues were extracted for histopathology and mechanistic studies (studying changes in protein expression), as well as blood for serum biochemistry tests.

2.14 Statistical analysis

Data and results were reported as Mean \pm SEM from three independent trials. Comparison of each group with the control was determined via one way ANOVA, and was considered statistically significant indicated by * $p < 0.05$, ** $p < 0.01$, $p < 0.001$ or **** $p < 0.000$. GraphPad prism 8 was used to evaluate statistics.

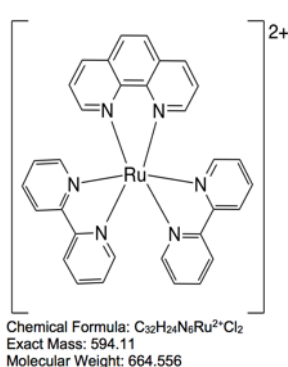
Chapter Three

Results

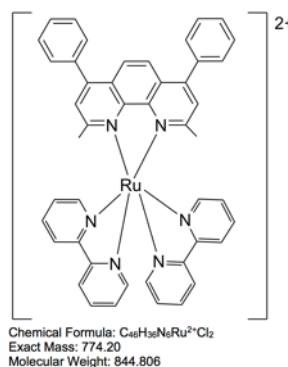
3.1 Compound Synthesized

The chemical structure of the ruthenium based complexes, $[\text{Ru}(\text{bpy})_2\text{phen}]\text{Cl}_2$, $[\text{Ru}(\text{bpy})_2\text{BC}]\text{Cl}_2$, $[\text{Ru}(\text{bpy})_2\text{dpphen}]\text{Cl}_2$, $[\text{Ru}(\text{bpy})(\text{dpphen})\text{CH}_3\text{OH}]\text{Cl}_2$, $[\text{Ru}(\text{bpy})(\text{dpphen})\text{H}_2\text{O}]\text{Cl}_2$, are represented below.

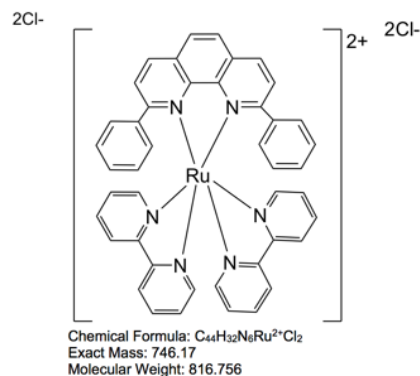
(A) $[\text{Ru}(\text{bpy})_2\text{phen}]\text{Cl}_2$



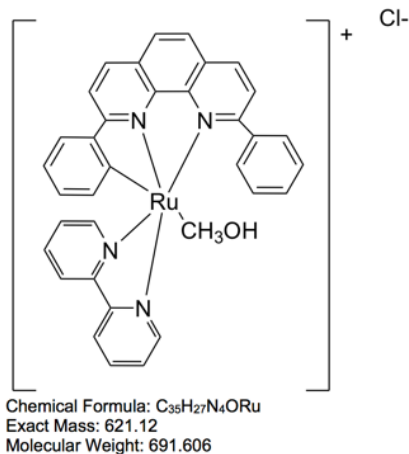
(B) $[\text{Ru}(\text{bpy})_2\text{BC}]\text{Cl}_2$



(C) $[\text{Ru}(\text{bpy})_2\text{dpphen}]\text{Cl}_2$



(D) $[\text{Ru}(\text{bpy})(\text{dpphen})\text{CH}_3\text{OH}]\text{Cl}_2$



(E) $[\text{Ru}(\text{bpy})(\text{dpphen})\text{H}_2\text{O}]\text{Cl}_2$

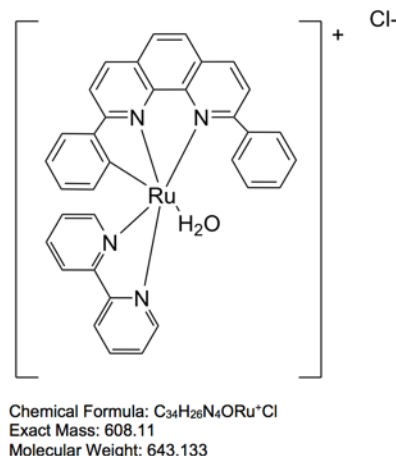


Figure 3.1: Chemical structure, formula and mass of the compounds synthesized
(A) $[\text{Ru}(\text{bpy})_2\text{phen}]\text{Cl}_2$ (B) $[\text{Ru}(\text{bpy})_2\text{BC}]\text{Cl}_2$ (C) $[\text{Ru}(\text{bpy})_2\text{dpphen}]\text{Cl}_2$ (D) $[\text{Ru}(\text{bpy})(\text{dpphen})\text{CH}_3\text{OH}]\text{Cl}_2$ (E) $[\text{Ru}(\text{bpy})(\text{dpphen})\text{H}_2\text{O}]\text{Cl}_2$

3.1.1. Ru(bpy)₂dpphen[H₂O].Cl₂

3.1.1.1 Generation through blue LED light irradiation

The system built for photoactivation of [Ru(bpy)₂dpphen]Cl is demonstrated below in figure 3.4

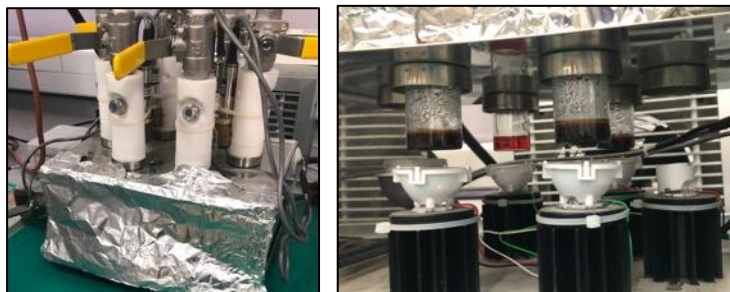


Figure 3.4. Blue LED light setup

3.1.1.1.i Absorption Spectra of [Ru(bpy)₂dpphen]Cl₂ as a function of time

Figure 3.5 demonstrates the prodrug is stable at room temperature as absorbance at 455 nm remained constant. The shifts observed in the absorption spectra of figure 3.6 and 3.7 denote the generation of [Ru(bpy)₂dpphen]Cl₂ photoproducts as a function of time indicated with arrows.

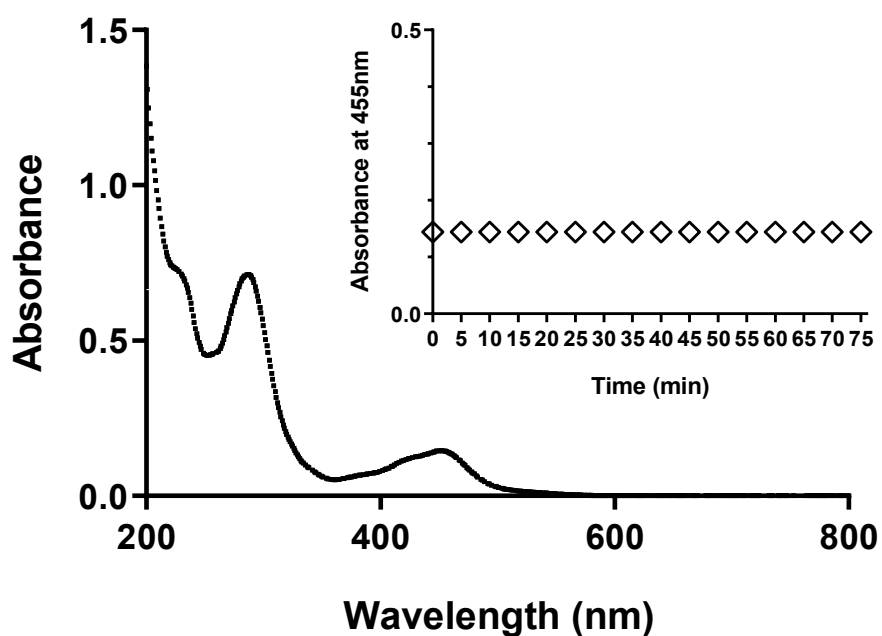


Figure 3.5. Absorption spectrum of [Ru(bpy)₂dpphen]Cl₂ in water as a function of time in the dark.

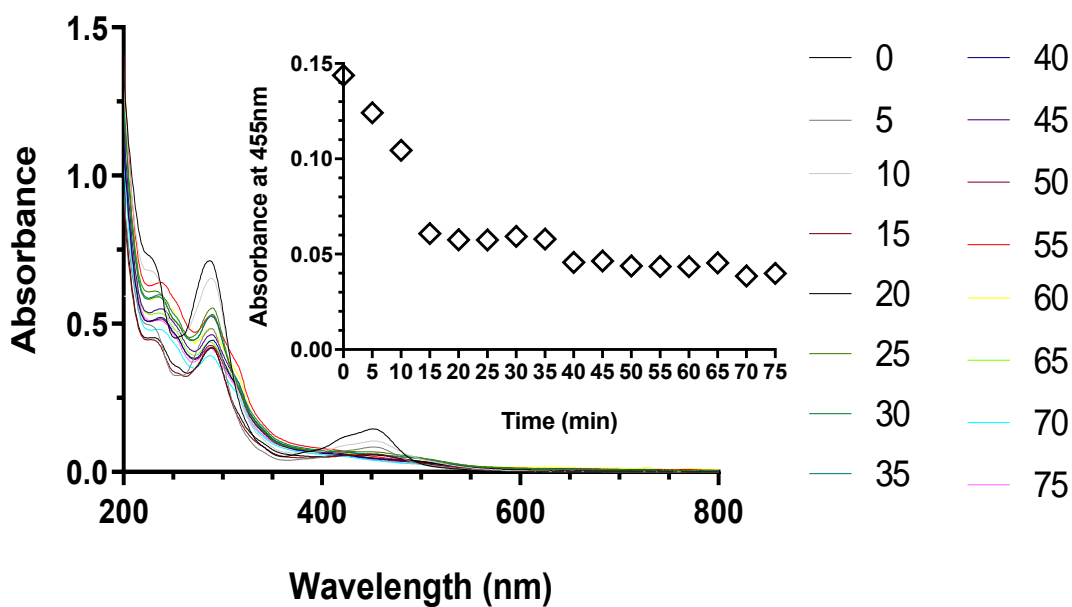


Figure 3.6. Absorption spectrum of [Ru(bpy)₂dpphen]Cl₂ in water as a function of time upon exposure to blue light (100 mWcm², 448nm)

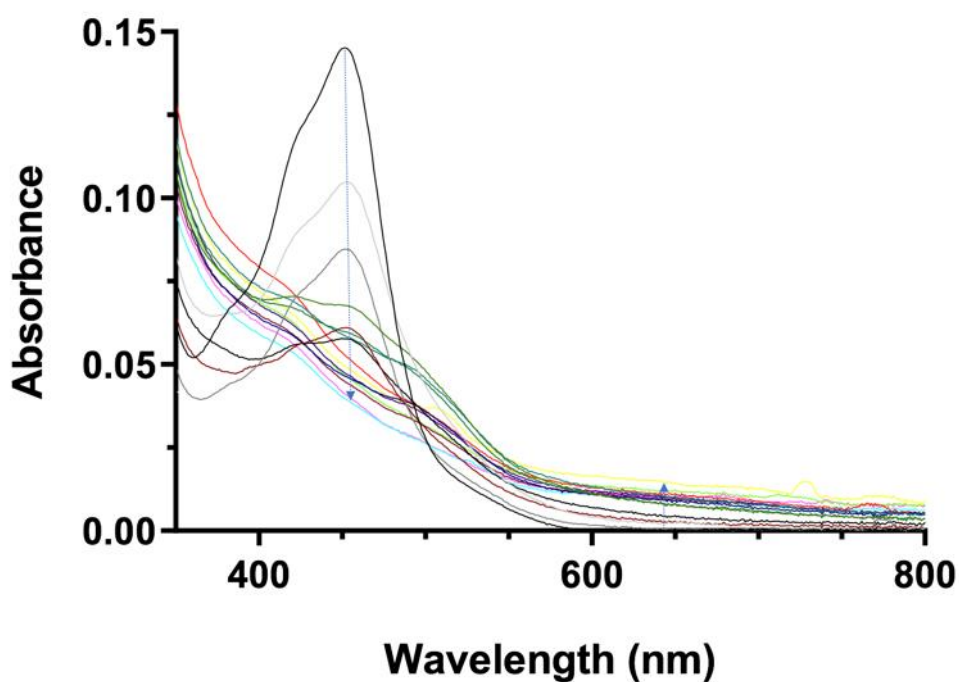


Figure 3.7. Closer picture at the absorption spectrum of [Ru(bpy)₂dpphen]Cl₂ in water as a function of time upon exposure to blue light (100 mWcm², 448nm). Arrows indicate the spectral changes trend throughout light exposure.

3.1.1.1.ii Photolysis products

Peaks assigned below in figure 3.8 (373.13), indicates $[\text{Ru}(\text{bpy})_2\text{dpphen}]\text{Cl}_2$ prior to irradiation. The aquated photoproduct formed upon irradiation, was confirmed by ESI/MS. At time 15, 30, 45 and 60 min, the aquated photoproduct $[\text{Ru}(\text{bpy})(\text{dpphen})\text{H}_2\text{O}]\text{Cl}_2$ was detected by peak 606. Peak 157 was the dissociating ligand. The precursors relative abundance decreased upon irradiation while that of the ligand increased. Accordingly, time of irradiation was depicted to attain maximal photoactivation of the prodrug $[\text{Ru}(\text{bpy})_2\text{dpphen}]\text{Cl}_2$.

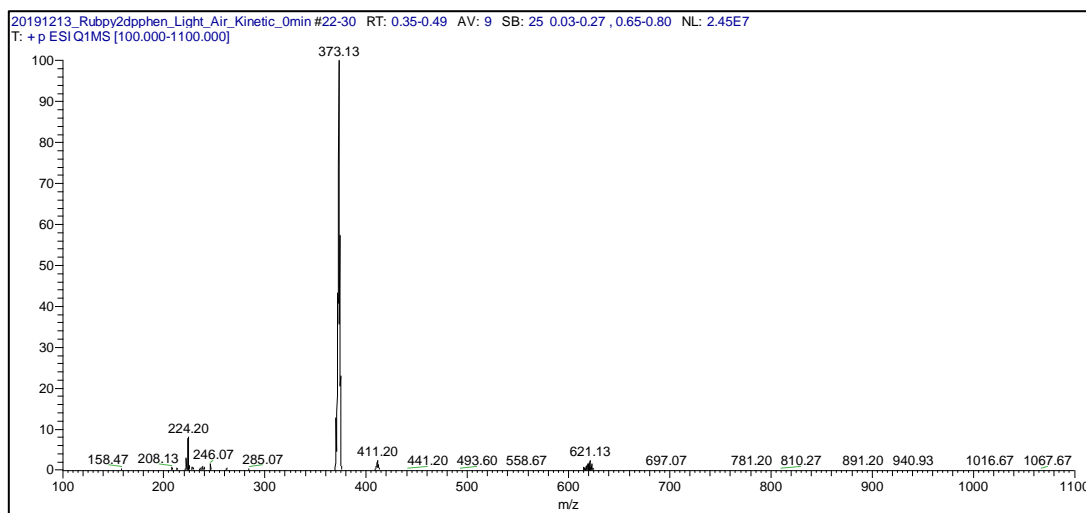
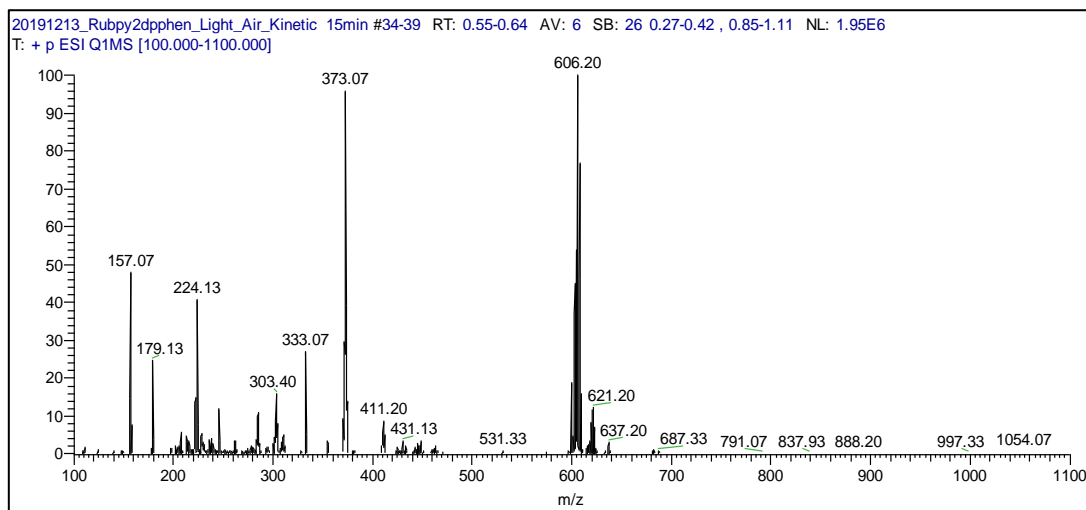
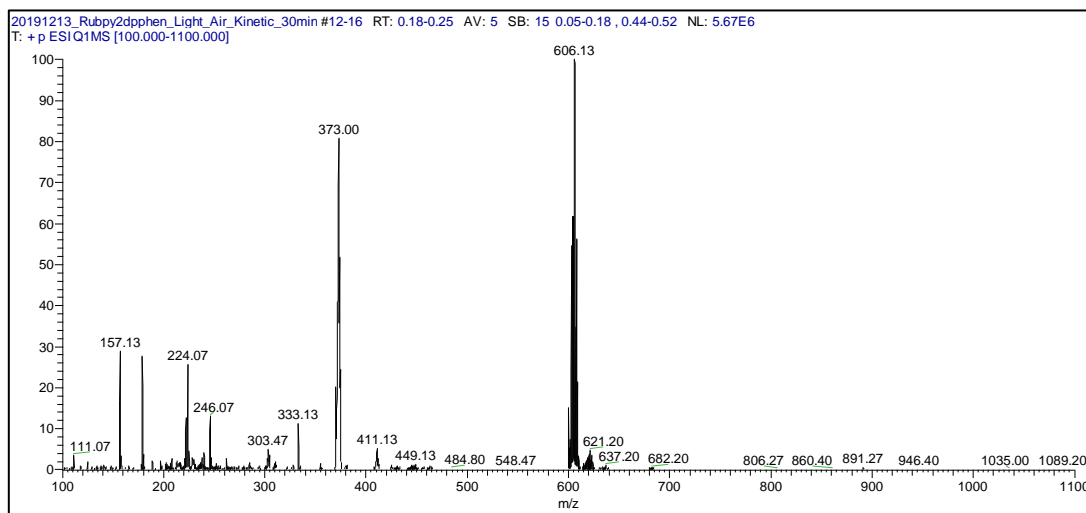


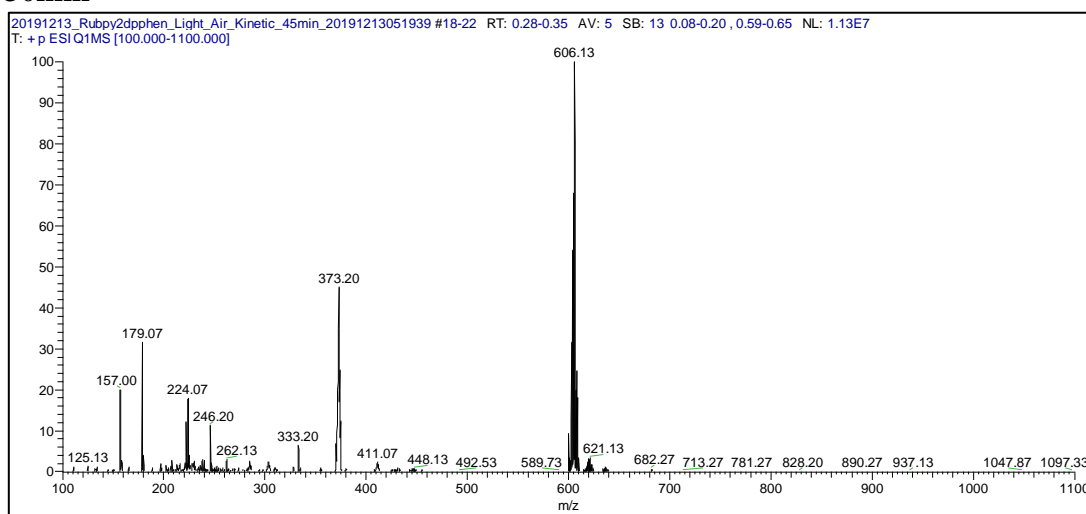
Figure 3.8. ESI-MS/MS spectrum $[\text{Ru}(\text{bpy})_2\text{dpphen}]\text{Cl}_2$ before irradiation. The m/z value assigned to the peaks, is as a function of the percent abundance of the signals (%). Peak at m/z $[\text{M} - 2\text{Cl}]^{++} = 373.13$ correspond to $[\text{Ru}(\text{bpy})_2\text{dpphen}]\text{Cl}_2$ confirming the absence of ligand dissociation. Tested in LC-MS grade water.



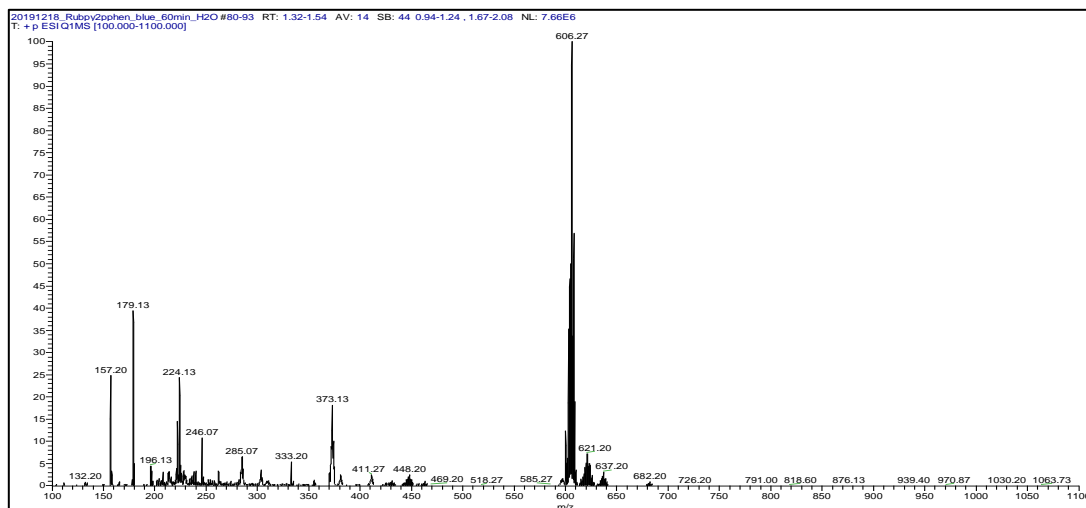
15min



30min



45min



60min

Figure 3.9. ESI-MS/MS spectrum $\text{Ru}(\text{bpy})_2\text{dpphen}.\text{Cl}_2$ after irradiation. $\text{Ru}(\text{bpy})_2\text{dpphen}.\text{Cl}_2$ was diluted in LCMS grade water and photoactivation was achieved by irradiation with blue LED light at a power of 100 mW/cm^2 and tested at 15, 30, 45, 60 min.

The m/z value assigned to the peaks, is as a function of the percent abundance of the signals (%). Peak at $m/z=157$ correspond to the ligand bpy and 373.13 to $[\text{Ru}(\text{bpy})_2\text{dpphen}]\text{Cl}_2$. Peak at $m/z=606.27$ correspond to $[\text{Ru}(\text{bpy})(\text{dpphen})\text{H}_2\text{O}]\text{Cl}_2$. As the time of irradiation were increased the relative abundance of peak $m/z=606.27$ increased while that of the prodrug ($[\text{Ru}(\text{bpy})_2\text{dpphen}]\text{Cl}_2$) and ligand (bpy) decreased.

3.1.2 Purification of $[\text{Ru}(\text{bpy})\text{dpphen}][\text{CH}_3\text{OH}]\text{Cl}_2$

The purification of $[\text{Ru}(\text{bpy})(\text{dpphen})\text{CH}_3\text{OH}]\text{Cl}_2$ was attained by column chromatography using Alumina as the stationary phase and DCM to methanol (99.7: 0.3) as the mobile phase. Figure 3.10 represents the elution of the irradiated $[\text{Ru}(\text{bpy})\text{dpphen}]\text{Cl}_2$. Fractions obtained are represented in figure 3.11, which were looked upon their absorption spectra and speculated the targeted fraction to be found between fraction (F) 2 and 3 (figure 3.11 and 3.12). This was confirmed via ESI-MS/MS (figure 3.13), at which we observe the isolation of the precursor $[\text{Ru}(\text{bpy})_2\text{dpphen}]\text{Cl}_2$ from the photoproduct $[\text{Ru}(\text{bpy})(\text{dpphen})\text{CH}_3\text{OH}]\text{Cl}_2$ and ligand(BPY).

3.1.2.1 Column 1 fractions

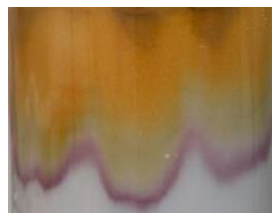


Figure 3.10. Column Chromatography (40/60) elution of irradiated $[\text{Ru}(\text{bpy})\text{dpphen}]\text{Cl}_2$. Eluting compounds in 99.7: 0.3 DCM to MeOH.

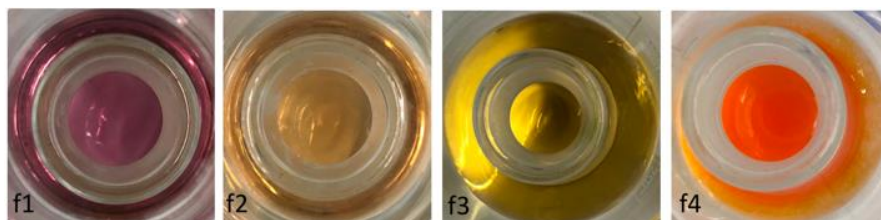


Figure 3.11. $[\text{Ru}(\text{bpy})_2\text{dpphen}]\text{Cl}_2$ photoproducts fractions eluted

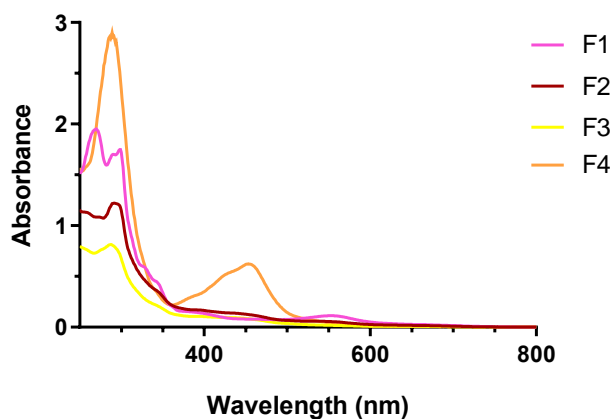
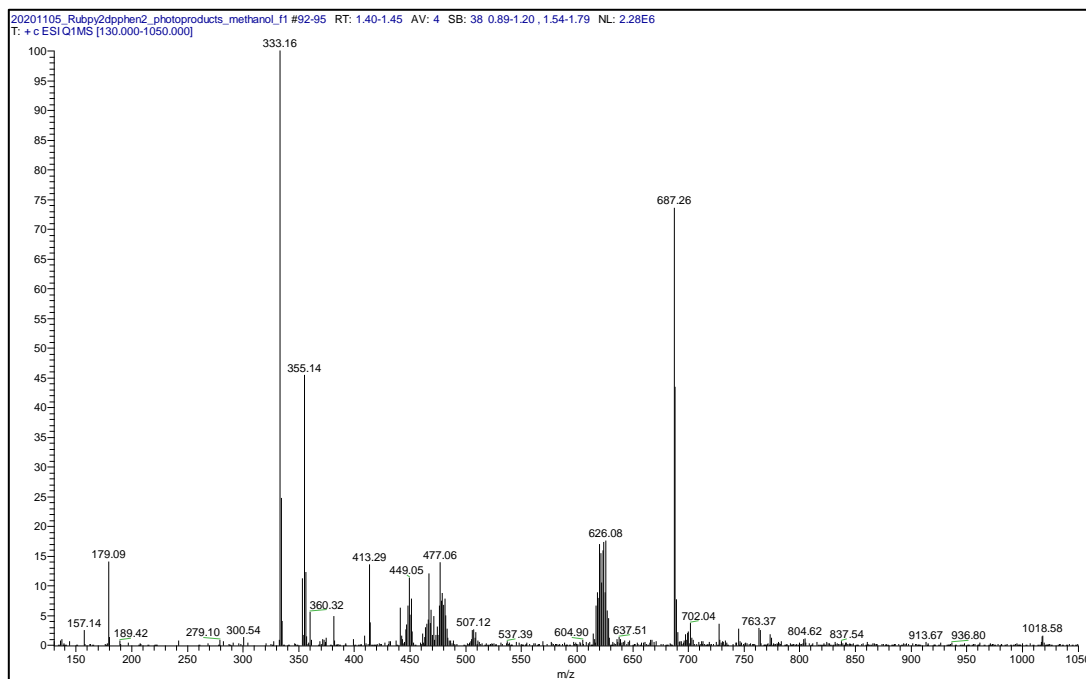
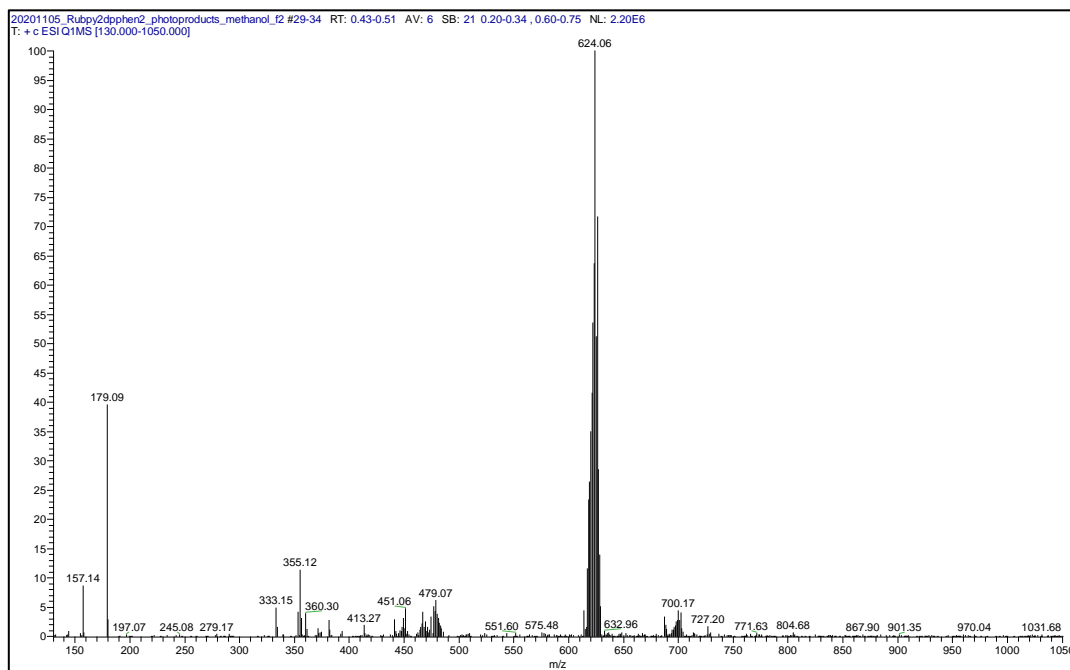


Figure 3.12. Absorption spectrum of eluted fractions of $[\text{Ru}(\text{bpy})_2\text{dpphen}]\text{Cl}_2$ photoproducts.

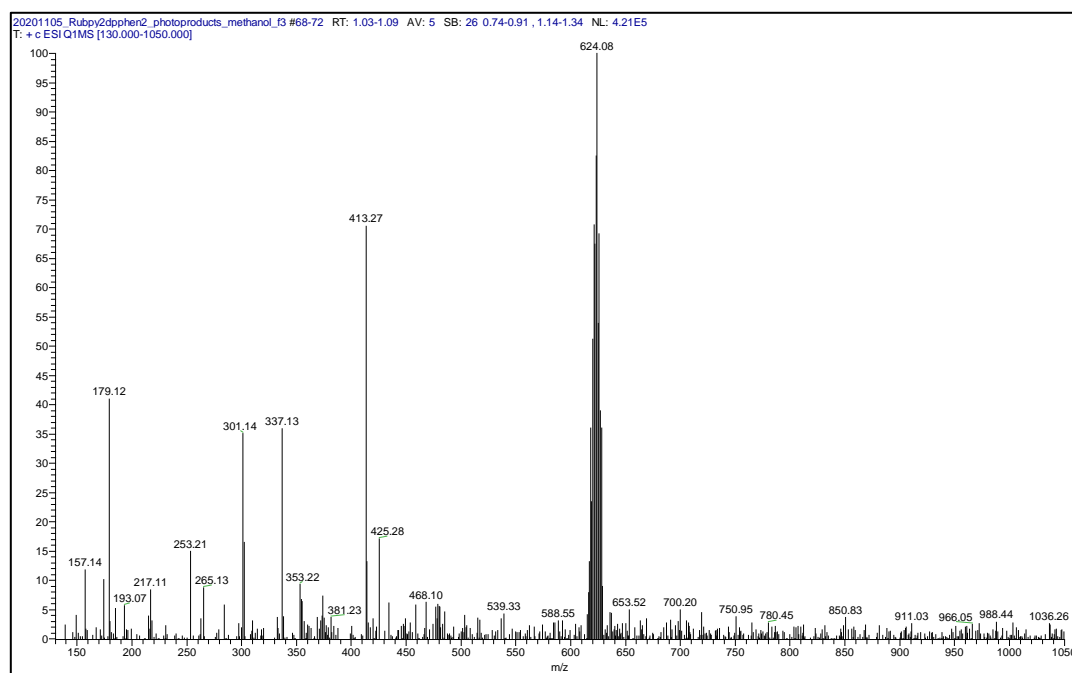
F1



F2



F3



F4

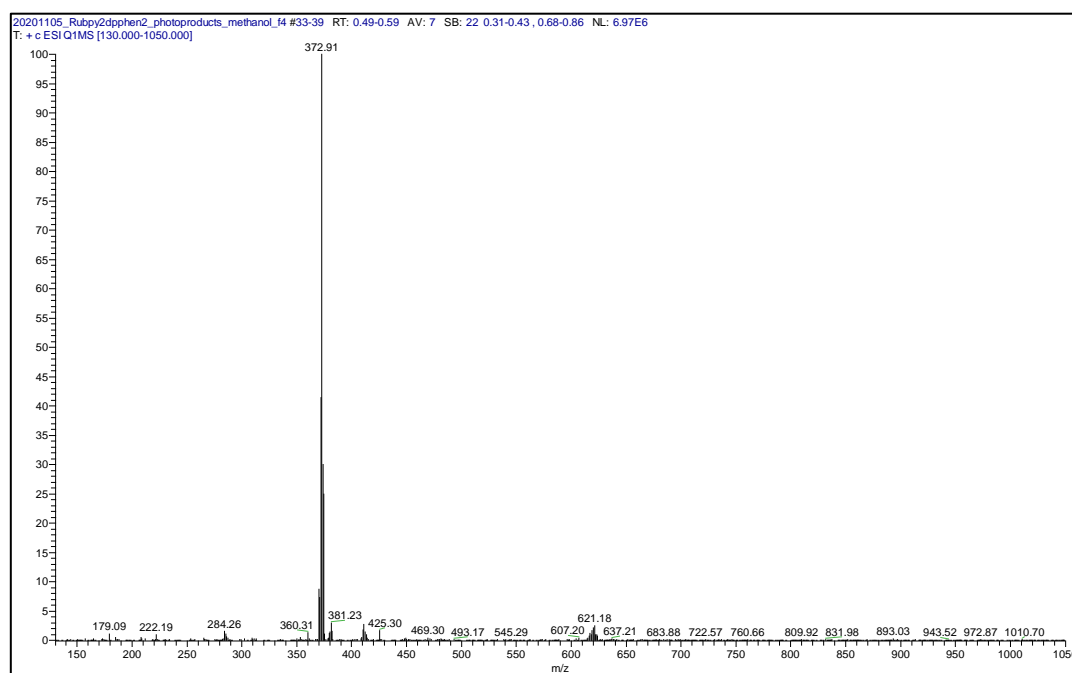
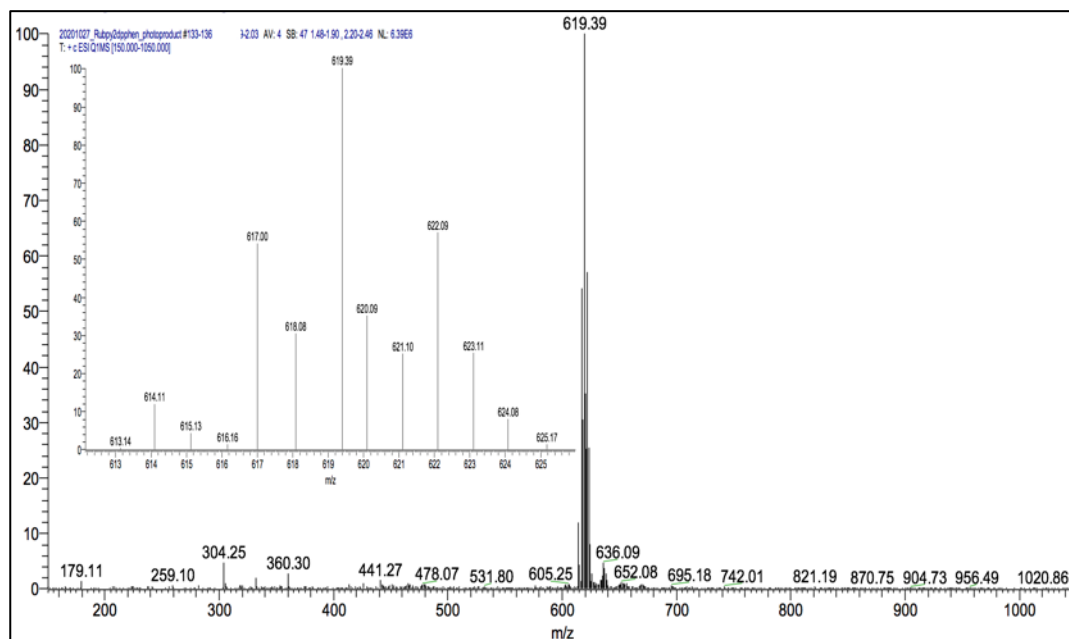


Figure 3.13. ESI-MS/MS spectrum for column 1 fraction characterization. F1,2,3,4 show the m/z value assigned to the peaks as a function of the percent abundance of the signals (%). (F1) Peaks at m/z of 687.26, 333.16, and 157.14 belong to $[\text{Ru}(\text{bpy})(\text{dpphen})\text{CH}_3\text{OFe}]\text{Cl}_2$, dpphen and bpy respectively. (F2) Peaks at m/z of 624.06, and 157.14 belong to $[\text{Ru}(\text{bpy})(\text{dpphen})\text{CH}_3\text{OH}]\text{Cl}_2$ and bpy respectively. (F3) Peaks at m/z of 624.06, and 157.14 belong to $[\text{Ru}(\text{bpy})(\text{dpphen})\text{CH}_3\text{OH}]\text{Cl}_2$ and bpy respectively. (F4) Peak at m/z of 372.91, belongs to $[\text{Ru}(\text{bpy})_2\text{dpphen}]\text{Cl}_2$.

3.1.2.2 Column 2 fractions via ESI/MS

Fraction two and three obtained from the first column were rerun on a sequential column with the same phases to further purify $[\text{Ru}(\text{bpy})(\text{dpphen})\text{CH}_3\text{OH}]\text{Cl}_2$ from the ligand BPY, which is separated in figure 3.15. Solubility and exchange was attained in 10% methanol. As well as, in pure LCMS-grade water by sonication. Both (figure 3.16 and 3.17) show a great increase in the relative abundance of the aquated photoproduct inferring the counter-ion exchange of methanol and the great ionizing



power of water.

Figure 3.14. ESI-MS/MS spectrum for column 2 fraction characterization. The m/z value assigned to the peaks, is as a function of the percent abundance of the signals (%). Peak at m/z $[\text{M} + \text{H}^+]^+ = 619.39$ correspond to $[\text{Ru}(\text{bpy})(\text{dpphen})\text{CH}_3\text{OH}]\text{Cl}_2$. Tested in Methanol.

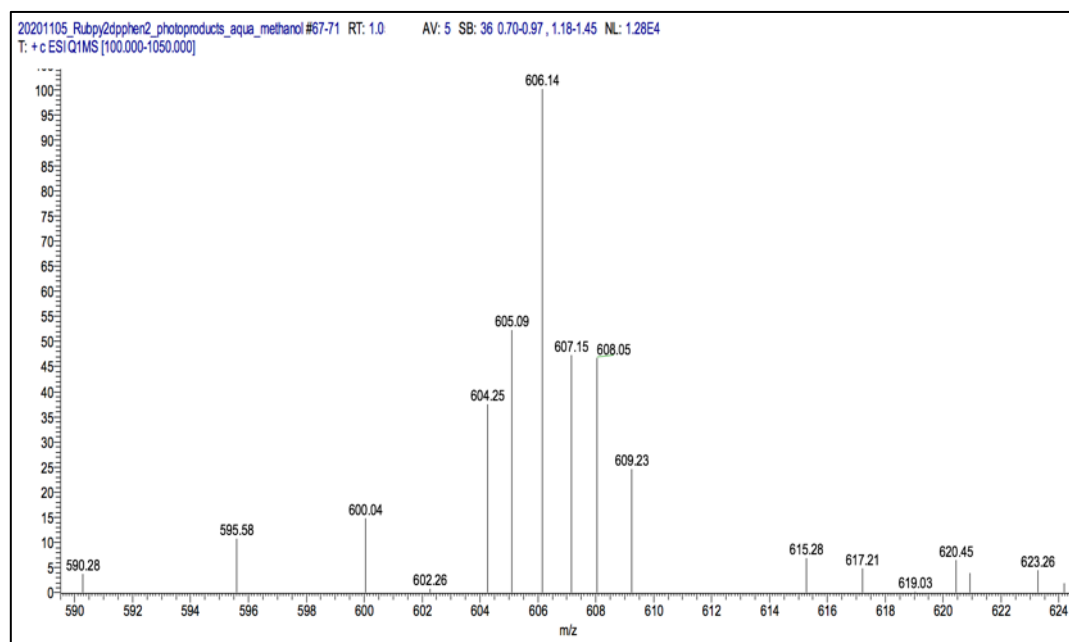


Figure 3.15. ESI-MS/MS spectrum for column 2 fraction characterization in 10% methanol. Compound was dissolved in 10% LC-MS grade methanol. The m/z value assigned

to the peaks, is as a function of the percent abundance of the signals (%). Peak at m/z $[M + H]^+ = 606.14$ correspond to $[\text{Ru}(\text{bpy})(\text{dpphen})\text{H}_2\text{O}]\text{Cl}_2$.

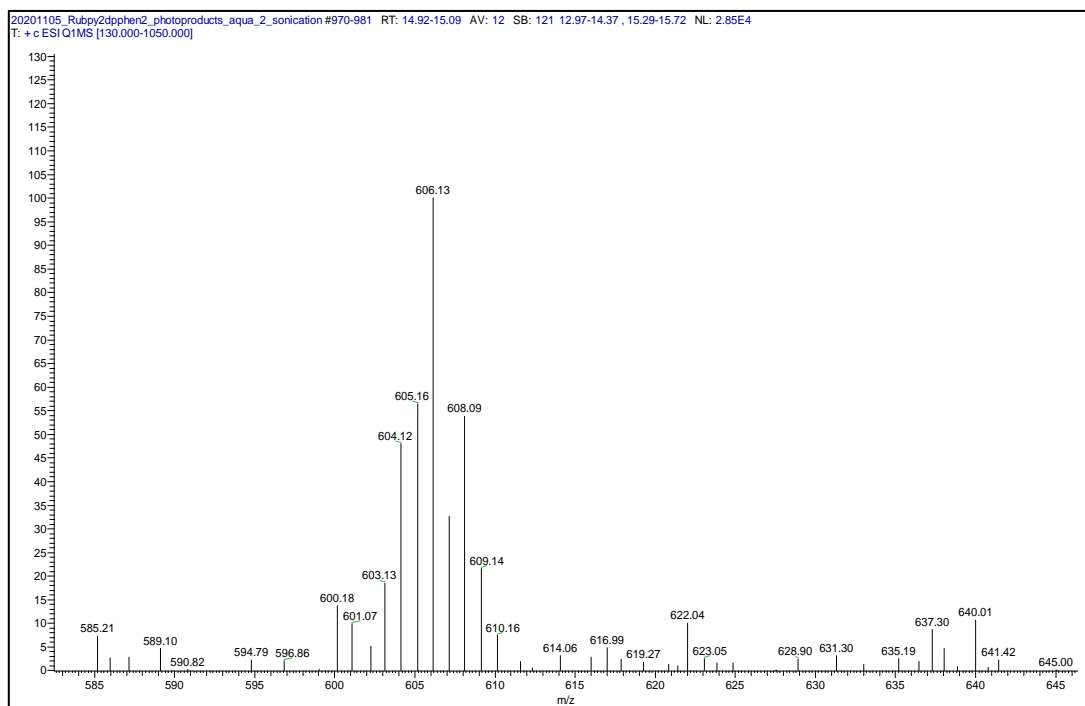


Figure 3.16. ESI-MS/MS spectrum for column 2 fraction characterization in miliQ water. Compound was dissolved in LC-MS grade water by sonication. The m/z value assigned to the peaks, is as a function of the percent abundance of the signals (%). Peak at m/z $[M + H]^+ = 606.13$ correspond to $[\text{Ru}(\text{bpy})(\text{dpphen})\text{H}_2\text{O}]\text{Cl}_2$.

3.1.2.2.i Absorption Spectra

The absorption spectra of the purified $[\text{Ru}(\text{bpy})(\text{dpphen})\text{H}_2\text{O}]\text{Cl}_2$ is represented below

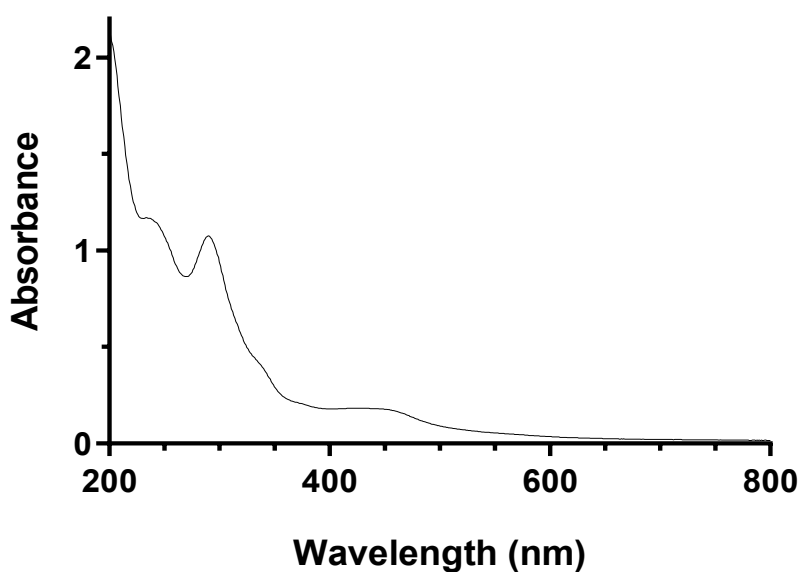


Figure 3.17. Absorption spectrum of $[\text{Ru}(\text{bpy})(\text{dpphen})\text{H}_2\text{O}]\text{Cl}_2$

3.2 Octanol-water partition coefficient

Cellular uptake of $[\text{Ru}(\text{bpy})_2\text{phen}]\text{Cl}_2$, $[\text{Ru}(\text{bpy})_2\text{BC}]\text{Cl}_2$, $[\text{Ru}(\text{bpy})_2\text{BC}]\text{Cl}_2$ photoproducts, $[\text{Ru}(\text{bpy})_2\text{dpphen}]\text{Cl}_2$ and $[\text{Ru}(\text{bpy})(\text{dpphen})\text{H}_2\text{O}]\text{Cl}_2$ is a function of lipophilicity, as determined by calculating the $\log P$ value or the partition coefficient between the hydrophobic octanol phase and the hydrophilic water phase (section 2.4).

The $\log P$ of $[\text{Ru}(\text{bpy})_2\text{BC}]\text{Cl}_2$ (Mehanna, et al., 2019) was found to be significantly higher than that of $[\text{Ru}(\text{bpy})_2\text{phen}]\text{Cl}_2$ (-1.57 ± 0.01 and -2.82 ± 0.10 , respectively, $p < 0.05$, Table 3.1). This, suggested that $[\text{Ru}(\text{bpy})_2\text{BC}]\text{Cl}_2$ was more lipophilic than $[\text{Ru}(\text{bpy})_2\text{phen}]\text{Cl}_2$. The $\log P$ of $[\text{Ru}(\text{bpy})_2\text{dpphen}]\text{Cl}_2$ was found to be slightly higher than that of $[\text{Ru}(\text{bpy})_2\text{phen}]\text{Cl}_2$ (-2.53 ± 0.06 and -2.82 ± 0.10 , respectively, Table 3.1), suggesting that $[\text{Ru}(\text{bpy})_2\text{dpphen}]\text{Cl}_2$ was slightly more lipophilic than $[\text{Ru}(\text{bpy})_2\text{phen}]\text{Cl}_2$. The $\log P$ of cisplatin is -2.21 , as reported in the literature (Qu et al., 2017), confirming that cisplatin is slightly more hydrophobic than $[\text{Ru}(\text{bpy})_2\text{phen}]\text{Cl}_2$ ($p < 0.05$). The dissociating ligands, BC and bpy were the most lipophilic since they had the highest $\log P$ values, reported to be 6.96 (Hageh et al., 2018) and 1.88 (as estimated by ChemDraw Professional, v15.0, CambridgeSoft), respectively.

Table 3.1. The partition coefficient between the hydrophobic octanol phase and the hydrophilic water phase ($\log P$) reported for $[\text{Ru}(\text{bpy})_2\text{phen}]\text{Cl}_2$, $[\text{Ru}(\text{bpy})_2\text{BC}]\text{Cl}_2$, $[\text{Ru}(\text{bpy})_2\text{dpphen}]\text{Cl}_2$, $[\text{Ru}(\text{bpy})(\text{dpphen})\text{H}_2\text{O}]\text{Cl}_2$, cisplatin, BC and bpy.

Compounds	$\log P$
$[\text{Ru}(\text{bpy})_2\text{Phen}]\text{Cl}_2$	-2.82 ± 0.10
$[\text{Ru}(\text{bpy})_2\text{BC}]\text{Cl}_2$	-1.57 ± 0.01
$[\text{Ru}(\text{bpy})_2\text{dpphen}]\text{Cl}_2$	-2.53 ± 0.06
$[\text{Ru}(\text{bpy})(\text{dpphen})\text{H}_2\text{O}]\text{Cl}_2$	-2.77 ± 0.05
Cisplatin	-2.21^{a}
BC	6.96^{b}
BPY	1.88^{c}

^{a, b} Values reported in the literature (Hageh et al., 2018; Qu et al., 2017)

^c Values estimated by ChemDraw Professional (v15.0, CambridgeSoft)

3.3 Cellular uptake of Ru(II) in A375 cancer cells

The cellular uptake of the $[\text{Ru}(\text{bpy})_2\text{BC}]\text{Cl}_2$ was measured by ICP-MS at different time points starting from 0 until 24 h after treatment based on internal and external standards (Indium and Ruthenium respectively). The uptake of $[\text{Ru}(\text{bpy})_2\text{BC}]\text{Cl}_2$ was analysed in A375 (Figure 3.19) cell lines, as well as its photoproducts. Figure 3.18 ensures the photoproduct formation, indicated by a peak shift from 456 (blue arrow) to 538nm (red arrow). In A375, the uptake of $[\text{Ru}(\text{bpy})_2\text{BC}]\text{Cl}_2$ showed a significant difference between the precursor and photoproduct at all time points. Whilst the precursor showed an uptake of $107.97 \mu\text{M}/\text{cell}$ at 0 hours, the photoproduct did not show any uptake until 3 hours. The precursor reached its maximum uptake of $1566.3 \mu\text{M}/\text{cell}$ at 24 hours, indicating the choice of blue LED light exposure post drug addition. $[\text{Ru}(\text{bpy})_2\text{BC}]\text{Cl}_2$ photoproduct did not reach its maximum by 24 h ($287.2 \mu\text{M}/\text{cell}$). This indicates that $[\text{Ru}(\text{bpy})_2\text{BC}]\text{Cl}_2$ precursor was the most readily internalized compound by the cancer cells.

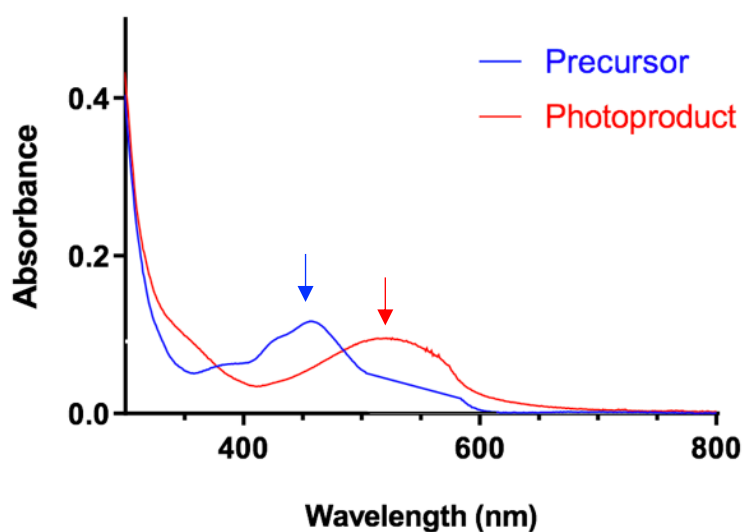


Figure 3.18. UV-vis absorbance spectrum of $[\text{Ru}(\text{bpy})_2\text{BC}]\text{Cl}_2$ precursor vs. photoproduct: $[\text{Ru}(\text{bpy})_2\text{BC}]\text{Cl}_2$ precursor (456 nm-blue arrow) and photoproduct (538nm- red arrow) indicate shift, representing ligand dissociation.

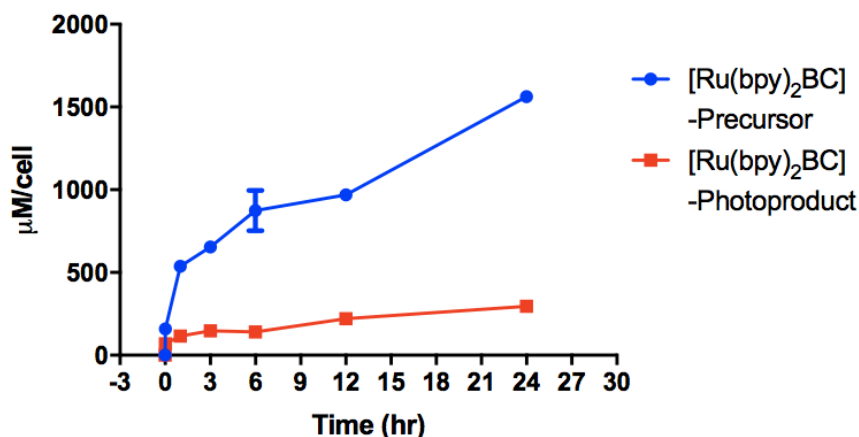


Figure 3.19. ICP-MS analysis for the uptake of Ru(II) in A375 cells. Ru(bpy)₂BC.Cl₂ precursor has the greatest cellular uptake n=3 from three independent experiments where samples were run in triplicates. Data points denote mean \pm SEM and expressed in $\mu\text{M}/\text{cell}$.

The maximum intracellular concentration of [Ru(bpy)₂BC]Cl₂ precursor and photoproduct was reported in μM (table 3.3). The ratio (intracellular concentration / extracellular concentration) was calculated knowing that the extracellular concentration was 3 μM . [Ru(bpy)₂BC]Cl₂ precursor had the greatest intracellular to extracellular ratios in comparison to its photoproducts.

Table 3.3. Intracellular concentration of [Ru(bpy)₂BC]Cl₂ precursor vs. photoproducts (μM cell) along with the ratio of intracellular/extracellular compound concentration in A375 cell line.

	Intracellular Concentration (μM)	Intracellular / Extracellular Concentration (μM)
Ru(bpy)₂BC.Cl₂ precursor	1566.3 \pm 1.7	522.1 \pm 0.5
Ru(bpy)₂BC.Cl₂ photoproducts	287.2 \pm 3.1	95.7 \pm 1.1

3.4. Mode of uptake of [Ru(bpy)₂BC]Cl₂ precursor

The mode of uptake of the [Ru(bpy)₂BC]Cl₂ into A375 cells was measured by ICP-MS based on internal and external standards (Indium and Ruthenium respectively). (Figure 3.20) The uptake was mostly inhibited at low temperatures, and uses an active form of transport to be further investigated.

Table 3.4. Intracellular concentration of [Ru(bpy)₂BC]Cl₂ precursor (μ M) along with the ratio of intracellular/extracellular compound concentration in A375 cell line, identifying the mode of uptake.

[Ru(bpy) ₂ BC]Cl ₂ precursor	Intracellular Concentration (μ M)	Intracellular/ Extracellular Concentration (μ M)
37 °C	639.9 \pm 3.6	160.6 \pm 1.4
4 °C	332.7 \pm 2.1	110.9 \pm 0.8
Transferrin Receptor	490.7 \pm 4.8	199.7 \pm 2.4

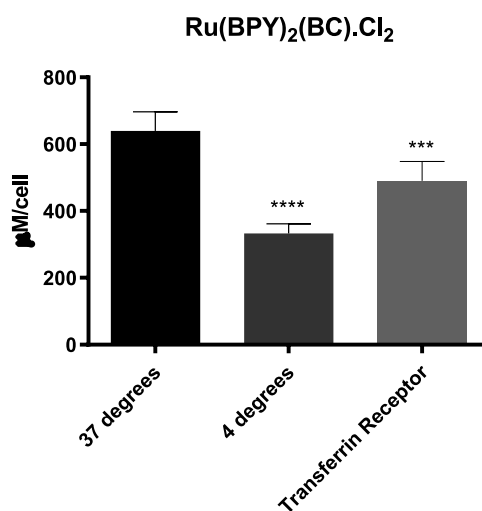


Figure 3.20. ICP-MS analysis for the mode of uptake of Ru(II) in A375 cells.

P<0.001 and *P<0.0001 in comparison to 37 degrees.

3.5 The cytotoxic effects of ruthenium complexes on cancer cells survival

The cytotoxic effect of Ru(II) was examined on A375 cancer cells for 72 hours in comparison to cisplatin (positive control).

3.5.1 Cytotoxicity of [Ru(bpy)₂BC]Cl₂ (dark vs. light), Ligands and Cisplatin

Cells were treated with multiple concentrations of [Ru(bpy)₂BC]Cl₂ drug in the dark and blue LED light. Results showed a dose-dependent activity and IC₅₀ values of 43.1 μM, 0.127 μM and 9.219 μM for [Ru(bpy)₂BC]Cl₂ drug in the dark, [Ru(bpy)₂BC]Cl₂ drug photo activated in blue LED light and Cisplatin respectively. IC₅₀ values (μM) of [Ru(bpy)₂Phen]Cl₂ (unstrained control), BC and BPY ligands (>100, 51.9 μM and >100 respectively) were measured on A375 cell line in dark conditions, as they are not affected by light (not sterically hindered) according to preliminary studies.

Table 3.5. IC₅₀ values (μM) of [Ru(bpy)₂BC]Cl₂, [Ru(bpy)₂phen]Cl₂, BC and BPY ligands along with IC₅₀ of the positive control cisplatin. The IC₅₀ values were measured on A375 cell line in both dark and light conditions. The phototoxicity index (PI) was calculated as IC₅₀ dark/IC₅₀ light.

IC ₅₀	Dark	Light	Phototoxicity Index (PI)
[Ru(BPY) ₂ BC]Cl ₂	43.1 ± 1.3	0.127 ± 1.5	339.3
Cisplatin	9.219 ± 1.5	-	-
[Ru(BPY) ₂ phen]Cl ₂ (Phen)	>100	-	-
Bathocuproine (BC)	51.9 ± 1.4	-	-
Cis-Dichlorobis(2,2'-bipyridine)Ruthenium(II) (BPY)	>100	-	-

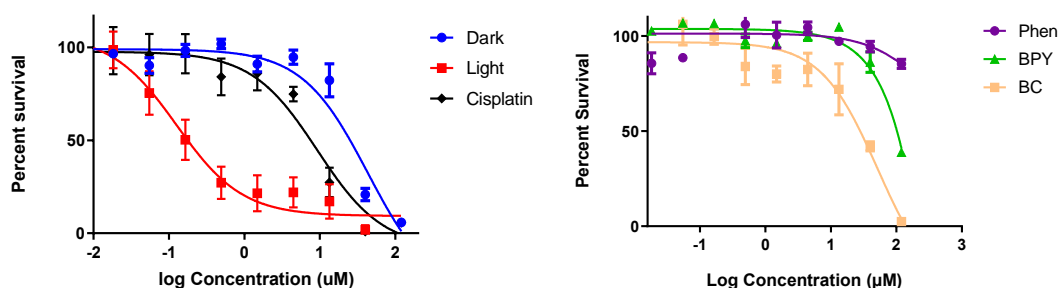


Figure 3.21. Cytotoxic effect of [Ru(bpy)₂BC]Cl₂ dark, [Ru(bpy)₂BC]Cl₂ light, cisplatin, Phen, BC, and BPY on A375. Cells were treated with a range of concentrations starting from maximum concentration of 120 μM to a minimum of 0.006 μM using threefold dilutions. Data points denote mean ± SEM. n = 3 from three independent experiments where samples were run in triplicate

3.5.2 Cytotoxicity of [Ru(bpy)₂BC]Cl₂ activated intracellularly in a Ru(bpy)₂BC.Cl₂ free medium and [Ru(bpy)₂BC]Cl₂ photoproducts on seeded A375.

Cells were treated with [Ru(bpy)₂BC]Cl₂, and activated intracellularly (Light – intracellular) by changing the supernatant prior to photoactivation. The effect of the photoproduct of [Ru(bpy)₂BC]Cl₂ was also studied by photoactivating the drug extracellularly and then allowing its uptake to test its cytotoxicity. There was no significant effect of the precursor being left in the supernatant whilst the photoactivation process as the photoproduct did not have a cytotoxic effect as the drugs activation intracellularly

Table 3.6. IC₅₀ values (μM) of [Ru(bpy)₂BC]Cl₂, light irradiated, light – Intracellular and photoproducts.

	Light	Light - Intracellular	Photoproducts
IC ₅₀	0.127 ± 1.5	0.2293 ± 1.4	15.74 ± 1.3

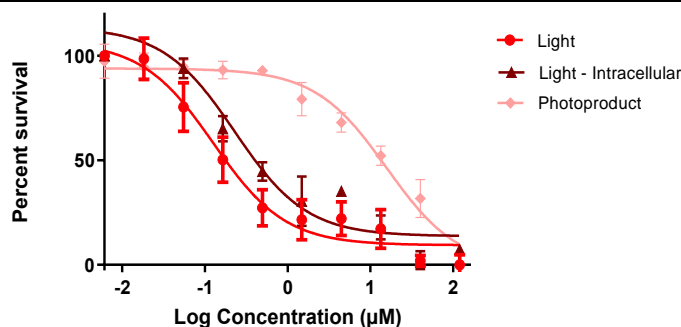


Figure 3.22. Cytotoxic effect of Ru(bpy)₂BC.Cl₂ photoactivated using blue LED light on A375. Cells were treated with a range of concentrations starting from maximum concentration of 120μM to a minimum of 0.006 μM using threefold dilutions. Light: photoactivated including drug remnants in supernatant not uptaken by A375 cells, vs. Light-non-uptaken drug removed from supernatant prior to activation and the photo activated products of [Ru(bpy)₂BC]Cl₂, as well as the extracellular photoactivation of [Ru(bpy)₂BC]Cl₂. Data points denote mean ± SEM. n = 3 from three independent experiments where samples were run in triplicate.

3.5.3 Cytotoxicity of Ru(bpy)₂dpphen.Cl₂ (dark vs. light)

Cells were treated with multiple concentrations of [Ru(bpy)₂dpphen]Cl₂ drug in the dark and blue LED light. Results showed a dose-dependent activity and IC₅₀ values of 71.83 μM and 1.43 μM (IC₅₀ values, table 3.7) for [Ru(bpy)₂dpphen]Cl₂ drug in the dark, and drug photo activated in blue LED light respectively.

Table 3.7. IC₅₀ values (μM) of [Ru(bpy)₂dpphen]Cl₂. The IC₅₀ values were measured on A375 cell line in both dark and light conditions. The phototoxicity index (PI) was calculated as IC₅₀ dark/IC₅₀ light.

	[Ru(bpy) ₂ dpphen]Cl ₂ -dark	[Ru(bpy) ₂ dpphen]Cl ₂ -light	Phototoxicity Index (PI)
IC ₅₀	71.83 ± 1.6	1.43 ± 1.2	50.2

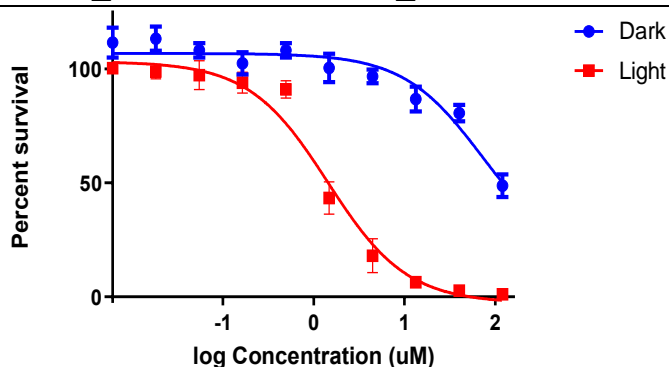


Figure 3.23. Cytotoxic effect of [Ru(bpy)₂dpphen]Cl₂ dark and light activated on A375. Cells were treated with a range of concentrations starting from maximum concentration of 120μM to a minimum of 0.006 μM using threefold dilutions. Data points denote mean ± SEM. n = 3 from three independent experiments where samples were run in triplicate.

3.5.4 Cytotoxicity of [Ru(bpy)(dpphen)H₂O]Cl₂

Cells were treated with multiple concentrations of [Ru(bpy)(dpphen)H₂O]Cl₂. Results showed an IC₅₀ value of 10.52 (IC₅₀ values, table 3.8) on A375 cell line.

Table 3.8. IC₅₀ values (μM) of [Ru(bpy)(dpphen)H₂O]Cl₂. The IC₅₀ values were measured on A375 cell line.

	[Ru(bpy)(dpphen)H ₂ O]Cl ₂
IC ₅₀	10.52 ± 1.4

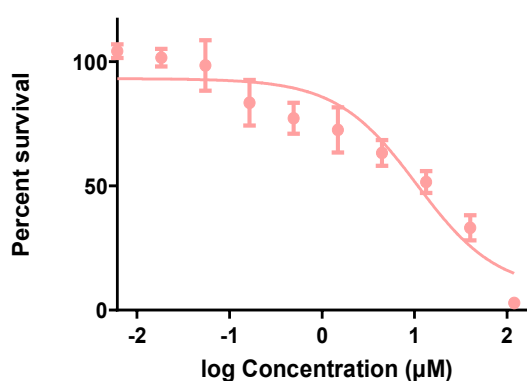


Figure 3.24. Cytotoxic effect of [Ru(bpy)(dpphen)H₂O].Cl₂ photoproducts on A375. Cells were treated with a range of concentrations starting from maximum concentration of 120μM to a minimum of 0.006 μM using threefold dilutions. Data points denote mean ± SEM. n =3 from three independent experiments where samples were run in triplicate.

3.6 ROS production

A375 cells were treated with $[\text{Ru}(\text{bpy})_2\text{BC}]\text{Cl}_2$, at IC_{50} stained by DCFDA and then blue LED light activated. Upon ROS production, the DCFDA produced a fluorescent product. The measured fluorescence was therefore proportional to the produced ROS. Cells treated with $[\text{Ru}(\text{bpy})_2\text{BC}]\text{Cl}_2$ prodrug, without light activation did not show any ROS production when compared to control group as well as the positive control (TBHP). However, upon light activation, $[\text{Ru}(\text{bpy})_2\text{BC}]\text{Cl}_2$ produced a significant increase in ROS production at the concentrations used compared to control. Control cells treated with only light also showed an increase in ROS activity (17 RFU) compared to cells without light exposure (<2 RFU). Data are presented in figure 3.25.

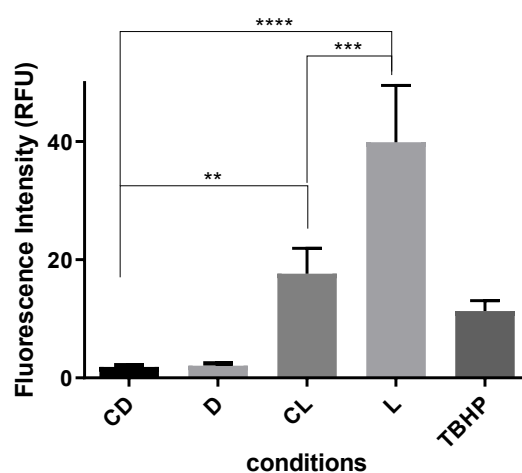


Figure 3.25. ROS production upon treatment with $[\text{Ru}(\text{bpy})_2\text{BC}]\text{Cl}_2$ compounds with or without light irradiation in A375. Control Dark: CD, Dark prodrug treated: D, Control Blue LED Light: CL, Light prodrug treated: L. **** indicates $P < 0.0001$ compared with control. *** indicates $P < 0.001$ comparing light with control light. ** indicates $P < 0.01$, control. Data points denote mean \pm SEM. $n = 3$ from three independent experiments where samples were run in triplicate.

3.7 Western Blots

The effect of Photo activated $[\text{Ru}(\text{bpy})_2\text{BC}]\text{Cl}_2$ on the expression of vital apoptotic proteins in A375 cells were measured. Results have shown that $[\text{Ru}(\text{bpy})_2\text{BC}]\text{Cl}_2$ (with light activation: L) treatment had a significant effect on the expression of all markers represented below, by 72hours of treatment. Cells were treated with light (figure 3.26.) double IC50 and Western blot results were presented as bands visualized by the ChemiDoc imaging system, quantified by ImageLab, normalized against actin and represented as Bar graphs. $n=3$ from three independent experiments. In the light irradiated cells, Pro (bax) and anti (bcl2) apoptotic proteins were significantly increased and decreased respectively by 72 hours, yet at 48 hours bax was significantly increased identifying a pro-apoptotic mechanism via the Bax/Bcl2 ratio at 48 and 72 hours. Cytochrome C, cleaved caspase 3, and cleaved PARP-1 were significantly increased at 48 with a surge increase at 72 hours conforming programmed cell death. Procaspase 8 was significantly decreased in light irradiated cells at 72 hours indicating an extrinsic pathway is interfering with cell death. Proteins P21, P-ERK and P-AKT were studied at 72 hours. P21 indicated a significant increase in light irradiated cells, while P-ERK and P-AKT were significantly inhibited over ERK and AKT respectively further indicating a pro-apoptotic cell death.

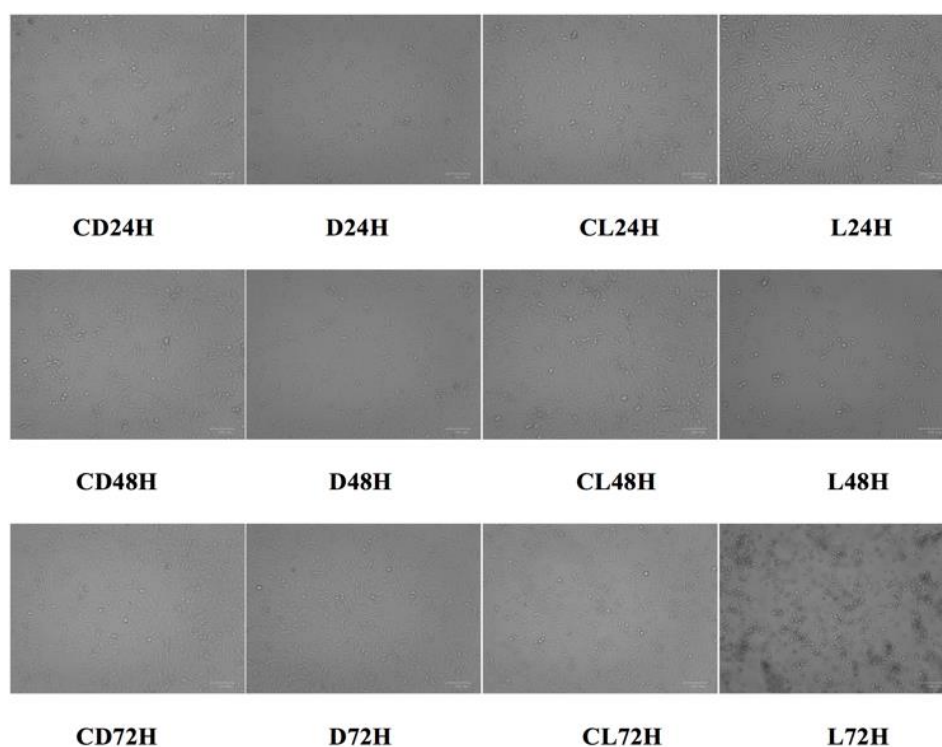


Figure 3.26. A375 cells treated with a concentration of double IC50 of the Light activated prodrug at 24,48 and 72 hours. (Control Dark: CD, Dark prodrug treated:

D, Control Blue LED Light: CL, Light prodrug treated: L). Microscopic images taken using ZOE TM Fluorescent Cell Imager (Biorad)

3.7.1 Bcl2-Associated X protein (Bax)

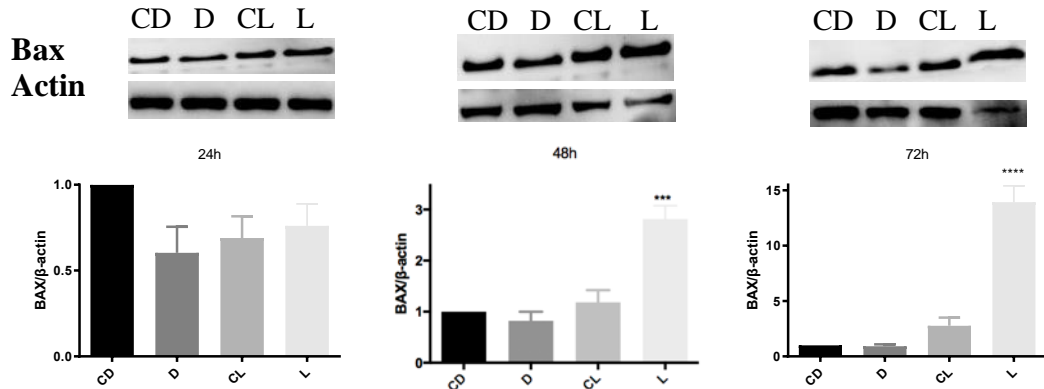


Figure 3.27. The western blot images of Bax and actin along with the ratios of the different samples normalized to CD at 24, 48 and 72 hours. Bands showed a significant increase in the expression of Bax in L compared to CD at 48h as well as a great significant increase in L compared to CD at 72h. Bars denote mean \pm SEM. *** $P < .001$ and **** $P < .0001$ versus Control group, as measured by one-way ANOVA.

3.7.2 B-cell lymphoma 2 (Bcl-2)

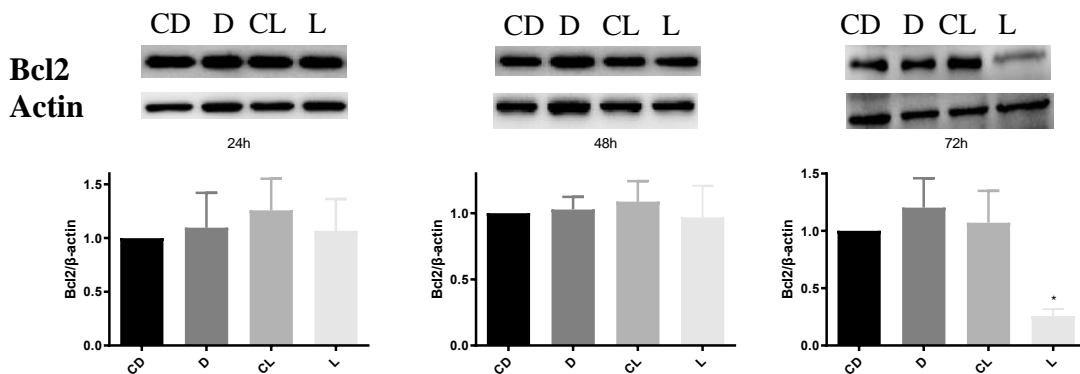


Figure 3.28. The western blot images of Bcl2 and actin along with the ratios of the different samples normalized to CD at 24, 48 and 72 hours. Bands showed a significant decrease in the expression of Bcl2 in L compared to D at 72h. Bars denote mean \pm SEM. * $P < .05$ versus Control group, as measured by one-way ANOVA.

Bax/Bcl2

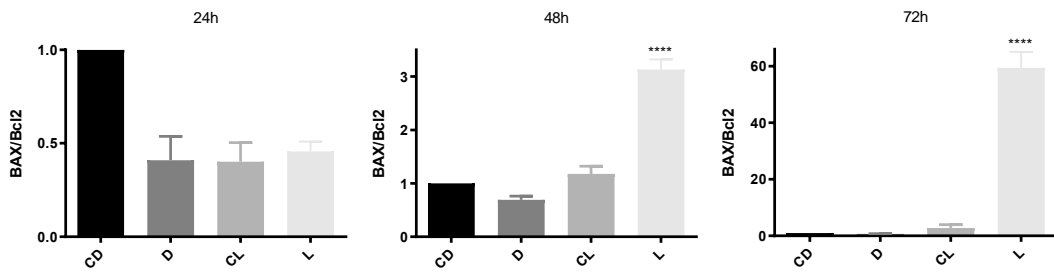


Figure 3.29. The ratio of Bax/Bcl2 at 24, 48 and 72h. A significant increase between CD and L is observed at 48 and 72h. Bars denote mean \pm SEM. **** P <.0001 versus Control group, as measured by one-way ANOVA.

3.7.3 Cytochrome c

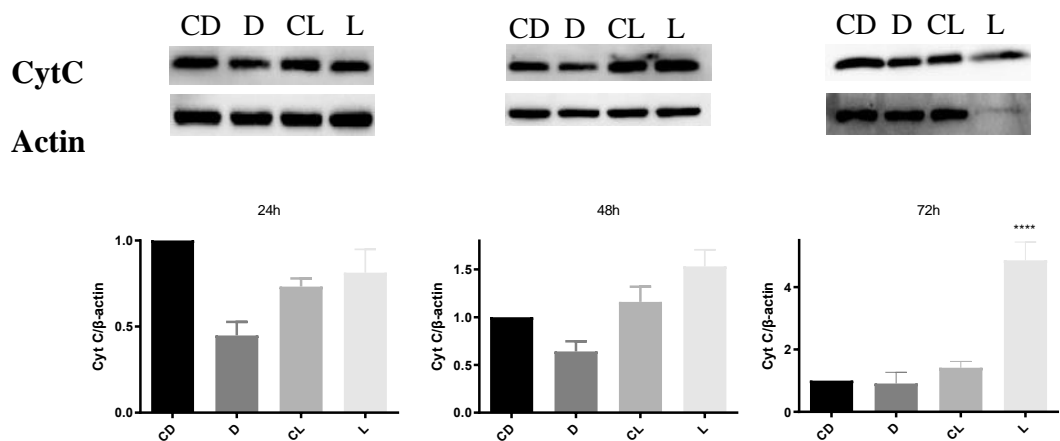


Figure 3.30. The western blot images of Cytochrome C and actin along with the ratios of the different samples normalized to CD at 24, 48 and 72 hours. Bands showed a significant increase in the expression of Cytochrome C in L compared to CD at 72h. Bars denote mean \pm SEM. **** P <.0001 versus Control group, as measured by one-way ANOVA.

3.7.4 Cleaved Caspase 3

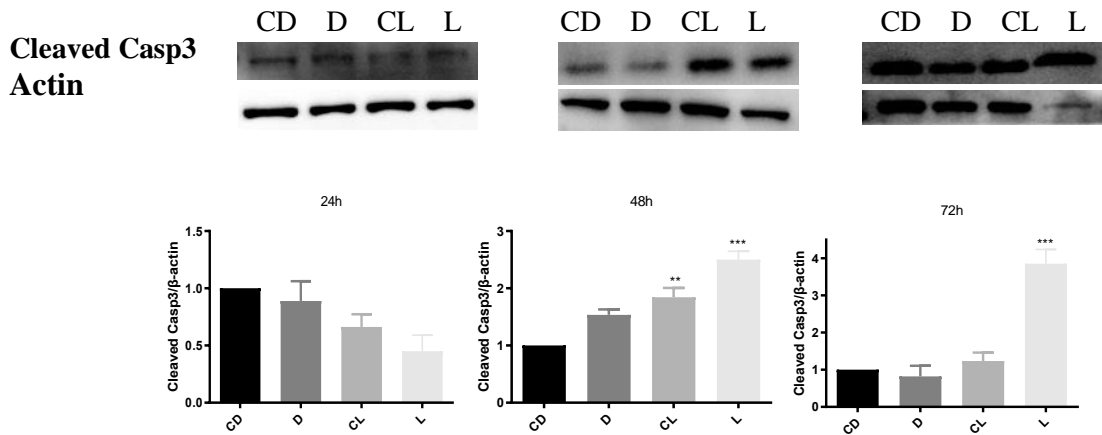


Figure 3.31. The western blot images of cleaved caspase-3 and actin along with the ratios of the different samples normalized to CD at 24, 48 and 72 hours. Bands showed a significant increase in the expression of Pro-casp3 in L compared to CD at 72h. Bands showed a significant increase in the expression of Cleaved Casp3 in CL and L compared to CD at 48h as well as in L compared to CD at 72h. Bars denote mean \pm SEM. ** P <.01 and *** P <.001 versus Control group, as measured by one-way ANOVA.

3.7.5 Cleaved Poly (ADP-ribose) polymerase (Cleaved- Parp-1)

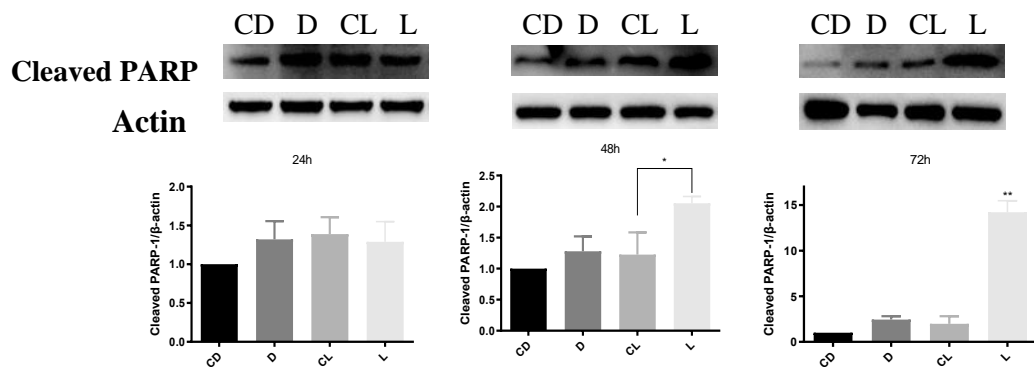


Figure 3.32. The western blot images of Cleaved PARP-1 and actin along with the ratios of the different samples normalized to CD at 24, 48 and 72 hours. Bands showed a significant increase in the expression of Cleaved PARP-1 in L compared to CL at 48h as well as a great significant increase in L compared to CD at 72h. Bars denote mean \pm SEM. * P <.05 and ** P <.01 versus Control group, as measured by one-way ANOVA.

3.7.6 Procaspase 8

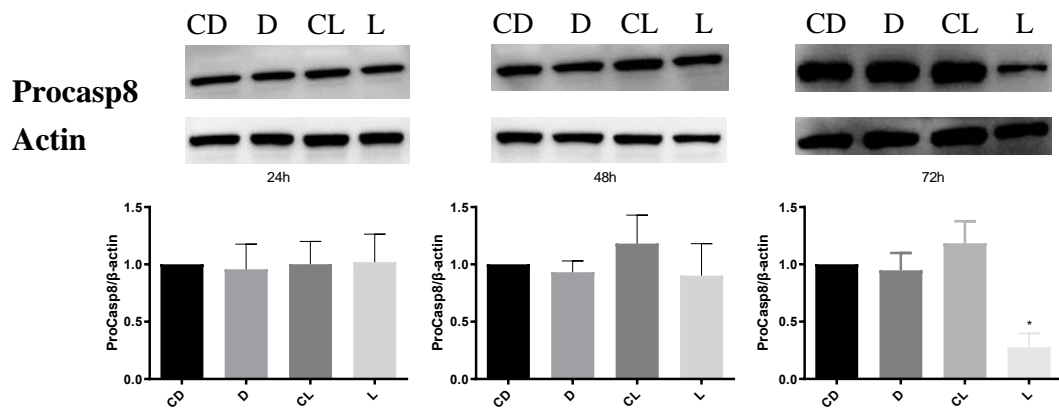


Figure 3.33. The western blot image of Procaspase 8 and actin along with the ratios of the different samples normalized to CD at 24, 48 and 72 hours. Bands showed a significant decrease in the expression of Bax in L compared to CD at 72h. Bars denote mean \pm SEM. * $P < .05$ versus Control group, as measured by one-way ANOVA.

3.7.7 Cyclin-dependent Kinase inhibitor 1 (P21)

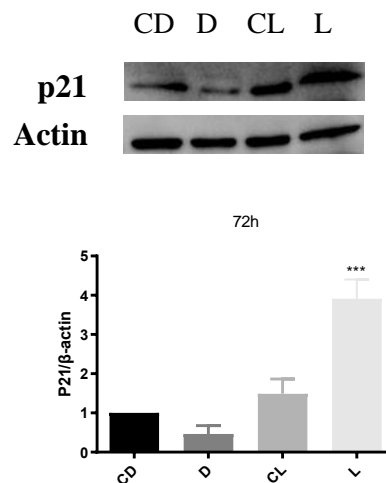


Figure 3.34. The western blot image of P21 and actin along with the ratios of the different samples normalized to CD at 72 hours. Bands showed a significant increase in the expression of P21 in L compared to CD at 72h. Bars denote mean \pm SEM. *** $P < .001$ versus Control group, as measured by one-way ANOVA.

3.7.8 Extracellular signal-regulated kinase (ERK)

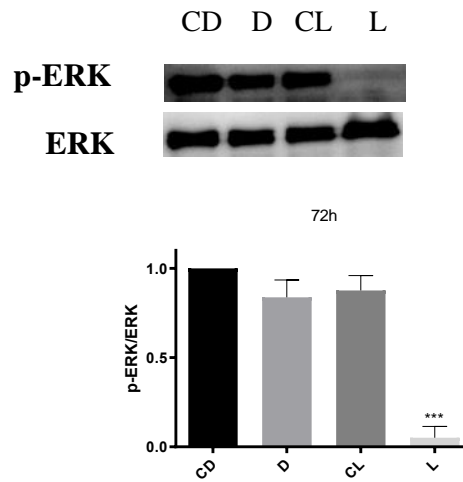


Figure 3.35. The western blot image of p-ERK and ERK along with the ratios of the different samples normalized to CD at 72 hours. Bands showed a great significant decrease in the expression of p-ERK to ERK in L compared to CD at 72h. Bars denote mean \pm SEM. *** $P < .001$ versus Control group, as measured by one-way ANOVA.

3.7.9 Protein Kinase B (AKT)

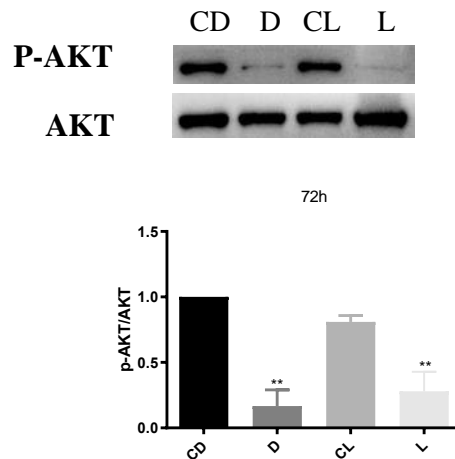


Figure 3.36. The western blot image of p-AKT and AKT along with the ratios of the different samples normalized to CD at 72 hours. Bands showed a significant decrease in the expression of p-ERK to ERK in D compared to CD as well as in L compared to CD at 72h. Bars denote mean \pm SEM. ** $P < .01$ versus Control group, as measured by one-way ANOVA.

3.7.10 Beclin-1

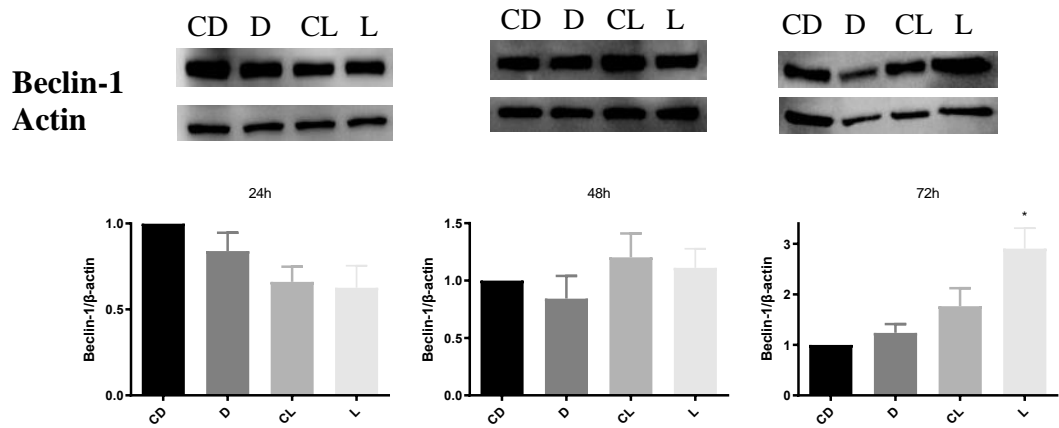


Figure 3.37. The western blot image of Beclin-1 and actin along with the ratios of the different samples normalized to CD at 24, 48 and 72 hours. A significant increase is seen in the expression of Beclin-1 in L compared to CD at 72h. Bars denote mean \pm SEM. * $P < .05$ versus Control group, as measured by one-way ANOVA.

3.8 Effect of Ru(II) on DNA damage in A375 cells via the Comet Assay

The DNA damaging potential of Ru(II) was assessed using alkaline comet assay. The DNA damage in A375 cells treated for 72 h with $[\text{Ru}(\text{bpy})_2\text{BC}]\text{Cl}_2$ both in the dark and blue LED light, were measured using multiple parameters including head length, tail length, comet length, head DNA content, tail DNA content and tail moment (table 3.9). To reflect DNA damage, the tail moment index (TMI) was calculated by multiplying the tail DNA content by the tail length divided by 1000. Data shown in figure 3.39 revealed a significant increase in TMI in both cells treated with KMnO_4 (positive control) and Ru(II) compared with PBS (negative control) and Ru(II) groups (dark vs. light treated). The latter group did not show any significant change in TMI compared with PBS treated A375 cells. Comet tails are greatly identified in light treated cells shown in figure 3.38. (Control Dark: CD, Dark prodrug treated: D, Control Blue LED Light: CL, Light prodrug treated: L).

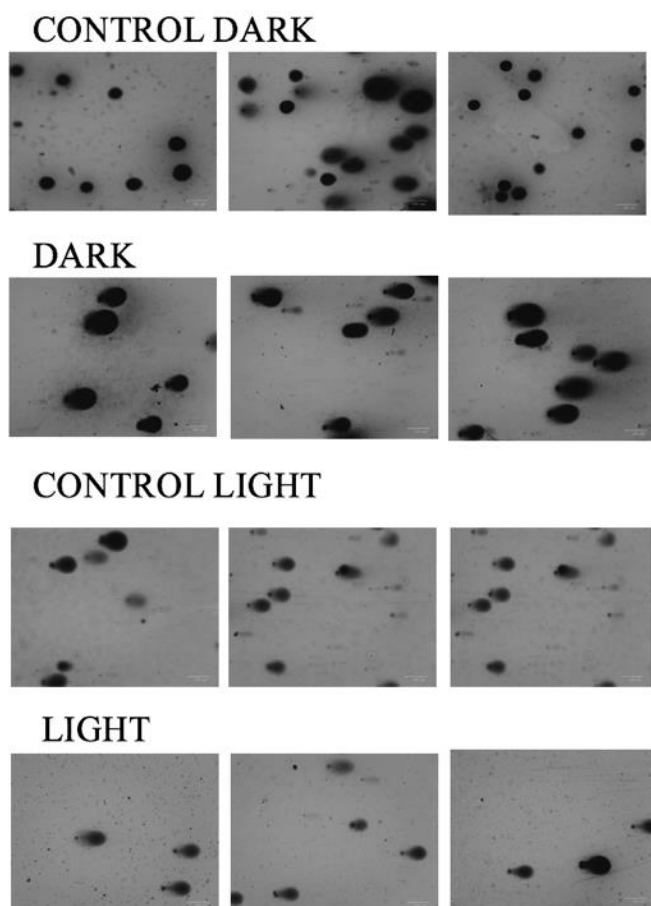


Figure 3.38. Microscopic images of the comet formations in comparison to controls. Control Dark (no treatment), Dark (treated with $[\text{Ru}(\text{bpy})_2\text{BC}]\text{Cl}_2$), Control light (blue LED light irradiated) and Light (treated with $[\text{Ru}(\text{bpy})_2\text{BC}]\text{Cl}_2$ photo activated).

Table 3.9. Effect of Ru(II) treatment on DNA in A375 cells. DNA damage in A375 cells exposed to No treatment (CD), [Ru(bpy)₂BC]Cl₂ dark (D), blue LED light (CL), [Ru(bpy)₂BC]Cl₂ light photo activated (L), PBS and KMnO₄ were measured by the comet assay and CASP (Comet assay software package) was used to measure the parameters present in the table below. Data points denote mean ± SEM. n = 3 from three independent experiments where 50 images were taken at random.

	Negative control (PBS)	Positive Control (KMnO ₄)	CD	D	CL	L
Head Length	225.4±7.9	87.3±1.9	237.5±6.3	247.2±7.4	242.1±10.6	66.3±8.1
Tail Length	33.3±3.5	282.7±17.3	35.3±3.4	36.8±2.9	68.92±6.8	131±6.01
Comet Length	258.7±8.4	370±17	272.7±7.71	277.7±10.3	311.1±13.2	197.4±13
Head DNA content	94.3±0.8	20.3±9.6	94±0.5	90.8±0.8	73.1±1.8	6.7±1.5
Tail DNA content	5.7±0.8	79.7±7.4	6±0.5	9.2±0.8	26.9±1.7	93.3±1.5
Tail moment	2.1±0.4	280.3±13.6	2.5±0.4	3.9±0.5	20.2±2.6	110.7±6.7
Overall Tail Moment	6.9±1.1	162.1±6.9	7.9±0.8	10.5±0.7	46.1±5.5	44.1 ±8.03

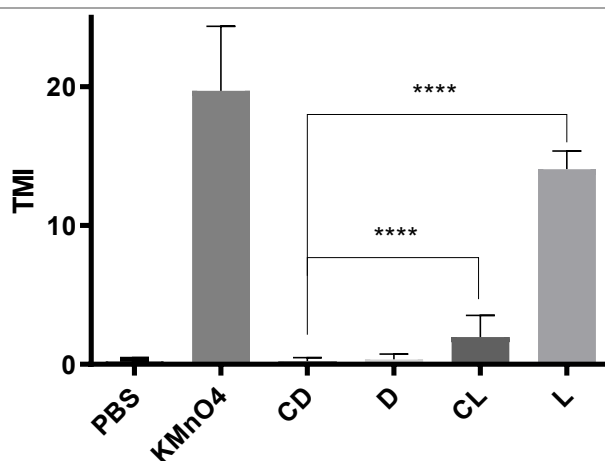
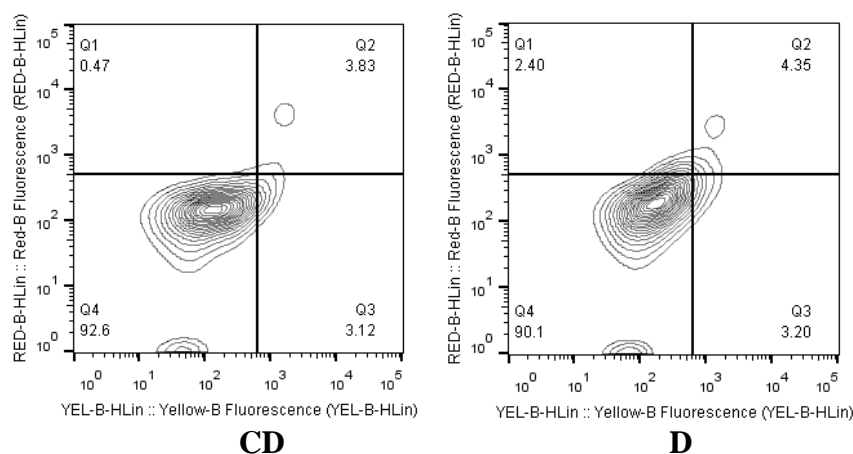


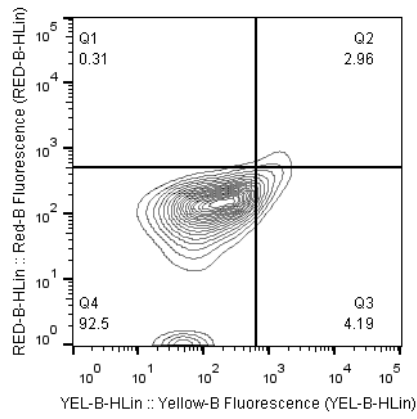
Figure 3.39. Tail moment index as calculated from the comet assay data. (n=3). TMI= [Tail DNA content x Tail length] ÷ 1000. **** indicates P<0.0001 compared with control. Data points denote mean ± SEM. n = 3 from three independent experiments where samples were run in triplicate.

3.9 Flow cytometry

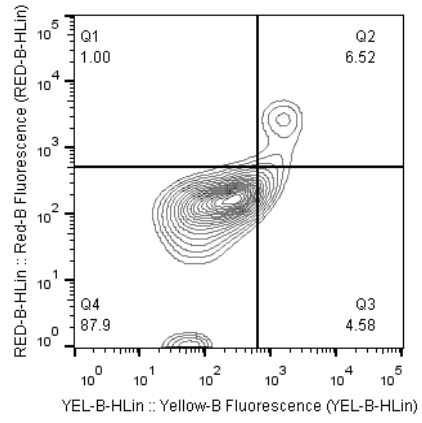
Annexin V/7-AAD staining was used in order to determine the type of cell death following the treatment of A375 cell line with double IC50 of [Ru(bpy)₂BC]Cl₂ light and of cisplatin (positive control). Flow cytometry result demonstrated significant increase ($P < 0.001$ in the percentage of apoptotic cells 48 hours post-treatment with [Ru(bpy)₂BC]Cl₂ light respectively compared to the control cells, while no significant cell death was observed at 24 hours (figure 3.40). These data confirm apoptotic cell death. (Control Dark: CD, Dark prodrug treated: D, Control Blue LED Light: CL, Light prodrug treated: L). One population was negative for both Annexin V and 7-AAD, and stated healthy (quadrant one), while another was either positive for Annexin V and negative for 7-AAD, or Annexin V positive and for 7-AAD positive, stated apoptotic (quadrant two and three respectively). Cells which were Annexin V negative but 7-AAD positive were stated necrotic (Herzenberg, et al., 2006). Cells treated with [Ru(bpy)₂BC]Cl₂ and light irradiated were distinguished to undergo early and late apoptosis significantly identified (***) $P < .001$ versus control group) at 48h post treatment (figure 3.40 & 3.42), leaving around 50% healthy cells, in comparison to cisplatin treated cells at 48h leaving approximately 30% cells healthy.

(A) 24 hours

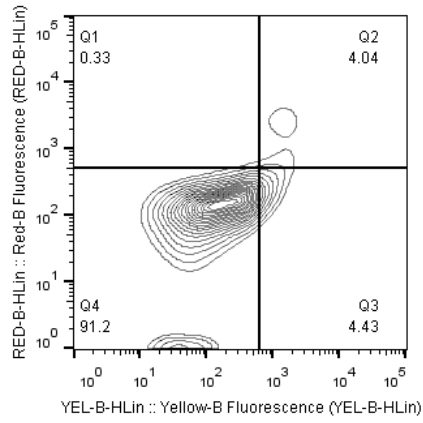




CL

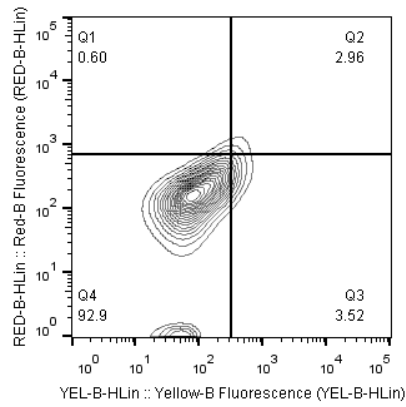


L

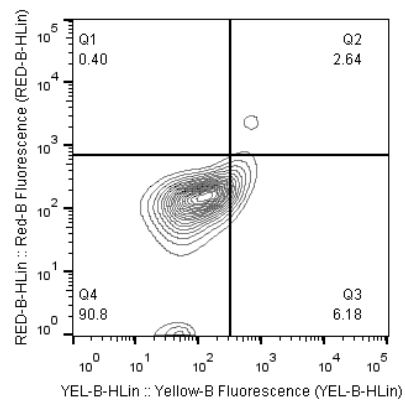


Cisplatin: +ve CTRL

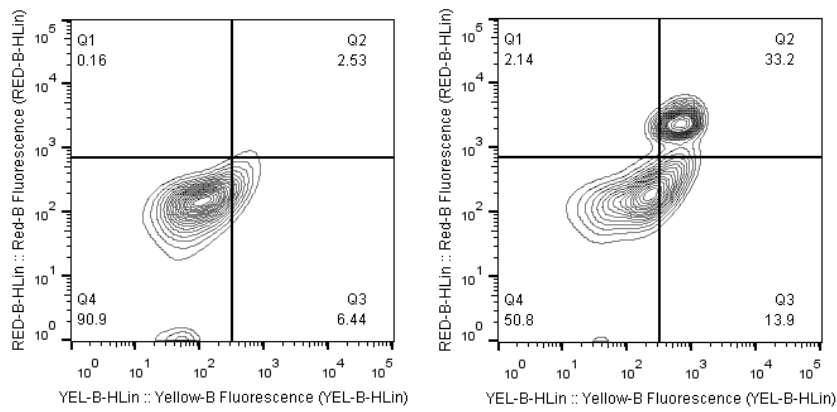
(B) 48 hours



CD

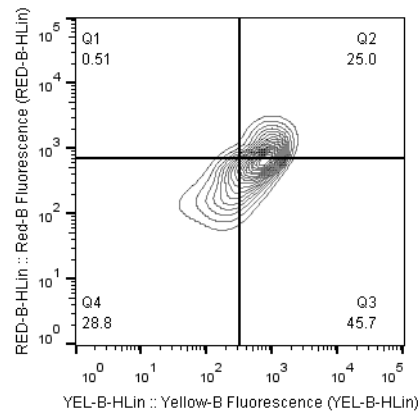


D



CL

L



Cisplatin: +ve CTRL

Figure 3.40. Cell death analysis at 24 and 48 hours. A375 cells were treated with double IC50 concentration to confirm mechanistic cell death. At (A) 24 hours, no significant death was observed, while at (B) 48 hours Annexin+/7AAD+ cells significantly increased in the those treated with [Ru(bpy)₂BC]Cl₂ light irradiation (L) in comparison to the control cells (CD). Data points denote mean ± SEM. n = 3 from three independent experiments where samples were run in triplicate.

24hours

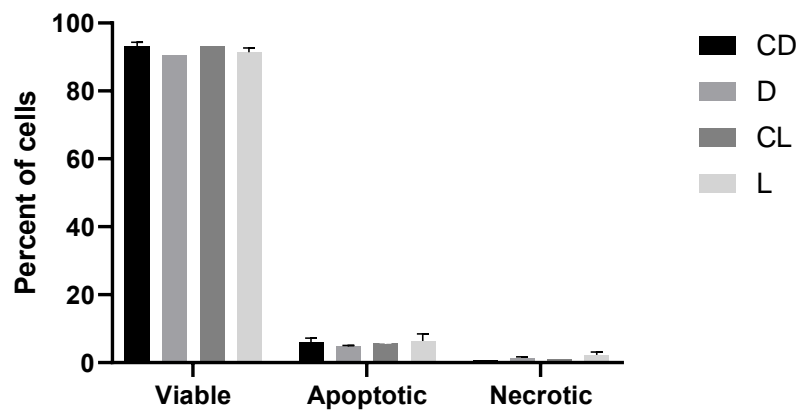


Figure 3.41. Bar graph representing percent viable, apoptotic and necrotic cells

at 24 hours. Data points denote mean \pm SEM. $n = 3$ from three independent experiments where samples were run in duplicates.

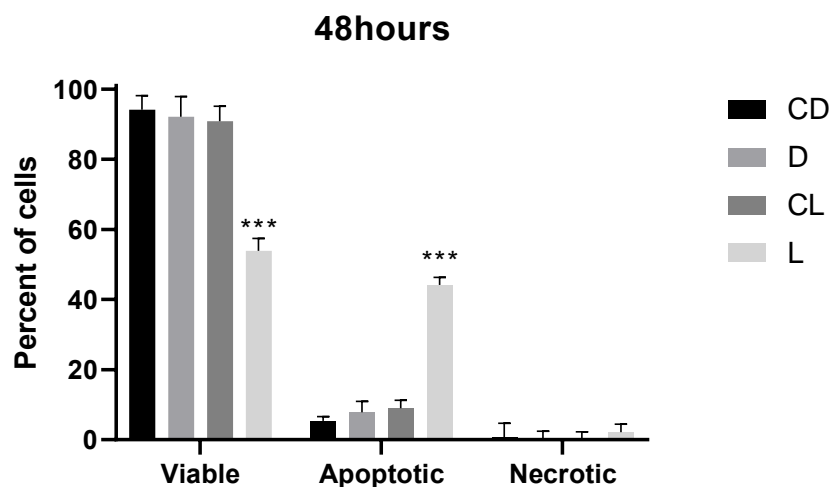


Figure 3.42. Bar graph representing percent viable, apoptotic and necrotic cells at 48 hours. A significant increase of apoptotic cells in Ru(bpy)₂BCl₂ light irradiated (L) cells in comparison to the control cells (CD) was observed. Data points denote mean \pm SEM. $n = 3$ from three independent experiments where samples were run in duplicates. *** $P < .001$ versus Control group, as measured by one-way ANOVA.

3.10 *In Vivo*

3.10.1 Lethal dose

Using the up and down procedure, the lethal dose was found to be in the range of 6-7 mg/kg (figure 3.43). Death at 10 mg/kg was seizure like within 30 minutes (Appendix C). Daily IP injections over a one month period of 0.2 mg/kg, 0.4 mg/kg, 1 mg/kg and 2.5 mg/kg showed no sign of toxicity/death, nor weight loss.

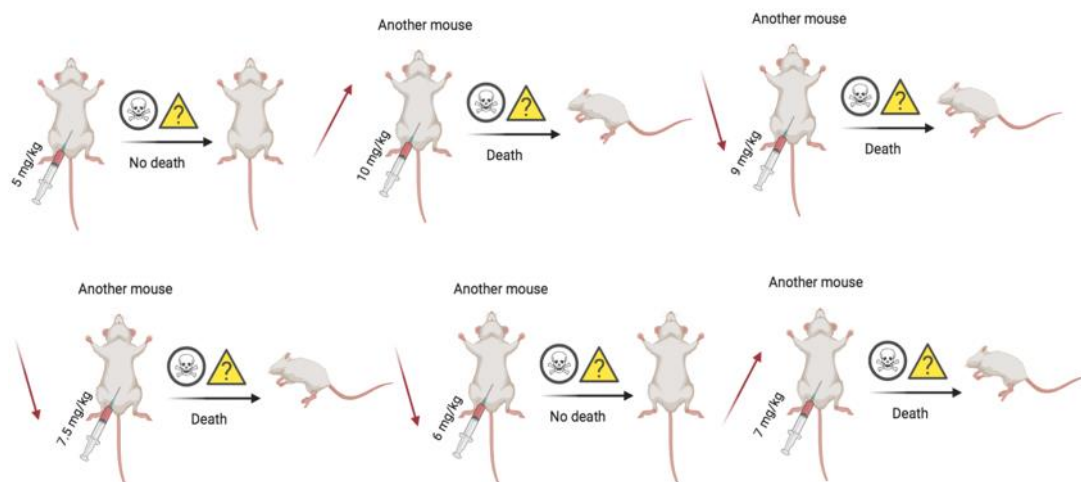


Figure 3.43. Lethal dose obtained via the up and down procedure.

3.10.2 Toxicity

3.10.2.1 Maximum Tolerated dose

Three groups of three mice administered 5, 2.5 or 1.25 mg/kg Ru(bpy)₂BCl₂ and a fourth group (control) was only administered saline for comparison. By week 4, 33% mice remained living, indicating 5mg/kg was not a dose to be considered for treatment.

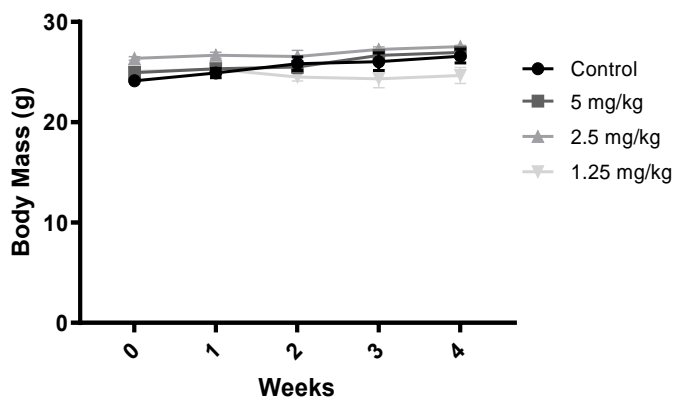


Figure 3.44. Body weight (g) of each mouse measured weekly. No significant decrease in body weight was observed in 5, 2.5 or 1.25 mg/kg [Ru(bpy)₂BC]Cl₂ administered mice in comparison to the control (saline)

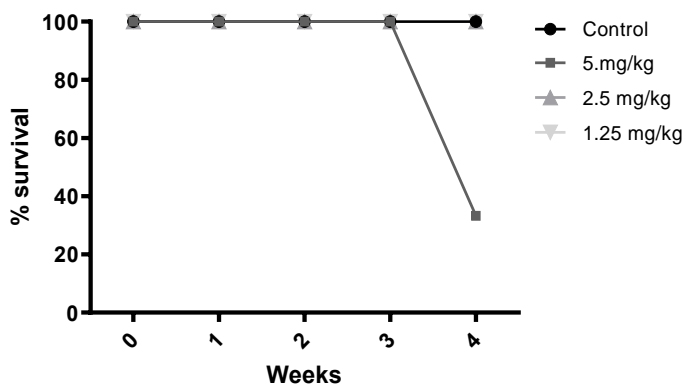


Figure 3.45. Percent survival per group. Survival remained 100% till mid week 4, at which it dropped to 33% after two of three animals in the 5 mg/kg [Ru(bpy)₂BC]Cl₂ administered mice died.

3.10.3 DMBA/TPA model induces skin carcinogenesis

After 12 weeks DMBA/TPA application, all 32 mice showed skin carcinogenesis represented in the images below (figure 3.46)



Figure 3.46. Random five of thirty-two mice represented, twelve weeks' post DMBA/TPA.

3.10.4 Efficacy

Preliminary data is represented up till week 3, while the treatments efficacy is understudy up till 8 wks. A significant decrease in tumor volume and incidence is seen at week 3 in all treated groups with a drastic tumor growth control in G2 and G3 (figure 3.48 and 3.49). In G1 and G4 there was a shift in growth at week 2 which then declined at week 3 (figure 3.49). Tumor incidence has also been significantly decreased at week 3 (figure 3.50).

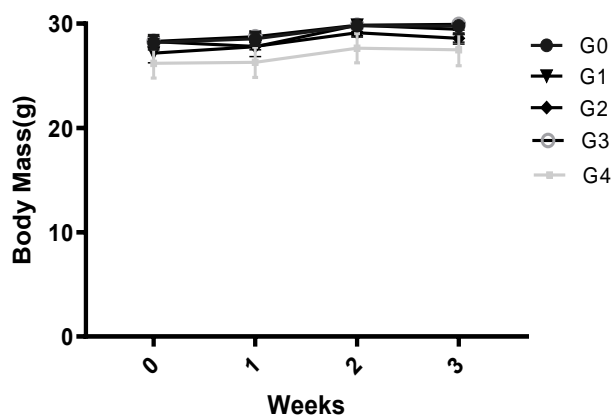





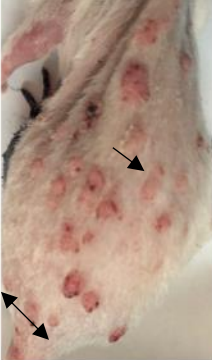

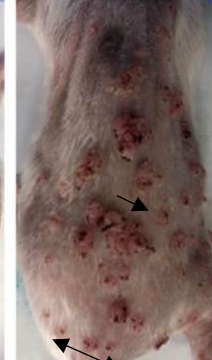
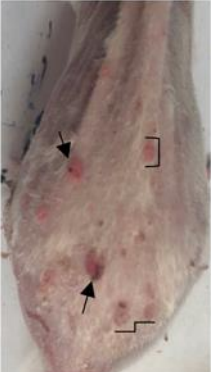

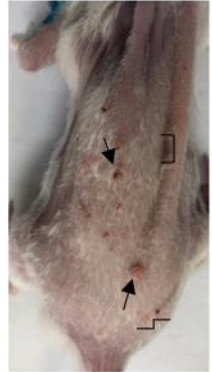



Figure 3.47. Body weight (g) measured weekly per group. No significant change in body weight was observed.

Day 0		Week 3	
G0: Saline			
M1	M2	M1	M2
			
G1: [Ru(bpy)2BC]Cl2 Precursor			
M1	M2	M1	M2
			
G2: [Ru(bpy)2BC]Cl2 photo activated			
M1	M2	M1	M2
			

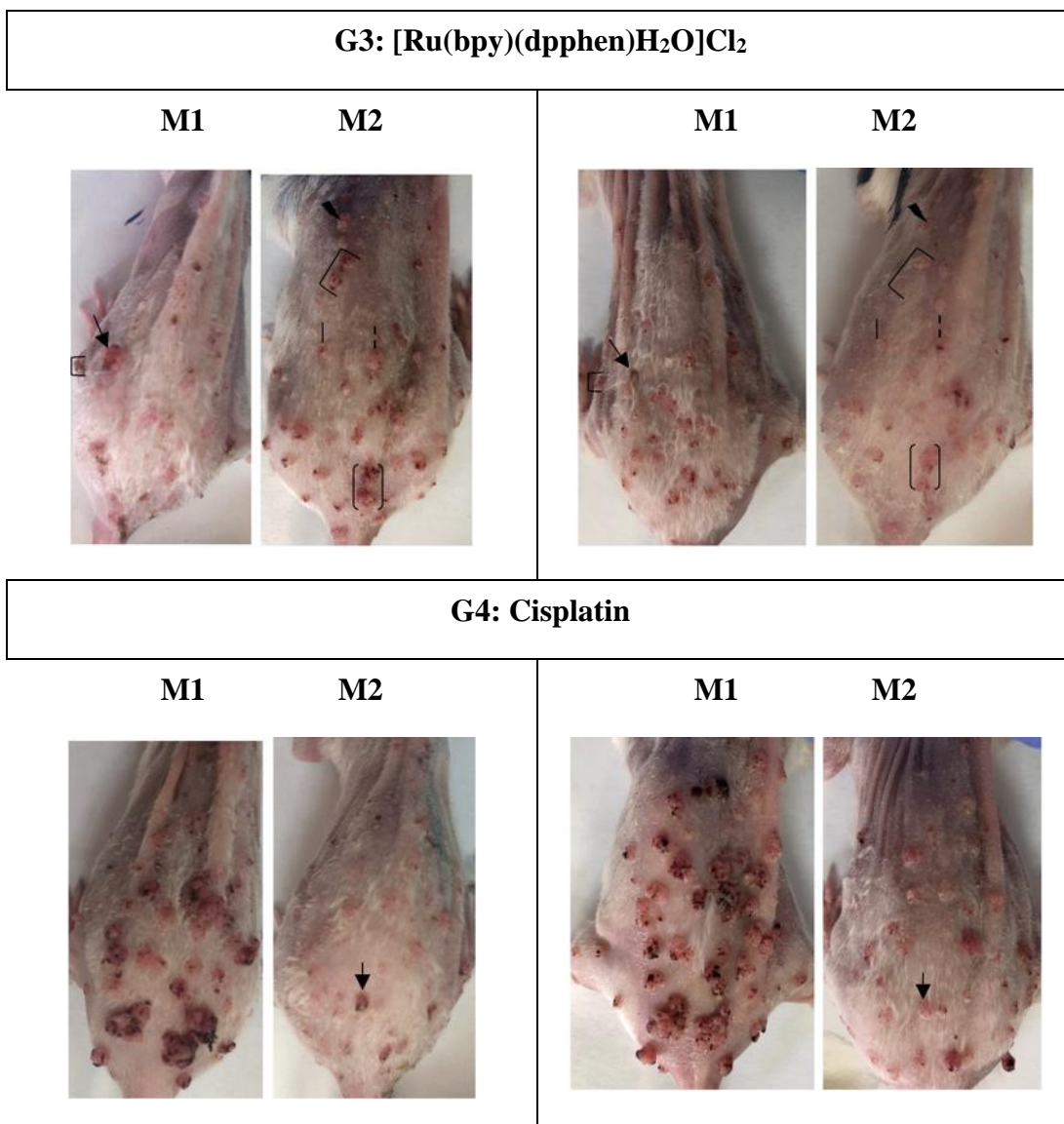


Figure 3.48. Two animals (M1/ M2) represented from each group at day 0 vs. week 4 of treatment. M = balb/c mouse. Arrows, brackets, lines and dashes indicate tumors at day 0 respective to week 3 in M1 or M2.

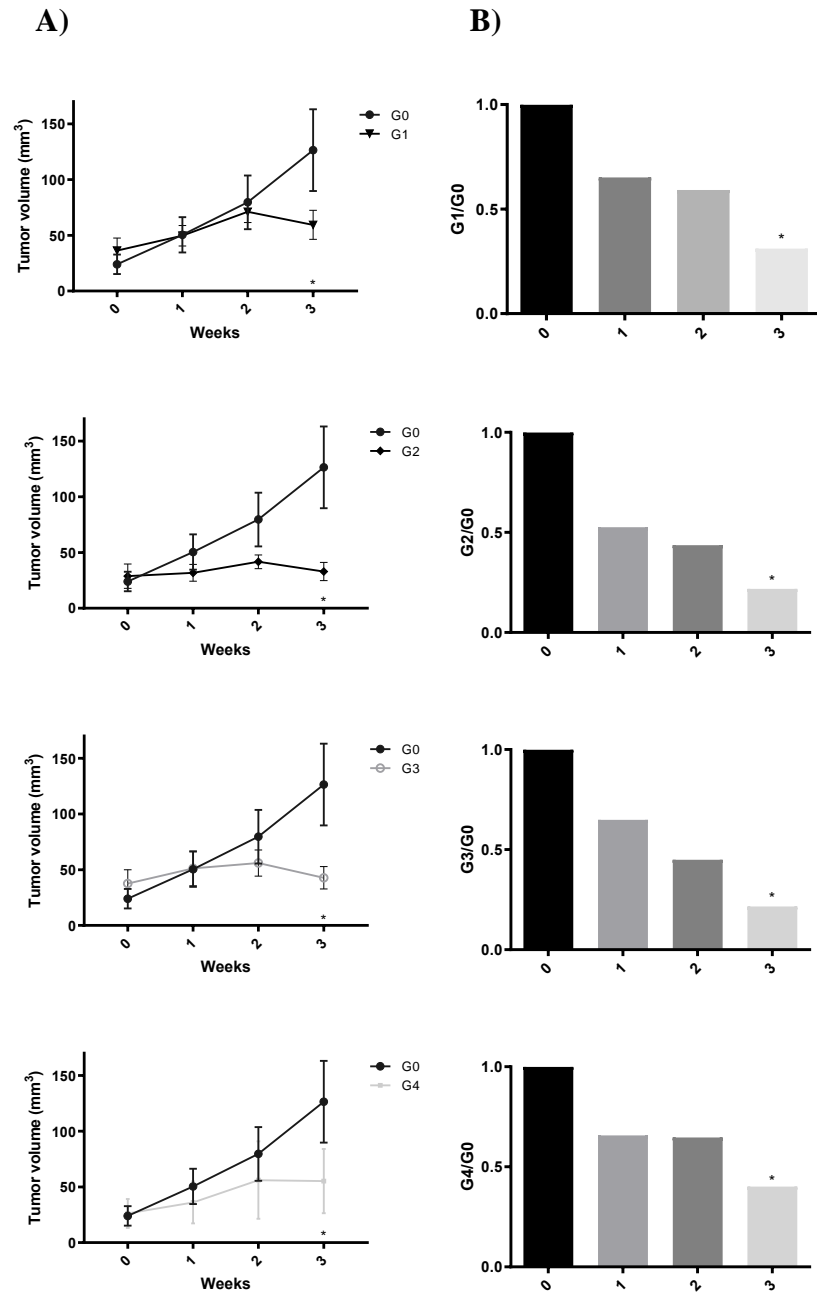


Figure 3.49. Tumor growth in Balb/c mice bearing DMBA/TPA induced skin tumors treated over 3 weeks as described in Table 2.2. Tumor volumes were estimated using a Vernier calliper and a reference model developed in our lab (Shebaby et al., 2017). (A) All groups were compared to the control group (G0) and values represent the mean \pm SEM (n = 6). (B) The fold decrease in comparison to G0 per group. *p < 0.05 versus G0.

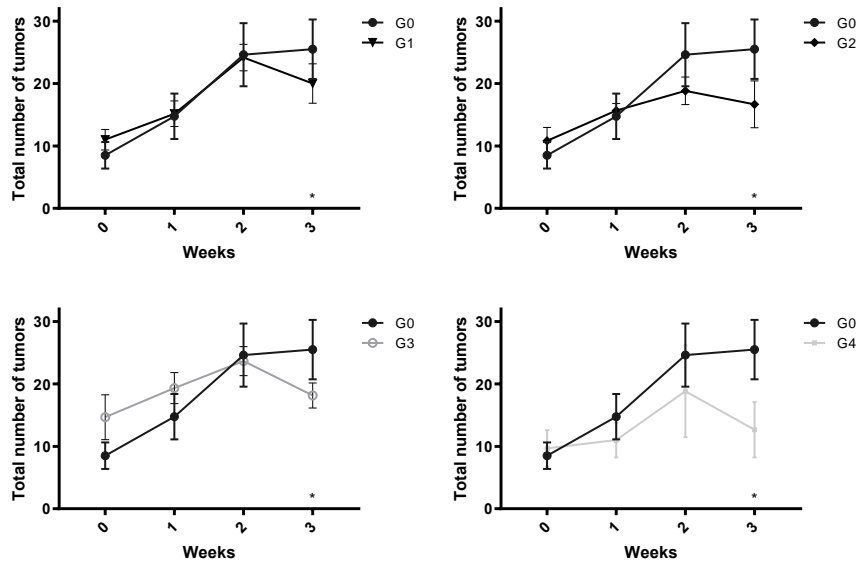


Figure 3.50. Tumor incidence in Balb/c mice bearing DMBA/TPA induced skin tumors treated over 3 weeks as described in Table 2.2. All groups were compared to the control group (G0) and values represent the mean \pm SEM (n = 6). *p < 0.05 versus G0.

Chapter Four

Discussion

Metallo drugs have gained great attention in chemotherapy, after cisplatin and its derivatives successfully treated various cancers (Groessler, et al., 2010; Golla et al., 2017). The platinum based compounds like cisplatin, which exhibited biological side effects, and acquired resistance against various cancers, reinvigorated the design of substitute metal complexes that may be less toxic (Hanif, et al., 2018; Galluzzi, et al., 2012). Ruthenium based complexes were developed upon their distinctive properties, and were predominantly tempting for the use in PACT, as they are easily altered photo-physically, kinetically inert and hold great absorption in the visible range (Mansouri, et al., 2003; Howerton et al., 2012; Mehanna, et al., 2019; Mansour, et al., 2018; Fayad et al., 2020). Once a Ru(II) polypyridyl complex holding an octahedral geometry is irradiated, its Ru-N bond will break, allowing ligand dissociation (Mari, et al., 2015; Mehanna, et al., 2019). The foremost purpose of PACT, is to produce local phototoxicity, to minimize cellular death in non-irradiated tissues (Dickerson et al., 2014). PACT provokes cytotoxicity through various mechanisms such as, the aquated complex formed via ligand photodissociation, or its active molecules caged by the metal center, binding DNA (Bonnet, et al., 2018; Mehanna, et al., 2019).

This study explores the photophysical and photochemical possessions of Ru(II) bipyridyl compounds and the photochemotherapeutic potentials of $[\text{Ru}(\text{bpy})_2\text{BC}]\text{Cl}_2$ in addition to the derivation and potential of $[\text{Ru}(\text{bpy})(\text{dpphen})\text{H}_2\text{O}]\text{Cl}_2$ from $[\text{Ru}(\text{bpy})_2\text{dpphen}]\text{Cl}_2$ *in vitro* and *in vivo*. $[\text{Ru}(\text{bpy})_2\text{phen}]\text{Cl}_2$ was used as an unstrained control, while the preceding complexes studied were strained via phenyl or methyl groups on the phenanthroline ligand at the 2,9-positions.

$[\text{Ru}(\text{bpy})_2\text{BC}]\text{Cl}_2$, a novel strained Ru(II) bipyridyl complex, was sterically hindered by the bathocuproine (2,9-Dimethyl-4,7-diphenyl-1,10-phenanthroline) ligand, and distorted the octahedral geometry of this compound, assembling it unstable photochemically, hence prone to photolysis, yet protected if not exposed to light (Mehanna, et al., 2019).

The absorption spectrum of $[\text{Ru}(\text{bpy})_2\text{BC}]\text{Cl}_2$ (Figure 3.18) and $[\text{Ru}(\text{bpy})_2\text{dpphen}]\text{Cl}_2$

(Figure 3.5) complexes presented maximal absorbance at 280 nm (the UV range) ascribed to the intra-ligand π to π^* transition and at 450 nm at which the MLCT (metal to ligand charge transfer) excitation followed (Mansour et al., 2018; Mehanna, et al., 2019). This was the basis for choosing to photo activate the compound using a blue LED light with a peak wavelength of 460 nm (100 mW/cm²). When investigating the *in vivo* photo activation strategy, penetration is an important consideration, as there is a maximal penetration among different tissue. Superficial tumors, may be considered for blue wavelength associated treatments, yet deeper tissue, would require an irradiated wavelength in the infrared range (650-850 nm) as it holds better penetrance (Szaciłowski, et al., 2005). This suggests that the present complexes of this study are best fit for superficial tumors.

Complexes [Ru(bpy)₂phen]Cl₂, [Ru(bpy)₂BC]Cl₂, [Ru(bpy)₂dpphen]Cl₂ were synthesized according to modified procedures, and their photochemistry and purity were identified and confirmed by ¹H NMR (Appendix A) post synthesis, at which a counter ion exchange mechanism was then implemented to conform solubility in water between hexafluorophosphate and chloride, to be biologically efficient. Noticing each compound was purified using different stationary phases of column chromatography, dependent on size (sephadex LH-20), and polarity (silica/alumina) of the molecule (Mansour et al., 2018; Mehanna et al., 2019).

The ability to characterize the photoproduct of [Ru(bpy)₂dpphen]Cl₂ upon intracellular photoactivation and understand the cytotoxicity behind the complexes PACT potential lead to the novel isolation and purification of [Ru(bpy)(dpphen)H₂O]Cl₂ from the photo activation of [Ru(bpy)₂dpphen]Cl₂, to be studied as a promising chemotherapeutic agent. Generating this ruthenium based complex, having a 5-coordinate bond due to the ligand ejection (BPY) upon irradiation and aquation (Akatsuka, et al., 2019). The kinetic photoactivation of [Ru(bpy)₂dpphen]Cl₂ in LCMS- grade water, seen in figure 3.5, 3.6 demonstrate the transition from a six-coordinate Ru(II) bipyridyl complex to a five-coordinate Ru(II) bipyridyl complex. Time points 0 (for comparison), 15, 30, 45 and 60 min were looked at on an ESI-MS/MS obtained spectra (figure 3.8 and 3.9), and studied for the definite formation of the aquated photoproduct, at which a time dependent manner ensured the photo formation and reduction in the abundance of the precursor. The purification method

was extensively studied for the isolation of $[\text{Ru}(\text{bpy})(\text{dpphen})\text{H}_2\text{O}]\text{Cl}_2$ from the precursor $[\text{Ru}(\text{bpy})_2\text{dpphen}]\text{Cl}_2$ and the ligand bpy. Sephadex LH-20, silica and aluminium oxide for column chromatography were all attempted with different mobile phases. Aluminium oxide, was found to be the best stationary phase using a mobile phase of dichloromethane to methanol (99.7:0.3) (Laemmel, Collin & Sauvage, 1999). Noting the use of methanol, will allow the counter-ion exchange between water and methanol and no form of exchange of chlorine (unlike chloride) from dichloromethane, making it the best fit. Two sequential columns were made. The first purification isolating, the precursor from the photoproduct $[\text{Ru}(\text{bpy})(\text{dpphen})\text{CH}_3\text{OH}]\text{Cl}_2$ and the ligand and the second purifying the photoproduct $[\text{Ru}(\text{bpy})(\text{dpphen})\text{CH}_3\text{OH}]\text{Cl}_2$ as seen in figure 3.14. Once the compound was obtained, the solubility and exchange was tested in nothing but methanol and water. Water was used to dissolve the solid $[\text{Ru}(\text{bpy})(\text{dpphen})\text{CH}_3\text{OH}]\text{Cl}_2$, as it holds great ionizing power, enforcing the exchange by sonication and was not chosen to dissolve in another to avoid counter-ion exchange of another form. The cytotoxic effect of $[\text{Ru}(\text{bpy})(\text{dpphen})\text{H}_2\text{O}]\text{Cl}_2$ which has a $\text{LogP} = -2.77 \pm 0.05$ (Table 3.1) has an IC_{50} of 10.52 ± 1.4 (figure 3.24) showing some toxicity on A375 in reference to the precursor in the dark with an IC_{50} of 71.83 ± 1.6 with a phototoxicity index of 50.2 (IC_{50} of the photo activated precursor was 1.43 ± 1.2) (figure 3.23). The mechanistic cell death associated with $[\text{Ru}(\text{bpy})_2\text{dpphen}]\text{Cl}_2$ photoproducts, exhibiting an apoptotic cell death has recently been reported (Masnour et al., 2020), yet the isolated aquated photoproduct is to be further investigated on various cell lines as well as its mode of death. Primary studies of $[\text{Ru}(\text{bpy})(\text{dpphen})\text{H}_2\text{O}]\text{Cl}_2$ on a skin carcinogenesis model is being undertaken, by administering 2.5 mg/kg in reference to cisplatin (2.5 mg/kg) to which results will be reported. In our lab, groundwork has shown the prodrug; $[\text{Ru}(\text{bpy})_2\text{dpphen}]\text{Cl}_2$ was lethal at a dose of 2.5 mg/kg as well as 1.5 mg/kg after a month of studying its MTD. $[\text{Ru}(\text{bpy})_2\text{dpphen}]\text{Cl}_2$ photoproduct reached a maximal of 5 mg/kg IP and IV and still showed no sign of death indicating the dose of choice for the purified aquated photoproduct.

The potential that $[\text{Ru}(\text{bpy})_2\text{BC}]\text{Cl}_2$ held as a photo activated cancer therapeutic (Mehanna et al., 2019) led to the further examination of the mechanism of cell death. The cell line A375 (human melanoma), was chosen for *in vitro* studies, as it holds the

closest characteristics to the skin carcinogenesis model which was to be implemented after the understanding of $[\text{Ru}(\text{bpy})_2\text{BC}]\text{Cl}_2$ hypothetical mechanistic cell death, to then study its efficacy *in vivo*.

Foremost, findings have shown that metal complexes cellular uptake improved with lipophilicity (Puckett & Barton, 2007). The LogP (partition coefficient) between the octanol (hydrophobic) and water (hydrophilic) phases were measured to establish the scope of lipophilicity defying the cellular uptake. Comparing to the unstrained control; $[\text{Ru}(\text{bpy})_2\text{phen}]\text{Cl}_2$, its LogP was found to be -2.82 while $[\text{Ru}(\text{bpy})_2\text{BC}]\text{Cl}_2$ was LogP = -1.57, which showed significant lipophilicity in comparison. The greater lipophilicity was due to the BC ligand having a LogP = 6.96 ($\text{IC}_{50} = 51.9 \pm 1.4$) conferring the immediate uptake of $[\text{Ru}(\text{bpy})_2\text{BC}]\text{Cl}_2$ precursor at 0h ($136 \mu\text{M}/\text{cell}$; figure 3.19) compared to its photoproduct ($23 \mu\text{M}/\text{cell}$; figure 3.19) in A375 cells. Noting $[\text{Ru}(\text{bpy})_2\text{dpphen}]\text{Cl}_2$, held a LogP = -2.53, it did not show any sign of uptake after immediate incubation with the precursor at 0h on A549 cells. $[\text{Ru}(\text{bpy})_2\text{phen}]\text{Cl}_2$ showed minimal uptake through cell membranes owing to its rather hydrophilic associated LogP value (Table 3.1) and associated IC_{50} (>100 ; table 3.5) (Mansour, et al. 2018, Mehanna et al., 2019). Figure 3.19 demonstrated the intracellular comparison of $[\text{Ru}(\text{bpy})_2\text{BC}]\text{Cl}_2$ precursor vs photoproduct. At 24 hours, the intracellular concentration of the precursor was $1566 \mu\text{M}/\text{cell}$, 522 folds greater than the extracellular concentration ($3 \mu\text{M}$), whilst the photoproducts only showed an intracellular concentration of $287 \mu\text{M}/\text{cell}$ at 24 hours and 95-fold greater than the extracellular concentration ($3 \mu\text{M}$).

$[\text{Ru}(\text{bpy})_2\text{BC}]\text{Cl}_2$ has a PACT potential due to its significant uptake and photochemical characteristics, yet, it is to be efficient, should the compound be activated intracellularly, prompting selective toxicity, thus curtailing side effects (Dickerson, et al., 2014). This was first assessed by studying the cytotoxicity *in vitro* on A375 cells and presenting a phototoxicity index (PI) of 339 ($\text{PI} = \text{IC}_{50} \text{ dark} / \text{IC}_{50} \text{ light}$). It is noteworthy that the dissociative ligand BPY held no effect on A375 cell lines (LogP = 1.88 and $\text{IC}_{50} >100$). To further assure the photolysis effect of the complex on A375 cells be due to the intra-activated complex, only the intracellular complex was photo irradiated and its cytotoxic effect compared to (Light; figure 3.23) that which was irradiated while still having non-uptaken precursor in the medium. No significance

was observed indicating irradiated complex in the medium did not confer the major cytotoxic effect. To further convene this, the complex was irradiated in media on a separate plate and then the photoproducts formed were then moved to the seeded cells to obtain their cytotoxicity ($IC_{50} = 15.74 \pm 1.3$; table 3.7, figure 3.23).

Pathways which $[Ru(bpy)_2BC]Cl_2$ can use as a route to enter cells, can be via the simple passive diffusion; down the concentration gradient, facilitated diffusion; via channels and carriers, active transport; using transport proteins or ATP power driven pumps versus the concentration gradient or by endocytosis; vesicular formation via the cell membrane (Kunjachan et al., 2014). The mode of uptake of $[Ru(bpy)_2BC]Cl_2$, suggested an active mode of transport considering its high intracellular concentration. This was set after observing a significant decrease in the precursors uptake at 4 °C, showing its obstruct of energy dependent, active mechanisms of transport (Puckett & Barton, 2007; Puckett & Barton, 2008). While the intracellular concentration did substantially decrease, it is still 110 folds greater than the extracellular concentration (3 μM), which proposes $[Ru(bpy)_2BC]Cl_2$ may also use another route of transport, as well as not achieving complete inhibition at 4 degrees (Puckett & Barton, 2007; Ghezzi, et al., 2004). A significant decrease is also observed in the transferrin receptor mediated uptake, indicating the complex would freely use this passage to enter (figure 3.20). This has been suggested and demonstrated on KP1019, a ruthenium based drug which used the transferrin receptor as the route of entry to cells. To further confirm our complexes route of entry via the transferrin receptor, complex KP1019 or iron itself can be used for comparison, for future implementations (Li & Qian, 2002). The mechanism of transport remains to be further clarified as a dual mechanism of transport seems to be the case. Substitute receptor-mediated paths like the Epithelial growth factor receptor (EGFR), or Low density lipoprotein (LDL) receptors, lipid raft/caveolae-mediated endocytosis (inhibit using Nystatin and Dynasore) or clathrin-mediated endocytosis using sucrose to block the route can be further looked into (Xiaoning, et al., 2018).

ROS formation may be formed by the disturbance of the membrane potential of the mitochondria or cell anti-oxidant system hindering. The production of ROS has been associated with type I programmed cell death (apoptosis), type II programmed cell death (autophagy) and type III programmed cell death (necroptosis) (Perillo et al.,

2020). Transition metal based complexes like ruthenium and platinum generated ROS and thus hydroxyl radicals producing oxidative DNA adducts (Cadet & Davies, 2017). ROS production was not exhibited in A375 cells treated with $[\text{Ru}(\text{bpy})_2\text{BC}]\text{Cl}_2$ in the dark but showed a significant production of ROS in $[\text{Ru}(\text{bpy})_2\text{BC}]\text{Cl}_2$ treated and light irradiated cells ($P < 0.0001$), 3-folds greater than TBHP (positive control). The control irradiated cells also showed a significant increase in ROS production ($P < 0.01$) (figure 3.25). The production of ROS due to blue light itself has been reported on melanoma cells in PDT and PACT (Akasov, et al., 2019; Hopkins, et al., 2016).

Western blots were performed to determine the route of cell death, which $[\text{Ru}(\text{bpy})_2\text{BC}]\text{Cl}_2$ holds as a PACT, conferring its potency. The intrinsic path, was first studied, by studying the protein expression of Bax and Bcl-2. The increase in Bax levels moved to the mitochondria, consequently increasing the cytochrome c release, whilst having low Bcl-2 levels, preventing the apoptotic inhibition (Shamas-Din, et al., 2013; Kilbride & Prehn, 2013). After a 24-hour incubation with $[\text{Ru}(\text{bpy})_2\text{BC}]\text{Cl}_2$ treated in the dark and light, no effect was observed in neither the expression of Bax nor Bcl-2, nor its ratio (Bax/Bcl-2; figure 3.29). Yet, after 48 hours, a 3-fold increase was observed in the protein level of Bax, yet Bcl-2 was still relatively functional, still showing a significant increase in the Bax/Bcl-2 ratio. When A375 cells were incubated 72 hours with irradiated $[\text{Ru}(\text{bpy})_2\text{BC}]\text{Cl}_2$, a noticeable increase was observed in Bax (15-folds) and a significant decrease in Bcl-2 was associated, inferring a Bax/Bcl-2 ratio of 60 folds, in comparison to the control cells (figure 3.27, 3.28, 3.29). The increase in mitochondrial cytochrome c release starting at 48h was the result of pro-apoptotic Bax surge at 48h, yet was not significantly increased till 72h post-treatment in comparison to the control (figure 3.30).

The executioner caspase, caspase 3, and end point of the intrinsic and extrinsic pathways, is an important event of apoptosis, as it holds effector caspase activity to downstream proteins, promoting cellular death (Walsh, et al., 2008). Western blot quantifications have shown a significant increase in cleaved caspase3 of the cells treated with $[\text{Ru}(\text{bpy})_2\text{BC}]\text{Cl}_2$ light irradiated (L) (figure 3.31) starting at 48h as well as in the control light treated cells (CL). At 72h cleaved caspase 3 showed an 8.3-fold increase in $[\text{Ru}(\text{bpy})_2\text{BC}]\text{Cl}_2$ light irradiated (L) cells, pounding the effect observed in light irradiated cells (CL) at 48h (figure 3.31). This infers the most efficient effect of apoptotic markers, was prominent at 72 hours.

Downstream of caspase 3 is an essential controller of apoptosis; PARP (Poly [ADP-ribose] polymerase 1), whose activated cleavage is associated with an increase in DNA disintegration in the nucleus and consequently cell death (Stennicke, et al., 1998; Caron et al., 2019). The cleavage of caspase 3 successively cleaves PARP (Segawa, Suzuki & Nagata, 2011). Analysis of the western blots (figure 3.32) expressed a significant increase in light treated (L) vs control light irradiated cells post 48 hours, at which a surge increase (14-folds) was not to be missed at 72 hours in the [Ru(bpy)₂BC]Cl₂ light irradiated (L) cells. This reinforces the observant apoptotic initiation at 48 hour and definite surge at 72 hours.

Caspase 3 is capably activated via an extrinsic pathway, primarily by the DISC complex activating procaspase 8. The stimulation of caspase 8 can either immediately activate caspase 3 or it can activate and cleave Bid, which will assist the discharge of cytochrome c from the mitochondria, consequently activating the intrinsic apoptotic path (Raychaudhuri, 2014; Park, 2012; Twiddy, et al., 2004). To observe whether this is applicable in the PACT treatment of [Ru(bpy)₂BC]Cl₂, procaspase 8 expression was quantified by western blotting (figure 3.33). Comparing to control cells and dark treated [Ru(bpy)₂BC]Cl₂, procaspase 8 was significantly downregulated in light irradiated [Ru(bpy)₂BC]Cl₂ treated A375 cells post 72 hours. This infers the activation of both intrinsic and extrinsic pathways at 72 hours post treatment of light treated cells. These were also the routes of cell death observed in the PACT potential of [Ru(bpy)₂dpphen]Cl₂ on MDA-MB-231 cells (Mansour et al., 2020).

The tumor suppressor p53 which controls the pro-apoptotic Bcl2 family members; Noxa and Puma, has control on many downstream protein like p21 (Ruhul, et al., 2015). Cyclin dependent kinases which hold an important role in cell cycle progression and, subsequently, proliferation is constrained by the universal inhibitor p21, which is essential in arresting cells in their G1 and G0 phases of the cell cycle post DNA damage (Han, et al., 2002). This being said, p21 was quantified at 72-hours post [Ru(bpy)₂BC]Cl₂ light irradiated treated (L) A375 cells (figure 3.34), knowing apoptosis was most significantly active at this time point. It was noticeably upregulated in comparison to the control cells.

As demonstrated in figure 1.3, Ras-ERK and PI3K-Akt have been associated with cell survival, and the ability to control cellular invasion and migration (Azad et al., 2010).

The downstream effectors of both pathways are capable and linked to effectors of apoptosis. Substrates that are controlled by ERK include Bid/ Bax and p21. The phosphorylation and activation of ERK (P-ERK), commits its translocation to the nucleus transcribing survival genes (Kondoh, et al., 2007; Sabio & Davis, 2014). Thus, the inhibition of P-ERK has been associated with the active apoptotic proteins, keeping P-ERK localized to the cytoplasm. The production of ROS has been linked to DNA damage, increasing p53 and subsequently p21 activity controlled by ERK (Subramaniam et al., 2004; Sabio & Davis, 2014). Western blot analysis of P-ERK/ERK was analysed at 72-hours post treatment (figure 3.35), exhibiting significant decrease/ inhibition of P-ERK, promoting apoptosis. The phosphorylation and activation of AKT inhibits apoptosis by preventing caspase 9 activity (important in activating and cleaving caspase 3), and inhibit MDM2 which will consequently down regulate p53 (Shi, et al., 2012). Western blot analysis of P-AKT/AKT showed significant inhibition of both dark (D) and light (L) treated [Ru(bpy)₂BC]Cl₂ (figure 3.36), inferring an apoptotic mechanism. Noting the significant inhibition in the dark treated A375 cells, holds a potential for [Ru(bpy)₂BC]Cl₂ as a chemotherapeutic agent considering its low toxicity (IC₅₀ 43.1 ± 1.3).

A complex made of the autophagic protein Beclin-1, and Bcl-2, the anti-apoptotic protein is associated with the inhibition of autophagy-related cell death. This phosphorylated inhibition of Bcl-2 allows for the crosstalk between apoptosis and autophagy (Marquez & Xu, 2012; Chen, et al., 2019). Noting the significant downregulated expression of Bcl-2 at 72 hours (figure 3.28), can explain the overexpression of Beclin-1 at 72 hours (figure 3.37), indicating the existence of both apoptotic and autophagic cell-death. Further proteins related to autophagy are to be studied. Noting the link of autophagy to AKT and mTOR (figure 1.3), the triggered activation of AKT, will phosphorylate and inhibit TSC1/2 thus, inducing mTOR and cell survival. Figure 3.36 demonstrates the significant inhibition of P-AKT/AKT, indicating, most probable inhibition of mTOR thus activating autophagy associated markers (Huang and Manning, 2008; Alayev and Holz, 2013).

Conferring the production of ROS (figure 3.25), the effect of [Ru(bpy)₂BC]Cl₂ on DNA damage was measured both on dark and light treated (irradiated) A375 cells using the comet assay (Hageh, et al., 2018). The DNA of healthy cells, remains

supercoiled and confined to the nucleus at which it is not affected and will not migrate upon electrophoresis. Cells having damaged DNA, will leave the nucleus (comet head), representing a longer migration upon electrophoresis generating a comet tail (Lu, et al., 2017; Hageh et al., 2018). Silver staining, provides the microscopic images for the observation of cells having damaged DNA, which show greater tail length, tail DNA content, overall tail moment and tail moment index (TMI). Only after $[\text{Ru}(\text{bpy})_2\text{BC}]\text{Cl}_2$ was light irradiated in A375 cells, did a significant ($P < 0.0001$) DNA damage occur, as calculated from the TMI (figure 3.39, table 3.9) and observed in the microscopic images (LIGHT; figure 3.38). No DNA damage was detected in dark treated cells, having DNA condensed at the comet head (DARK; figure 3.38). The effect seen in light treated cells was not attributed to light itself as slight damage was observed in comparison to that irradiated with $[\text{Ru}(\text{bpy})_2\text{BC}]\text{Cl}_2$. These results reflect that observed in the ROS production (figure 3.25). Various studies have stressed the part of DNA modifications by metal-based aqua complexes and their effect on cell cytotoxicity, and associated apoptotic characteristics (Han et al., 2002; Garner, et al., 2011; Sabio & Davis, 2014; Haghe, et al., 2018). The results we obtained are in line with other ruthenium based complexes like, $\text{Ru}(\text{bathophenanthroline})_3$, and more, which showed to have great affinity to binding DNA, subsequently DNA damage upon treatment (Komor & Barton, 2013; Dickerson et al., 2014; Cadet & Davies, 2017).

To confirm the mode of cell death, induced by $[\text{Ru}(\text{bpy})_2\text{BC}]\text{Cl}_2$, flow cytometry was done on A375 cells. Annexin V and 7-AAD known to bind phosphatidylserine (PS) on the outer leaflet of the cell membrane (a hallmark of apoptotic cell death) and DNA respectively, were used to bind and fluoresce to detect percent apoptotic or necrotic cells (Leber, et al., 2012; Zemruski, et al., 2012). Cisplatin was used as a positive control, knowing its apoptotic choice of cell death (Basu & Krishnamurthy, 2010; Del Bello, et al., 2013). Cells were distinguished as populations of cells. No significant effect was observed in that of dark treated cells (D) nor in light irradiated cells (CL) (figure 3.40 B & 3.42). Noticing very little death at 24h post treatment in all conditions (figure 3.40 A & 3.41), including cisplatin leaving roughly 90% healthy cells. Cells treated with $[\text{Ru}(\text{bpy})_2\text{BC}]\text{Cl}_2$ for 72 hours, dark vs. light remain to be investigated. Many PACT ruthenium complexes showed similar mode of cell death, like $[\text{Ru}(\text{bpy})_2\text{dpphen}]\text{Cl}_2$, which was pro-apoptotic on MDA-MB-231 cells most

effectively starting at 48h and similar at 72h, with no significant death at 24h (leaving 94% healthy cells) (Mansour et al., 2020).

The Lethal dose of $[\text{Ru}(\text{bpy})_2\text{BC}]\text{Cl}_2$, was obtained via the UDP (Erhirhie, et al., 2018). Preliminary studies of daily IP injections over a one month period of 0.2 mg/kg, 0.4 mg/kg, 1 mg/kg and 2.5 mg/kg showed no sign of toxicity/death, nor weight loss. This directed a starting dose of 5 mg/kg, at which no death was obtained, to then move to 10mg/kg and observe seizure like death. The lethal dose was obtained to be in the range of 6-7 mg/kg, observing death at 7 mg/kg (Figure 3.43; Appendix C).

The Maximum tolerated dose of $[\text{Ru}(\text{bpy})_2\text{BC}]\text{Cl}_2$ was then studied over 28 days, showed no sign of physical or behavioural changes in all groups except that of the group administered 5 mg/kg $[\text{Ru}(\text{bpy})_2\text{BC}]\text{Cl}_2$, at which two of three mice died on the 23rd day. This indicated a one month period of 5 mg/kg has caused some form of intoxication to be further studied. Accordingly, the dose of treatment was decided (table 2.2).

A BALB/c mouse, skin cancer model was induced by multi-stage DMBA/TPA chemical carcinogenesis following a modified protocol (Kwitniewski, et al., 2009). After 12 weeks, mice were divided into five groups (table 2.2), ensuring a homogeneous division of tumors in each group. Five random images in figure 3.46, are shown 12 weeks after two rounds of DMBA (initiator) and continual TPA (pro-inflammatory) indicating all 32 mice developed skin carcinogenesis. TPA was added topically twice a week over the course of the experiment to avoid tumor regression (Kong & Xu, 2018). This model was designed to test the efficacy of $[\text{Ru}(\text{bpy})_2\text{BC}]\text{Cl}_2$ photo activated chemotherapeutic potential and test the chemotherapeutic potential of $[\text{Ru}(\text{bpy})(\text{dpphen})\text{H}_2\text{O}]\text{Cl}_2$ over a period of 8 weeks. This study is to be yet completed, but records of up till three weeks are reported. At 3 weeks' post treatments, all groups have exhibited a significant decrease in tumor volume in reference to the control. The tumor growth has been controlled greatly in G2 in and G3 in comparison to G0 from the beginning to week 3 with no surge increase in tumor volume. In G1 and G4 there was a surge increase in tumor volume at week 2 which then was decreased at week 3 indicating the initiation of the treatments activity against carcinogenesis. Tumor incidence has significantly declined in all groups at week 3 (figure 3.50). The study is

to be continued up till 8 weeks of treatment to observe how long the complexes in study can control tumor volume and incidence and if complete regression can be obtained.

Chapter Five

Conclusion

Overall, we have explored the PACT potential of $[\text{Ru}(\text{bpy})_2\text{BC}]\text{Cl}_2$, and isolated $[\text{Ru}(\text{bpy})(\text{dpphen})\text{H}_2\text{O}]\text{Cl}_2$ to study its chemotherapeutic potential. In conclusion, $[\text{Ru}(\text{bpy})_2\text{BC}]\text{Cl}_2$ was found to be more lipophilic than $[\text{Ru}(\text{bpy})_2\text{dpphen}]\text{Cl}_2$, linking to the presence of $[\text{Ru}(\text{bpy})_2\text{BC}]\text{Cl}_2$ at 0h and absence of $[\text{Ru}(\text{bpy})_2\text{dpphen}]\text{Cl}_2$ upon cellular uptake by ICP-MS. The phototoxicity index of $[\text{Ru}(\text{bpy})_2\text{BC}]\text{Cl}_2$ was 339 compared to 39 for $[\text{Ru}(\text{bpy})_2\text{dpphen}]\text{Cl}_2$. The mechanism of $[\text{Ru}(\text{bpy})_2\text{BC}]\text{Cl}_2$ as a PACT was identified, exhibiting the production of ROS, associated with DNA damage detected from comet tail formations, linked to the intrinsic apoptotic pathway. The intrinsic and extrinsic apoptotic pathways identified via flow cytometry exhibiting significant percent of apoptotic cells in $[\text{Ru}(\text{bpy})_2\text{BC}]\text{Cl}_2$ light treated cells after 48 hours of treatment and apoptotic proteins further studied by western blotting. The participation of the MAPK and PI3K pathways exhibited a significant decrease in their phosphorylated substrates, further indicating a pro-apoptotic mechanism. The significant increase in Beclin-1 at 72 hours identifies an autophagy dependent cell death. The efficacy of $[\text{Ru}(\text{bpy})_2\text{BC}]\text{Cl}_2$ PACT and $[\text{Ru}(\text{bpy})(\text{dpphen})\text{H}_2\text{O}]\text{Cl}_2$ chemotherapeutic potential were studied on a skin tumorigenesis model exhibiting significant tumor regression on the third week and is to be further reported after a total of eight weeks of treatment have been finalised. Further studies on the pharmacokinetics and bio-distribution as well as the mode of excretion of $[\text{Ru}(\text{bpy})_2\text{BC}]\text{Cl}_2$ are to be studied to assist drug dosage and most efficient delivery mode. The exhibition of $[\text{Ru}(\text{bpy})_2\text{BC}]\text{Cl}_2$ PACT being cell-line dependent suggests the next model to be designed is a colorectal induced carcinogenic model due to the high cytotoxicity shown on HT-29 cells which are cisplatin resistant (Mehanna, et al., 2019; Hector et al., 2001). Further investigation on the mode of cell death of $[\text{Ru}(\text{bpy})(\text{dpphen})\text{H}_2\text{O}]\text{Cl}_2$ is to be done.

References

- Abou-Ghali, Majdouline & Stiban, Johnny. (2015). Regulation of Ceramide Channel Formation and Disassembly: Insights on the Initiation of Apoptosis. *Saudi Journal of Biological Sciences*, 274. 10.1016/j.sjbs.2015.03.005.
- Abraha, I., Aristei, C., Palumbo, I., Lupattelli, M., Trastulli, S., Cirocchi, R., De Florio, R., & Valentini, V. (2018). Preoperative radiotherapy and curative surgery for the management of localised rectal carcinoma. *The Cochrane database of systematic reviews*, 10(10), CD002102. <https://doi.org/10.1002/14651858.CD002102.pub3>
- Akasov, R., Sholina, N., Khochenkov, D. Alova, A., Gorelkin, P., Erofeev, A., Khaydukov, E. (2019). Photodynamic therapy of melanoma by blue-light photoactivation of flavin mononucleotide. *Sci Rep* 9, 9679 (2019). <https://doi.org/10.1038/s41598-019-46115-w>
- Akatsuka, K., Abe, R., Takase, T., & Oyama, D. (2019). Coordination Chemistry of Ru(II) Complexes of an Asymmetric Bipyridine Analogue: Synergistic Effects of Supporting Ligand and Coordination Geometry on Reactivities. *Molecules (Basel, Switzerland)*, 25(1), 27. <https://doi.org/10.3390/molecules25010027>
- Al Hageh, C., Al Assaad, M., El Masri, Z., Samaan, N., El-Sibai, M., Khalil, C., & Khnayzer, R. S. (2018). A long-lived cuprous bis-phenanthroline complex for the photodynamic therapy of cancer. *Dalton Transactions (Cambridge, England: 2003)*, 47(14), 4959-4967. <https://doi.org/10.1039/C8DT00140E>
- Alayev, A., & Holz, M. K. (2013). mTOR signaling for biological control and cancer. *Journal of cellular physiology*, 228(8), 1658–1664. <https://doi.org/10.1002/jcp.24351>
- Alessio, E., & Messori, L. (2019). NAMI-A and KP1019/1339, Two Iconic Ruthenium Anticancer Drug Candidates Face-to-Face: A Case Story in Medicinal Inorganic Chemistry. *Molecules (Basel, Switzerland)*, 24(10), 1995. <https://doi.org/10.3390/molecules24101995>
- Anand, P., Kunnumakkara, A. B., Sundaram, C., Harikumar, K. B., Tharakan, S. T., Lai, O. S., Sung, B., & Aggarwal, B. B. (2008). Cancer is a preventable disease that requires major lifestyle changes. *Pharmaceutical research*, 25(9), 2097–2116. <https://doi.org/10.1007/s11095-008-9661-9>
- Arruebo, M., Vilaboa, N., Sáez-Gutierrez, B., Lambea, J., Tres, A., Valladares, M., & González-Fernández, A. (2011). Assessment of the evolution of cancer treatment therapies. *Cancers*, 3(3), 3279-3330. <https://doi.org/10.3390/cancers3033279>
- Arvelo, F., Sojo, F., Cotte, C. (2016) Tumour progression and metastasis. *ecancer* 10; 617. <https://doi.org/10.617/ecancer.org>
- Azad, M. B., & Gibson, S. B. (2010). Role of BNIP3 in proliferation and hypoxia-induced autophagy: implications for personalized cancer therapies. *Annals of the New York Academy of Sciences*, 1210, 8–16. <https://doi.org/10.1111/j.1749->

- Baba, A. I., & Cătoi, C. (2007). *TUMOR CELL MORPHOLOGY*. The Publishing House of the Romanian Academy. <https://www.ncbi.nlm.nih.gov/books/NBK9553>
- Bajaj, A., Miranda, O. R., Kim, I. B., Phillips, R. L., Jerry, D. J., Bunz, U. H., & Rotello, V. M. (2009). Detection and differentiation of normal, cancerous, and metastatic cells using nanoparticle-polymer sensor arrays. *Proceedings of the National Academy of Sciences of the United States of America*, *106*(27), 10912–10916. <https://doi.org/10.1073/pnas.0900975106>
- Baldwin, E. L., & Osheroff, N. (2005). Etoposide, topoisomerase II and cancer. *Current medicinal chemistry. Anti-cancer agents*, *5*(4), 363–372. <https://doi.org/10.2174/1568011054222364>
- Basu, A., & Krishnamurthy, S. (2010). Cellular responses to Cisplatin-induced DNA damage. *Journal of nucleic acids*, *2010*, 201367. <https://doi.org/10.4061/2010/201367>
- Berg, K., & Moan, J. (1994). Lysosomes as photochemical targets. *International Journal of Cancer*, *59*(6), 814–822. <https://doi.org/10.1002/ijc.2910590618>
- Bergamo, A., Masi, A., Jakupec, M. A., Keppler, B. K., & Sava, G. (2009). Inhibitory Effects of the Ruthenium Complex KP1019 in Models of Mammary Cancer Cell Migration and Invasion. *Metal-based drugs*, *2009*, 681270. <https://doi.org/10.1155/2009/681270>
- Bergsbaken, T., Fink, S. L., & Cookson, B. T. (2009). Pyroptosis: host cell death and inflammation. *Nature reviews. Microbiology*, *7*(2), 99–109. <https://doi.org/10.1038/nrmicro2070>
- Bhakar, A. L., Howell, J. L., Paul, C. E., Salehi, A. H., Becker, E. B., Said, F., Bonni, A., & Barker, P. A. (2003). Apoptosis induced by p75NTR overexpression requires Jun kinase-dependent phosphorylation of Bad. *The Journal of neuroscience: the official journal of the Society for Neuroscience*, *23*(36), 11373–11381. <https://doi.org/10.1523/JNEUROSCI.23-36-11373.2003>
- Bharat, B. (2004). Nuclear factor- κ B. *Cancer Cell*. *6*(3) 203-208 <https://doi.org/10.1016/j.ccr.2004.09.003>
- Billen, L. P., Kokoski, C. L., Lovell, J. F., Leber, B., & Andrews, D. W. (2008). Bcl-XL inhibits membrane permeabilization by competing with Bax. *PLoS biology*, *6*(6), e147. <https://doi.org/10.1371/journal.pbio.0060147>
- Blasco, M. A. (2005). Telomeres and human disease: Ageing, cancer and beyond. *Nature Reviews Genetics*, *6*(8), 611–622. <https://doi.org/10.1038/nrg1656>
- Bozzuto, G., Ruggieri, P., & Molinari, A. (2010). Molecular aspects of tumor cell migration and invasion. *Annali Dell'Istituto Superiore Di Sanita*, *46*(1), 66–80.

https://doi.org/10.4415/ANN_10_01_09

- Bravo-Sagua, R., Rodriguez, A. E., Kuzmicic, J., Gutierrez, T., Lopez-Crisosto, C., Quiroga, C., Díaz-Elizondo, J., Chiong, M., Gillette, T. G., Rothermel, B. A., & Lavandero, S. (2013). Cell death and survival through the endoplasmic reticulum-mitochondrial axis. *Current molecular medicine*, *13*(2), 317–329. <https://doi.org/10.2174/156652413804810781>
- Cadet, J., & Davies, K. (2017). Oxidative DNA damage & repair: An introduction. *Free radical biology & medicine*, *107*, 2–12. <https://doi.org/10.1016/j.freeradbiomed.2017.03.030>
- Campagna, S., Puntoriero, F., Nastasi, F., Bergamini, G., & Balzani, V. (2007). Photochemistry and photophysics of coordination compounds: Ruthenium. In V. Balzani, & S. Campagna (Eds.), *Photochemistry and photophysics of coordination compounds I* (pp. 117-214). Berlin, Heidelberg: Springer Berlin Heidelberg. Retrieved from https://doi.org/10.1007/128_2007_133
- Cancer Research UK, (2017). Melanoma skin cancer mortality statistics. Retrieved from <https://www.cancerresearchuk.org/health-professional/cancer-statistics/statistics-by-cancer-type/melanoma-skin-cancer/mortality#heading-Zero>
- Cao, L., Shi, X., Chang, H., Zhang, Q., & He, Y. (2015). pH-Dependent recognition of apoptotic and necrotic cells by the human dendritic cell receptor DEC205. *Proceedings of the National Academy of Sciences of the United States of America*, *112*(23), 7237–7242. <https://doi.org/10.1073/pnas.1505924112>
- Caron, M., Sharma, A. K., O’Sullivan, J., Myler, L. R., Ferreira, M. T., Rodrigue, A., . . . Masson, J. (2019). Poly(ADP-ribose) polymerase-1 antagonizes DNA resection at double-strand breaks. *Nature Communications*, *10*(1), 1-16. <https://doi.org/10.1038/s41467-019-10741-9>
- Castellano, E and Downward, J. (2011). RAS Interaction with PI3K: More Than Just Another Effector Pathway. *Genes and Cancer*. *2*(3).<https://doi.org/10.1177/1947601911408079>
- Caspar, J. V., & Meyer, T. J. (1983). Photochemistry of tris(2,2'-bipyridine)ruthenium(2+) ion (Ru(bpy)₃²⁺). Solvent effects. *Journal of the American Chemical Society*, *105*(17), 5583– 5590. <https://doi.org/10.1021/ja00355a009>
- Chen, C. Y., Chen, J., He, L., & Stiles, B. L. (2018). PTEN: Tumor Suppressor and Metabolic Regulator. *Frontiers in endocrinology*, *9*, 338. <https://doi.org/10.3389/fendo.2018.00338>
- Chen, Y., Zhang, W., Guo, X. *et al.* (2019). The crosstalk between autophagy and apoptosis was mediated by phosphorylation of Bcl-2 and beclin1 in benzene-induced hematotoxicity. *Cell Death Dis* **10**, 772 <https://doi.org/10.1038/s41419-019-2004-4>

- Cheng, E., Cwei, M., Weiler, S., AFlavell, E., Wmak, T. (2001). BCL-2, BCL-XL Sequester BH3 Domain-Only Molecules Preventing BAX- and BAK-Mediated Mitochondrial Apoptosis. *Molecular Cell*, 8(3) [https://doi.org/10.1016/S1097-2765\(01\)00320-3](https://doi.org/10.1016/S1097-2765(01)00320-3)
- Cheng, N., Chytil, A., Shyr, Y., Joly, A., & Moses, H.. (2008). Transforming growth factor- β Signaling-Deficient fibroblasts enhance hepatocyte growth factor signalling in mammary carcinoma cells to promote scattering and invasion. *Molecular Cancer Research*, 6(10), 1521. <https://doi.org/10.1158/1541-7786.MCR-07-2203>
- Chung, Y. W., Kim, H. K., Kim, I. Y., Yim, M. B., & Chock, P. B. (2011). Dual function of protein kinase C (PKC) in 12-O-tetradecanoylphorbol-13-acetate (TPA)-induced manganese superoxide dismutase (MnSOD) expression: activation of CREB and FOXO3a by PKC-alpha phosphorylation and by PKC-mediated inactivation of Akt, respectively. *The Journal of biological chemistry*, 286(34), 29681–29690. <https://doi.org/10.1074/jbc.M111.264945>
- Croce C. M. (2009). Causes and consequences of microRNA dysregulation in cancer. *Nature reviews. Genetics*, 10(10), 704–714. <https://doi.org/10.1038/nrg2634>
- Commandeur, S., Sparks, S. J., Chan, H. L., Gao, L., Out, J. J., Gruis, N. A., van Doorn, R., & El Ghalbzouri, A. (2014). In-vitro melanoma models: invasive growth is determined by dermal matrix and basement membrane. *Melanoma research*, 24(4), 305–314. <https://doi.org/10.1097/CMR.0000000000000079>
- Côrte-Real, L. Matos, A., Alho, I., Morais, T., Tomaz, A., Garcia, M.,...Marques, F. (2013). Cellular Uptake Mechanisms of an Ant-tumor Ruthenium Compound: The Endosomal/Lysosomal System as a Target for Anticancer Metal-Based Drugs. *Microscopy and Microanalysis*, 19(5). <https://doi.org/10.1017/S143192761300175X>
- Corti, A., Milani, M., Lecis, D., Seneci, P., de Rosa, M., Mastrangelo, E., & Cossu, F. (2018). Structure-based design and molecular profiling of Smac-mimetics selective for cellular IAPs. *The FEBS journal*, 285(17), 3286–3298. <https://doi.org/10.1111/febs.14616201>
- Dahle, J., Steen, H. B., & Moan, J. (1999). The mode of cell death induced by photodynamic treatment depends on cell density. *Photochemistry and Photobiology*, 70(3), 363–367.
- Daniels, T. R., Bernabeu, E., Rodríguez, J. A., Patel, S., Kozman, M., Chiappetta, D. A., Holler, E., Ljubimova, J. Y., Helguera, G., & Penichet, M. L. (2012). The transferrin receptor and the targeted delivery of therapeutic agents against cancer. *Biochimica et biophysica acta*, 1820(3), 291–317. <https://doi.org/10.1016/j.bbagen.2011.07.016>
- Darvin, P., Toor, S. M., Sasidharan Nair, V., & Elkord, E. (2018). Immune checkpoint

- inhibitors: recent progress and potential biomarkers. *Experimental & molecular medicine*, 50(12), 1–11. <https://doi.org/10.1038/s12276-018-0191-1>
- Del Bello, B., Toscano, M., Moretti, D., & Maellaro, E. (2013). Cisplatin-induced apoptosis inhibits autophagy, which acts as a pro-survival mechanism in human melanoma cells. *PloS one*, 8(2), e57236. <https://doi.org/10.1371/journal.pone.0057236>
- Dickerson, M., Sun, Y., Howerton, B., & Glazer, E. C. (2014). Modifying Charge and Hydrophilicity of Simple Ru(II) Polypyridyl Complexes Radically Alters Biological Activities: Old Complexes, Surprising New Tricks. *Inorganic Chemistry*, 53(19), 10370–10377. <https://doi.org/10.1021/ic5013796>
- Dietrick-Buchecker, C. O., Marnot, P. A., Sauvage J. P., (1982) *Tetrahedron Lett.* 23, 5291–5294.
- Duijf, P. H., Nanayakkara, D., Nones, K., Srihari, S., Kalimutho, M., & Khanna, K. K. (2019). Mechanisms of genomic instability in breast cancer. *Trends in Molecular Medicine*. 25(7), 595–611. <https://doi.org/10.1016/j.molmed.2019.04.004>
- El-Tanani. M., El-Habib. D., Raynor. B. and Morgan. R. (2016). Mechanisms of Nuclear Export in Cancer and Resistance to Chemotherapy. *Cancers*. 8(3), 35; <https://doi.org/10.3390/cancers8030035>
- Elmore S. (2007). Apoptosis: a review of programmed cell death. *Toxicologic pathology*, 35(4), 495–516. <https://doi.org/10.1080/01926230701320337>
- Erhirhie, E. O., Ihekwereme, C. P., & Ildigwe, E. E. (2018). Advances in acute toxicity testing: Strengths, weaknesses and regulatory acceptance. *Interdisciplinary Toxicology*, 11(1), 5–12. <https://doi.org/10.2478/intox-2018-0001>
- Fayad, C., Audi, H., Khnayzer, R., Daher, C. (2020). The anti-cancer effect of series of strained photoactivatable Ru(II) polypyridyl complexes on non-small-cell lung cancer and triple negative breast cancer cells. *Journal of Biological Inorganic Chemistry*. <https://doi.org/10.1007/s00775-020-01835-7>
- Feitelson, M. A., Arzumanyan, A., Kulathinal, R. J., Blain, S. W., Holcombe, R. F., Mahajna, J., Marino, M., Martinez-Chantar, M. L., Nawroth, R., Sanchez-Garcia, I., Sharma, D., Saxena, N. K., Singh, N., Vlachostergios, P. J., Guo, S., Honoki, K., Fujii, H., Georgakilas, A. G., Bilsland, A., Amedei, A., ... Nowsheen, S. (2015). Sustained proliferation in cancer: Mechanisms and novel therapeutic targets. *Seminars in cancer biology*, 35 Suppl(Suppl), S25–S54. <https://doi.org/10.1016/j.semcancer.2015.02.006>
- Flusberg, D. A., & Sorger, P. K. (2015). Surviving apoptosis: life-death signaling in single cells. *Trends in cell biology*, 25(8), 446–458. <https://doi.org/10.1016/j.tcb.2015.03.003>
- Frugtuet, B., Jiang, W. G., & Martin, T. A. (2015). Role of the WASP and WAVE

- family proteins in breast cancer invasion and metastasis. *Breast cancer (Dove Medical Press)*, 7, 99–109. <https://doi.org/10.2147/BCTT.S59006>
- Fulda, S., Debatin, K. Extrinsic versus intrinsic apoptosis pathways in anticancer chemotherapy. *Oncogene* 25, 4798–4811 (2006). <https://doi.org/10.1038/sj.onc.1209608>
- Galluzzi, L., Senovilla, L., Vitale, I. *et al.* (2012). Molecular mechanisms of cisplatin resistance. *Oncogene* 31, 1869–1883. <https://doi.org/10.1038/onc.2011.384>
- Garner, R. N., Joyce, L. E., & Turro, C. (2011). Effect of Electronic Structure on the Photoinduced Ligand Exchange of Ru(II) Polypyridine Complexes. *Inorganic Chemistry*, 50(10), 4384–4391. <https://doi.org/10.1021/ic102482c>
- Gavine, P.R., Wang, M., Yu, D. *et al.* (2015). Identification and validation of dysregulated MAPK7 (ERK5) as a novel oncogenic target in squamous cell lung and esophageal carcinoma. *BMC Cancer* 15, 454 <https://doi.org/10.1186/s12885-015-1455-y>
- Georgescu M. M. (2010). PTEN Tumor Suppressor Network in PI3K-Akt Pathway Control. *Genes & cancer*, 1(12), 1170–1177. <https://doi.org/10.1177/1947601911407325>
- Ghezzi, A., Aceto, M., Cassino, C., Gabano, E., & Osella, D. (2004). Uptake of antitumor platinum (II)-complexes by cancer cells, assayed by inductively coupled plasma mass spectrometry (ICP-MS). *Journal of Inorganic Biochemistry*, 98(1), 73–78.
- Gillet, C. E., & Barnes, D. M. (2000). The Molecular Basis of Cell Cycle and Growth Control: Stein GS, Baserga R, Giordano A, *et al*, eds. Wiley, 1998. ISBN 0 471 15706 6. *Molecular Pathology*, 53(6), 337.
- Golla, U., Swagatika, S., Chauhan, S., & Tomar, R. S. (2017). A systematic assessment of chemical, genetic, and epigenetic factors influencing the activity of anticancer drug KP1019 (FFC14A). *Oncotarget*, 8(58), 98426–98454. <https://doi.org/10.18632/oncotarget.21416>
- Golubnitschaja, O., Baban, B., Boniolo, G., Wang, W., Bubnov, R., Kapalla, M., Krapfenbauer, K., Mozaffari, M. S., & Costigliola, V. (2016). Medicine in the early twenty-first century: paradigm and anticipation - EPMA position paper 2016. *The EPMA journal*, 7(1), 23. <https://doi.org/10.1186/s13167-016-0072-4>
- Gomez, N., Erazo, T., & Lizcano, J. M. (2016). ERK5 and Cell Proliferation: Nuclear Localization Is What Matters. *Frontiers in cell and developmental biology*, 4, 105. <https://doi.org/10.3389/fcell.2016.00105>
- Groessl, M., Tsybin, Y. O., Hartinger, C. G., Keppler, B. K., & Dyson, P. J. (2010). Ruthenium versus platinum: interactions of anticancer metallodrugs with duplex oligonucleotides characterised by electrospray ionisation mass spectrometry. *Journal of biological inorganic chemistry: JBIC: a publication of*

the Society of Biological Inorganic Chemistry, 15(5), 677–688.
<https://doi.org/10.1007/s00775-010-0635-0>

- Guan X. (2015). Cancer metastases: challenges and opportunities. *Acta pharmaceutica Sinica. B*, 5(5), 402–418. <https://doi.org/10.1016/j.apsb.2015.07.005>
- Guo, W., Zheng, W., Luo, Q., Li, X., Zhao, Y., Xiong, S., & Wang, F. (2013). Transferrin serves as a mediator to deliver organometallic ruthenium(II) anticancer complexes into cells. *Inorganic chemistry*, 52(9), 5328–5338. <https://doi.org/10.1021/ic4002626>
- Gupta, S., Kass, G. E., Szegezdi, E., & Joseph, B. (2009). The mitochondrial death pathway: a promising therapeutic target in diseases. *Journal of cellular and molecular medicine*, 13(6), 1004–1033. <https://doi.org/10.1111/j.1582-4934.2009.00697.x>
- Hageh, C. A., Assaad, M. A., Masri, Z. E., Samaan, N., El-Sibai, M., Khalil, C., & Khnayzer, R. S. (2018). A long-lived cuprous bis-phenanthroline complex for the photodynamic therapy of cancer. *Dalton Transactions*, 47(14), 4959–4967. <https://doi.org/10.1039/C8DT00140E>
- Han, Z., Wei, W., Dunaway, S., Darnowski, J. W., Calabresi, P., Sedivy, J., Hendrickson, E. A., Balan, K. V., Pantazis, P., & Wyche, J. H. (2002). Role of p21 in apoptosis and senescence of human colon cancer cells treated with camptothecin. *The Journal of biological chemistry*, 277(19), 17154–17160. <https://doi.org/10.1074/jbc.M112401200>
- Hanahan, D., & Weinberg, R. A. (2000). The Hallmarks of Cancer. *Cell*, 100(1), 57–70. [https://doi.org/10.1016/S0092-8674\(00\)81683-9](https://doi.org/10.1016/S0092-8674(00)81683-9)
- Hanahan, D., & Weinberg, R. A. (2011). Hallmarks of Cancer: The Next Generation. *Cell*, 144(5), 646–674. <https://doi.org/10.1016/j.cell.2011.02.013>
- Hanif, M., Hartinger, C. (2018). Anticancer Metallodrugs: Where is the next Cisplatin? *Future Medicinal Chemistry*. 10(6). <https://doi.org/10.4155/fmc-2017-0317>
- Harr, M. W., & Distelhorst, C. W. (2010). Apoptosis and autophagy: decoding calcium signals that mediate life or death. *Cold Spring Harbor perspectives in biology*, 2(10), a005579. <https://doi.org/10.1101/cshperspect.a005579>
- Harris, A.L. (2002). Hypoxia - a key regulatory factor in tumor growth. *Nature Reviews Cancer*. 2:38–47.
- Hector, S., Bolanowska-Higdon, W., Zdanowicz, J., Hitt, S., & Pendyala, L. (2001). In vitro studies on the mechanisms of oxaliplatin resistance. *Cancer chemotherapy and pharmacology*, 48(5), 398–406. <https://doi.org/10.1007/s002800100363>
- Heffeter, P., Atil, B., Kryeziu, K., Groza, D., Koellensperger, G., Körner, W., Jungwirth, U., Mohr, T., Keppler, B. K., & Berger, W. (2013). The ruthenium

- compound KP1339 potentiates the anticancer activity of sorafenib in vitro and in vivo. *European journal of cancer (Oxford, England: 1990)*, 49(15), 3366–3375.
- Herzenberg, L. A., Tung, J., Moore, W. A., Herzenberg, L. A., & Parks, D. R. (2006). Interpreting flow cytometry data: a guide for the perplexed. *Nature immunology*, 7(7), 681–685. <https://doi.org/10.1038/ni0706-681>
- Himuro, M., Miyatsuka, T., Suzuki, L., Miura, M., Katahira, T., Goto, H., Nishida, Y., Sasaki, S., Koike, M., Shiota, C., Gittes, G. K., Fujitani, Y., & Watada, H. (2019). Cellular Autophagy in α Cells Plays a Role in the Maintenance of Islet Architecture. *Journal of the Endocrine Society*, 3(11), 1979–1992. <https://doi.org/10.1210/js.2019-00075>
- Hodson, R. (2016). Precision medicine. *Nature* 537, S49 <https://doi.org/10.1038/537S49a>
- Hoffmann, G. (2007). Principles and working mechanisms of water-filtered infrared-A (wIRA) in relation to wound healing. *GMS Krankenhaushygiene Interdisziplinär*, 2(2). <https://www.ncbi.nlm.nih.gov/pmc/articles/PMC2831244/>
- Hopkins, S., Siewert, B., Askes, S., Veldhuizen, P., Zwier R., Heger M., and Bonnet, S. (2016). An in vitro cell irradiation protocol for testing photopharmaceuticals and the effect of blue, green, and red light on human cancer cell lines. *Photobiological Sciences*. 15, 644-653 <https://doi.org/10.1039/C5PP00424A>
- Howells, C. C., Baumann, W. T., Samuels, D. C., & Finkielstein, C. V. (2011). The Bcl-2-associated death promoter (BAD) lowers the threshold at which the Bcl-2-interacting domain death agonist (BID) triggers mitochondria disintegration. *Journal of theoretical biology*, 271(1), 114–123. <https://doi.org/10.1016/j.jtbi.2010.11.040>
- Howerton, B. S., Heidary, D. K., & Glazer, E. C. (2012). Strained Ruthenium Complexes Are Potent Light-Activated Anticancer Agents. *Journal of the American Chemical Society*, 134(20), 8324–8327. <https://doi.org/10.1021/ja3009677>
- Huang, J., & Manning, B. D. (2008). The TSC1-TSC2 complex: a molecular switchboard controlling cell growth. *The Biochemical journal*, 412(2), 179–190. <https://doi.org/10.1042/BJ20080281>
- Ikner, A., & Ashkenazi, A. (2011). TWEAK induces apoptosis through a death-signaling complex comprising receptor-interacting protein 1 (RIP1), Fas-associated death domain (FADD), and caspase-8. *The Journal of biological chemistry*, 286(24), 21546–21554. <https://doi.org/10.1074/jbc.M110.203745>
- Jean, S., & Kiger, A. A. (2014). Classes of phosphoinositide 3-kinases at a glance. *Journal of cell science*, 127(Pt 5), 923–928. <https://doi.org/10.1242/jcs.093773>
- Ji, X., Wang, L., Wu, B., Han, R., Han, L., Wang, T., Yang, J., & Ni, C. (2015).

- Associations of MMP1, MMP2 and MMP3 Genes Polymorphism with Coal Workers' Pneumoconiosis in Chinese Han Population. *International journal of environmental research and public health*, 12(11), 13901–13912. <https://doi.org/10.3390/ijerph121113901>
- Junttila, M. R., & Evan, G. I. (2009). p53 — a jack of all trades but master of none. *Nature Reviews Cancer*, 9, 821. Retrieved from <https://doi.org/10.1038/nrc2728>
- Kakarla, R., Hur, J., Kim, Y. J., Kim, J., & Chwae, Y. J. (2020). Apoptotic cell-derived exosomes: messages from dying cells. *Experimental & molecular medicine*, 52(1), 1–6. <https://doi.org/10.1038/s12276-019-0362-88>
- Kang, R., Zeh, H. J., Lotze, M. T., & Tang, D. (2011). The Beclin 1 network regulates autophagy and apoptosis. *Cell death and differentiation*, 18(4), 571–580. <https://doi.org/10.1038/cdd.2010.191>
- Karch, J., & Molkenin, J. D. (2015). Regulated necrotic cell death: The passive aggressive side of bax and bak. *Circulation Research*, 116(11), 1800–1809. <https://doi.org/10.1161/CIRCRESAHA.116.305421>
- Karsch-Bluman, A., Feiglin, A., Arbib, E., Stern, T., Shoval, H., Schwob, O., Berger, M., & Benny, O. (2019). Tissue necrosis and its role in cancer progression. *Oncogene*, 38(11), 1920–1935. <https://doi.org/10.1038/s41388-018-0555>
- Kaspler, P., Lazic, S., Forward, S., Arenas, Y., Mandel, A., & Lilge, L. (2016). A ruthenium(ii) based photosensitizer and transferrin complexes enhance photo-physical properties, cell uptake, and photodynamic therapy safety and efficacy. *Photochemical & photobiological sciences: Official journal of the European Photochemistry Association and the European Society for Photobiology*, 15(4), 481–495. <https://doi.org/10.1039/c5pp00450k>
- Katt, M. E., Wong, A. D., & Searson, P. C. (2018). Dissemination from a solid tumor: Examining the multiple parallel pathways. *Trends in Cancer*, 4(1), 20–37. <https://doi.org/10.1016/j.trecan.2017.12.002>
- Kaufmann, K. B., Büning, H., Galy, A., Schambach, A., & Grez, M. (2013). Gene therapy on the move. *EMBO molecular medicine*, 5(11), 1642–1661. <https://doi.org/10.1002/emmm.201202287>
- Kessel, D., & Poretz, R. D. (2000). Sites of photodamage induced by photodynamic therapy with a chlorin e6 triacetoxymethyl ester (CAME). *Photochemistry and Photobiology*, 71(1), 94–96. [https://doi.org/10.1562/0031-8655\(2000\)071<0094:sopibp>2.0.co;2](https://doi.org/10.1562/0031-8655(2000)071<0094:sopibp>2.0.co;2)
- Kew, C., Lui, P. Y., Chan, C. P., Liu, X., Au, S. W., Mohr, I., Jin, D. Y., & Kok, K. H. (2013). Suppression of PACT-induced type I interferon production by herpes simplex virus 1 Us11 protein. *Journal of virology*, 87(24), 13141–13149. <https://doi.org/10.1128/JVI.02564-13>
- Khaddour, K., Hana, C. K., & Mewawalla, P. (2020). Hematopoietic Stem Cell

Transplantation. In *StatPearls*. StatPearls Publishing.

- Khavari, T. A., & Rinn, J. (2007). Ras/Erk MAPK signaling in epidermal homeostasis and neoplasia. *Cell Cycle* (Georgetown, Tex.), 6(23), 2928–2931. <https://doi.org/10.4161/cc.6.23.4998>
- Khosravi-Far, R., & Esposti, M. D. (2004). Death receptor signals to mitochondria. *Cancer biology & therapy*, 3(11), 1051–1057. <https://doi.org/10.4161/cbt.3.11.1173>
- Kilbride, S., Prehn, J. (2013). Central roles of apoptotic proteins in mitochondrial function. *Oncogene* 32, 2703–2711. <https://doi.org/10.1038/onc.2012.348>
- Kim, W. B., Shelley, A. J., Novice, K., Joo, J., Lim, H. W., & Glassman, S. J. (2018). Drug-induced phototoxicity: A systematic review. *Journal of the American Academy of Dermatology*, 79(6), 1069–1075. <https://doi.org/10.1016/j.jaad.2018.06.061>
- Komor, A. C., & Barton, J. K. (2013). The path for metal complexes to a DNA target. *Chemical communications (Cambridge, England)*, 49(35), 3617–3630. <https://doi.org/10.1039/c3cc00177f>
- Kondoh, K., & Nishida, E. (2007). Regulation of MAP kinases by MAP kinase phosphatases. *Biochimica Et Biophysica Acta*, 1773(8), 1227–1237. <https://doi.org/10.1016/j.bbamcr.2006.12.002>
- Kong, Y. H., & Xu, S. P. (2018). Salidroside prevents skin carcinogenesis induced by DMBA/TPA in a mouse model through suppression of inflammation and promotion of apoptosis. *Oncology reports*, 39(6), 2513–2526. <https://doi.org/10.3892/or.2018.6381>
- Korbelik M. (2006). PDT-associated host response and its role in the therapy outcome. *Lasers in surgery and medicine*, 38(5), 500–508. <https://doi.org/10.1002/lsm.20337>
- Kordes, M., Matuschewski, K., & Hafalla, J. C. (2011). Caspase-1 activation of interleukin-1 β (IL-1 β) and IL-18 is dispensable for induction of experimental cerebral malaria. *Infection and immunity*, 79(9), 3633–3641. <https://doi.org/10.1128/IAI.05459-11>
- Koval, J., Mikes, J., Jendzelovský, R., Kello, M., Solár, P., & Fedorocko, P. (2010). Degradation of HER2 receptor through hypericin-mediated photodynamic therapy. *Photochemistry and Photobiology*, 86(1), 200–205. <https://doi.org/10.1111/j.1751-1097.2009.00639.x>
- Kunjachan, S., Pola, R., Gremse, F., Theek, B., Ehling, J., Moeckel, D., Hermanns-Sachweh, B., Pechar, M., Ulbrich, K., Hennink, W. E., Storm, G., Lederle, W., Kiessling, F., & Lammers, T. (2014). Passive vs. Active Tumor Targeting using RGD-and NGR-modified Polymeric Nanomedicines. *Nano Letters*, 14(2), 972–981. <https://doi.org/10.1021/nl404391r>

- Kus, K., Kij, A., Zakrzewska, A., Jaształ, A., Stojak, M., Walczak, M., & Chlopicki, S. (2018). Alterations in arginine and energy metabolism, structural and signalling lipids in metastatic breast cancer in mice detected in plasma by targeted metabolomics and lipidomics. *Breast cancer research: BCR*, 20(1), 148. <https://doi.org/10.1186/s13058-018-1075-y>
- Kwitniewski, M., Jankowski, D., Jaskiewicz, K., Dziadziuszko, H., Juzeniene, A., Moan, J., Ma, L.-W., Peksa, R., Kunikowska, D., Graczyk, A., Kwasny, M., Kaliszewski, M., & Glosnicka, R. (2009). Photodynamic therapy with 5-aminolevulinic acid and diamino acid derivatives of protoporphyrin IX reduces papillomas in mice without eliminating transformation into squamous cell carcinoma of the skin. *International Journal of Cancer*, 125(7), 1721–1727. <https://doi.org/10.1002/ijc.24488>
- Laemmel, A.-C., Collin, J.-P., & Sauvage, J.-P. (1999). Efficient and Selective Photochemical Labilization of a Given Bidentate Ligand in Mixed Ruthenium(II) Complexes of the Ru(phen)2L2+ and Ru(bipy)2L2+ Family (L = Sterically Hindering Chelate). *European Journal of Inorganic Chemistry*, 1999(3), 383–386. [https://doi.org/10.1002/\(SICI\)10990682\(199903\)1999:3<383::AIDEJIC383>3.0.CO;2-9](https://doi.org/10.1002/(SICI)10990682(199903)1999:3<383::AIDEJIC383>3.0.CO;2-9)
- Lash, B. W., & Gilman, P. B. (2013). Chapter 12—Principles of Cytotoxic Chemotherapy. In G. C. Prendergast & E. M. Jaffee (Eds.), *Cancer Immunotherapy (Second Edition)* (pp. 167– 185). Academic Press. <https://doi.org/10.1016/B978-0-12-394296-8.00012-9>
- Lawler, P. R., & Lawler, J. (2012). Molecular basis for the regulation of angiogenesis by thrombospondin-1 and -2. *Cold Spring Harbor Perspectives in Medicine*, 2(5), a006627. <https://doi.org/10.1101/cshperspect.a006627>
- Leber, B., Mayrhauser, U., Leopold, B., Koestenbauer, S., Tscheliessnigg, K., Stadlbauer, V., & Stiegler, P. (2012). Impact of temperature on cell death in a cell-culture model of hepatocellular carcinoma. *Anticancer research*, 32(3), 915–921.
- Lee, J., Hong, F., Kwon, S., Kim, S. S., Kim, D. O., Kang, H. S., Lee, S. J., Ha, J., & Kim, S. S. (2002). Activation of p38 MAPK induces cell cycle arrest via inhibition of Raf/ERK pathway during muscle differentiation. *Biochemical and biophysical research communications*, 298(5), 765–771. [https://doi.org/10.1016/s0006-291x\(02\)02562-7](https://doi.org/10.1016/s0006-291x(02)02562-7)
- Lee, D. H., Kim, C., Zhang, L., & Lee, Y. J. (2008). Role of p53, PUMA, and Bax in wogonin-induced apoptosis in human cancer cells. *Biochemical pharmacology*, 75(10), 2020–2033. <https://doi.org/10.1016/j.bcp.2008.02.023>
- Lee, Y., Hur, I., Park, S. Y., Kim, Y. K., Suh, M. R., & Kim, V. N. (2006). The role of PACT in the RNA silencing pathway. *The EMBO journal*, 25(3), 522–532. <https://doi.org/10.1038/sj.emboj.7600942>
- Lenihan, C. R., & Taylor, C. T. (2013). The impact of hypoxia on cell death

- pathways. *Biochemical Society transactions*, 41(2), 657–663. <https://doi.org/10.1042/BST20120345>
- Li, Y., Lin, A. W., Zhang, X., Wang, Y., Wang, X., & Goodrich, D. W. (2007). Cancer cells and normal cells differ in their requirements for Thoc1. *Cancer research*, 67(14), 6657–6664. <https://doi.org/10.1158/0008-5472.CAN-06-3234>
- Li, H., & Qian, Z. M. (2002). Transferrin/transferrin receptor-mediated drug delivery. *Medicinal Research Reviews*, 22(3), 225–250. <https://doi.org/10.1002/med.10008>
- Lin, K., Zhao, Z.-Z., Bo, H.-B., Hao, X.-J., & Wang, J.-Q. (2018). Applications of Ruthenium Complex in Tumor Diagnosis and Therapy. *Frontiers in Pharmacology*, 9. <https://doi.org/10.3389/fphar.2018.01323>
- Linhao, Xu., Yong Z., Chen, J., Yizhou, Xu. (2020). Thrombospondin-1 A Key Protein That Induces Fibrosis in Diabetic Complications. *Journal of Diabetes Research*. 14. <https://doi.org/10.1155/2020/8043135>
- Linkermann, A., & Green, D. R. (2014). Necroptosis. *The New England journal of medicine*, 370(5), 455–465. <https://doi.org/10.1056/NEJMra1310050>
- Lippert, B. 1999. Cisplatin: Chemistry and Biochemistry of a Leading Anticancer Drug. John Wiley & Sons.
- Liu, H., Remedi, M. S., Pappan, K. L., Kwon, G., Rohatgi, N., Marshall, C. A., & McDaniel, M. L. (2009). Glycogen synthase kinase-3 and mammalian target of rapamycin pathways contribute to DNA synthesis, cell cycle progression, and proliferation in human islets. *Diabetes*, 58(3), 663–672. <https://doi.org/10.2337/db07-1208>
- Liu, P., Cheng, H., Roberts, T. M., & Zhao, J. J. (2009). Targeting the phosphoinositide 3-kinase pathway in cancer. *Nature reviews. Drug discovery*, 8(8), 627–644. <https://doi.org/10.1038/nrd2926>
- Liu, W. Q., Chen, S. Q., Bai, H. Q., Wei, Q. M., Zhang, S. N., Chen, C., Zhu, Y. H., Yi, T. W., Guo, X. P., Chen, S. Y., Yin, M. J., Sun, C. F., & Liang, S. H. (2020). The Ras/ERK signaling pathway couples antimicrobial peptides to mediate resistance to dengue virus in *Aedes* mosquitoes. *PLoS neglected tropical diseases*, 14(8), e0008660. <https://doi.org/10.1371/journal.pntd.0008660>
- Liu, F., Sun, D., Zhou, X., Ding, Y., Ma, Y., Hou, Y., Kong, X., & Wang, Z. (2018). Effect of adjuvant hormone therapy in patients with prostate cancer: A meta-analysis of randomized controlled trials. *Medicine*, 97(50), e13145. <https://doi.org/10.1097/MD.00000000000013145>
- Lu, Y., Liu, Y., & Yang, C. (2017). Evaluating In Vitro DNA Damage Using Comet Assay. *Journal of visualized experiments: JoVE*, (128), 56450. <https://doi.org/10.3791/56450>
- Luo, X., He, Q., Huang, Y., & Sheikh, M. S. (2005). Transcriptional upregulation of

- PUMA modulates endoplasmic reticulum calcium pool depletion-induced apoptosis via Bax activation. *Cell death and differentiation*, 12(10), 1310–1318. <https://doi.org/10.1038/sj.cdd.4401659>
- Makeeva, N., Myers, J. W., & Welsh, N. (2006). Role of MKK3 and p38 MAPK in cytokine-induced death of insulin-producing cells. *The Biochemical journal*, 393(Pt 1), 129–139. <https://doi.org/10.1042/BJ20050814>
- Mansour, N., Mehanna, S., Mroueh, M. A., Audi, H., Bodman-Smith, K., Daher, C. F., Taleb, R. I., El-Sibai, M., & Khnayzer, R. S. (2018). Photoactivatable RuII Complex Bearing 2,9- Diphenyl-1,10-phenanthroline: Unusual Photochemistry and Significant Potency on Cisplatin-Resistant Cell Lines. *European Journal of Inorganic Chemistry*, (22), 2524– 2532. <https://doi.org/10.1002/ejic.201800194>
- Mansour, N., Bodman-Smith, K., Khnayzer, R., Daher, C. (2020). A photoactivatable Ru (II) complex bearing 2,9-diphenyl-1,10-phenanthroline: A potent chemotherapeutic drug inducing apoptosis in Triple Negative Human Breast Adenocarcinoma cells. *Biological Inorganic Chemistry*. <https://doi.org/10.1007/s00775-020-01835-7>
- Mansouri, A., Ridgway, L. D., Korapati, A. L., Zhang, Q., Tian, L., Wang, Y., Siddik, Z. H., Mills, G. B., & Claret, F. X. (2003). Sustained activation of JNK/p38 MAPK pathways in response to cisplatin leads to Fas ligand induction and cell death in ovarian carcinoma cells. *The Journal of Biological Chemistry*, 278(21), 19245–19256. <https://doi.org/10.1074/jbc.M208134200>
- Mari, C., Pierroz, V., Ferrari, S., & Gasser, G. (2015). *Combination of Ru(II) complexes and light: New frontiers in cancer therapy*. 6(5), 2660–2686. <https://doi.org/10.1039/C4SC03759F>
- Marques, J. T., White, C. L., Peters, G. A., Williams, B. R., & Sen, G. C. (2008). The role of PACT in mediating gene induction, PKR activation, and apoptosis in response to diverse stimuli. *Journal of interferon & cytokine research: the official journal of the International Society for Interferon and Cytokine Research*, 28(8), 469–476. <https://doi.org/10.1089/jir.2007.0006>
- Marquez, R. T., & Xu, L. (2012). Bcl-2:Beclin 1 complex: multiple, mechanisms regulating autophagy/apoptosis toggle switch. *American journal of cancer research*, 2(2), 214–221.
- Martin G. S. (2003). Cell signaling and cancer. *Cancer cell*, 4(3), 167–174. [https://doi.org/10.1016/s1535-6108\(03\)00216-2](https://doi.org/10.1016/s1535-6108(03)00216-2)
- Martinvalet, D., Zhu, P., Lieberman, J. (2005). Granzyme A Induces Caspase-Independent Mitochondrial Damage, a Required First Step for Apoptosis. *Immunity*. 22(3). <https://doi.org/10.1016/j.immuni.2005.02.004>
- Mayo Clinic. (2020). Melanoma. Retrieved from <https://www.mayoclinic.org/diseases-conditions/melanoma/symptoms-causes/syc-20374884>

- Maytin, E. V., Kaw, U., Ilyas, M., Mack, J. A., & Hu, B. (2018). Blue light versus red light for photodynamic therapy of basal cell carcinoma in patients with Gorlin syndrome: A bilaterally controlled comparison study. *Photodiagnosis and photodynamic therapy*, 22, 7–13. <https://doi.org/10.1016/j.pdpdt.2018.02.009>
- Mehanna, S., Mansour, N., Audi, H., Bodman-Smith, K., Mroueh, M. A., Taleb, R. I., Daher, C. F., & Khnayzer, R. S. (2019). Enhanced cellular uptake and photochemotherapeutic potential of a lipophilic strained Ru(II) polypyridyl complex. *RSC Advances*, 9(30), 17254–17265. <https://doi.org/10.1039/C9RA02615K>
- Meng, X., Leyva, M., Marjorie, J., Gross, I., Benosman, S., Fricker, B., Harlepp, S., ... Gaiddon, C. (2009). A Ruthenium-Containing Organometallic Compound Reduces Tumor Growth through Induction of the Endoplasmic Reticulum Stress Gene *CHOP*. *Cancer Research*, 69(13). <https://doi.org/10.1158/0008-5472.CAN-08-4408>
- McCubrey, J. A., Steelman, L. S., Chappell, W. H., Abrams, S. L., Wong, E. W. T., Chang, F., Lehmann, B., Terrian, D. M., Milella, M., Tafuri, A., Stivala, F., Libra, M., Basecke, J., Evangelisti, C., Martelli, A. M., & Franklin, R. A. (2007). Roles of the Raf/MEK/ERK pathway in cell growth, malignant transformation and drug resistance. *Biochimica et Biophysica Acta (BBA) - Molecular Cell Research*, 1773(8), 1263–1284. <https://doi.org/10.1016/j.bbamcr.2006.10.001>
- Meister, M., Tomasovic, A., Banning, A., & Tikkanen, R. (2013). Mitogen-Activated Protein (MAP) Kinase Scaffolding Proteins: A Recount. *International journal of molecular sciences*, 14(3), 4854–4884. <https://doi.org/10.3390/ijms14034854>
- Mezzacappa, C., Komiya, Y., & Habas, R. (2012). Activation and function of small GTPases Rho, Rac, and Cdc42 during gastrulation. *Methods in molecular biology (Clifton, N.J.)*, 839, 119–131. https://doi.org/10.1007/978-1-61779-510-7_10
- Mirochnik, Y., Kwiatek, A., & Volpert, O. (2008). Thrombospondin and apoptosis: Molecular mechanisms and use for design of complementation treatments. *Current Drug Targets*, 9(10), 851–862.
- Mott, H. R., & Owen, D. (2014). Structure and function of RLIP76 (RalBP1): an intersection point between Ras and Rho signalling. *Biochemical Society transactions*, 42(1), 52–58. <https://doi.org/10.1042/BST20130231>
- Murthy, D., Attri, K. S., & Singh, P. K. (2018). Phosphoinositide 3-Kinase Signaling Pathway in Pancreatic Ductal Adenocarcinoma Progression, Pathogenesis, and Therapeutics. *Frontiers in physiology*, 9, 335. <https://doi.org/10.3389/fphys.2018.00335>
- Nakajima, W., Hicks, M., Tanaka, N. *et al.* (2014). Noxa determines localization and stability of MCL-1 and consequently ABT-737 sensitivity in small cell lung cancer. *Cell Death Dis* 5, e1052. <https://doi.org/10.1038/cddis.2014.6>
- Nasti, T. H., Cochran, J. B., Tsuruta, Y., Yusuf, N., McKay, K. M., Athar, M., Timares,

- L., & Elmets, C. A. (2016). A murine model for the development of melanocytic nevi and their progression to melanoma. *Molecular carcinogenesis*, 55(5), 646–658. <https://doi.org/10.1002/mc.22310>
- National Cancer Institute. (2015). Metastatic cancer. Retrieved from <https://www.cancer.gov/types/metastatic-cancer>
- Nguyen, L. T., McKall-Faienza, K., Zakarian, A., Speiser, D. E., Mak, T. W., & Ohashi, P. S. (2000). TNF receptor 1 (TNFR1) and CD95 are not required for T cell deletion after virus infection but contribute to peptide-induced deletion under limited conditions. *European journal of immunology*, 30(2), 683–688. [https://doi.org/10.1002/1521-4141\(200002\)30:2<683::AID-IMMU683>3.0.CO;2-5](https://doi.org/10.1002/1521-4141(200002)30:2<683::AID-IMMU683>3.0.CO;2-5)
- Nishida, N., Yano, H., Nishida, T., Kamura, T., & Kojiro, M. (2006). Angiogenesis in Cancer. *Vascular Health and Risk Management*, 2(3), 213–219.
- Orgován, Z., & Keserű, G. M. (2020). Small molecule inhibitors of RAS proteins with oncogenic mutations. *Cancer metastasis reviews*, 39(4), 1107–1126. <https://doi.org/10.1007/s10555-020-09911-9>
- Oun, R., , Moussa, Y. E., , & Wheate, N. J., (2018). The side effects of platinum-based chemotherapy drugs: a review for chemists. *Dalton transactions (Cambridge, England: 2003)*, 47(19), 6645–6653. <https://doi.org/10.1039/c8dt00838h>
- Padma V. V. (2015). An overview of targeted cancer therapy. *BioMedicine*, 5(4), 19. <https://doi.org/10.7603/s40681-015-0019-4>
- Park H. H. (2012). Structural features of caspase-activating complexes. *International journal of molecular sciences*, 13(4), 4807–4818. <https://doi.org/10.3390/ijms13044807>
- Perillo, B., Di Donato, M., Pezone, A. *et al.* (2020). ROS in cancer therapy: the bright side of the moon. *Exp Mol Med* 52, 192–203 <https://doi.org/10.1038/s12276-020-0384-2>
- Peters, G. A., Hartmann, R., Qin, J., & Sen, G. C. (2001). Modular structure of PACT: distinct domains for binding and activating PKR. *Molecular and cellular biology*, 21(6), 1908–1920. <https://doi.org/10.1128/MCB.21.6.1908-1920.2001>
- Pickup, M., Novitskiy, S., & Moses, H. L. (2013). The roles of TGFβ in the tumour microenvironment. *Nature Reviews: Cancer*, 13(11), 788–799. <https://doi.org/10.1038/nrc3603>
- Plaetzer, K., Krammer, B., Berlanda, J., Berr, F., & Kiesslich, T. (2009). Photophysics and photochemistry of photodynamic therapy: Fundamental aspects. *Lasers in Medical Science*, 24(2), 259–268. <https://doi.org/10.1007/s10103-008-0539-1>
- Puckett, C. A., & Barton, J. K. (2007). Methods to Explore Cellular Uptake of Ruthenium Complexes. *Journal of the American Chemical Society*, 129(1), 46–47. <https://doi.org/10.1021/ja0677564>

- Puckett, C. A., & Barton, J. K. (2008a). Mechanism of cellular uptake of a ruthenium polypyridyl complex. *Biochemistry*, 47(45), 11711–11716. <https://doi.org/10.1021/bi800856t>
- Purring-Koch, C., & McLendon, G. (2000). Cytochrome c binding to Apaf-1: the effects of dATP and ionic strength. *Proceedings of the National Academy of Sciences of the United States of America*, 97(22), 11928–11931. <https://doi.org/10.1073/pnas.220416197>
- Qiang, L., Wu, T., Zhang, H. W., Lu, N., Hu, R., Wang, Y. J., Zhao, L., Chen, F. H., Wang, X. T., You, Q. D., & Guo, Q. L. (2012). HIF-1 α is critical for hypoxia-mediated maintenance of glioblastoma stem cells by activating Notch signaling pathway. *Cell death and differentiation*, 19(2), 284–294. <https://doi.org/10.1038/cdd.2011.95>
- Qu, F., Park, S., Martinez, K., Gray, J. L., Thowfeik, F. S., Lundeen, J. A., Kuhn, A. E., Charboneau, D. J., Gerlach, D. L., Lockart, M. M., Law, J. A., Jernigan, K. L., Chambers, N., Zeller, M., Piro, N. A., Kassel, W. S., Schmehl, R. H., Paul, J. J., Merino, E. J., ... Papish, E. T. (2017). Ruthenium Complexes are pH-Activated Metallo Prodrugs (pHAMPs) with Light-Triggered Selective Toxicity Toward Cancer Cells. *Inorganic Chemistry*, 56(13), 7519–7532. <https://doi.org/10.1021/acs.inorgchem.7b01065>
- Rademaker, J. M., van den Bongard, D., Pluim, D., Beijnen, J. H., & Schellens, J. H. M. (2004). A Phase I and pharmacological study with imidazolium-trans-DMSO-imidazole-tetrachlororuthenate, a novel ruthenium anticancer agent. *Clinical Cancer Research: An Official Journal of the American Association for Cancer Research*, 10(11), 3717–3727. <https://doi.org/10.1158/1078-0432.CCR-03-0746>
- Rastrelli, M., Tropea, S., Rossi, C. R., & Alaibac, M. (2014). Melanoma: epidemiology, risk factors, pathogenesis, diagnosis and classification. *In vivo (Athens, Greece)*, 28(6), 1005–1011.
- Rauh, C., Schuetz, F., Rack, B., Stickeler, E., Klar, M., Orlowska-Volk, M., Windfuhr-Blum, M., Heil, J., Rom, J., Sohn, C., Andergassen, U., Jueckstock, J., Fehm, T., Loehberg, C. R., Hein, A., Schulz-Wendtland, R., Hartmann, A., Beckmann, M. W., Janni, W., Fasching, P. A., ... Häberle, L. (2015). Hormone Therapy and its Effect on the Prognosis in Breast Cancer Patients. *Geburtshilfe und Frauenheilkunde*, 75(6), 588–596. <https://doi.org/10.1055/s-0035-1546149>
- Raychaudhuri, S., & Raychaudhuri, S. C. (2014). Death ligand concentration and the membrane proximal signaling module regulate the type 1/type 2 choice in apoptotic death signaling. *Systems and synthetic biology*, 8(1), 83–97. <https://doi.org/10.1007/s11693-013-9124-4>
- Rieder, C. R., Parsons, R. B., Fitch, N. J., Williams, A. C., & Ramsden, D. B. (2000). Human brain cytochrome P450 1B1: immunohistochemical localization in human temporal lobe and induction by dimethylbenz(a)anthracene in astrocytoma cell line (MOG-G-CCM). *Neuroscience letters*, 278(3), 177–180.

[https://doi.org/10.1016/s0304-3940\(99\)00932-5](https://doi.org/10.1016/s0304-3940(99)00932-5)

- Riley, R. S., June, C. H., Langer, R., & Mitchell, M. J. (2019). Delivery technologies for cancer immunotherapy. *Nature reviews. Drug discovery*, *18*(3), 175–196. <https://doi.org/10.1038/s41573-018-0006-z>
- Rodriguez, L. G., Wu, X., & Guan, J. L. (2005). Wound-healing assay. *Methods in molecular biology (Clifton, N.J.)*, *294*, 23–29. <https://doi.org/10.1385/1-59259-860-9:023>
- Roh, M. R., Eliades, P., Gupta, S., Grant-Kels, J. M., & Tsao, H. (2015). Cutaneous melanoma in women. *International Journal of Women's Dermatology*, *1*(1), 21–25. doi:10.1016/j.ijwd.2015.01.001
- Rocha, C., Silva, M. M., Quinet, A., Cabral-Neto, J. B., & Menck, C. (2018). DNA repair pathways and cisplatin resistance: an intimate relationship. *Clinics (Sao Paulo, Brazil)*, *73*(suppl 1), e478s. <https://doi.org/10.6061/clinics/2018/e478s>
- Ruhul Amin, A., Karpowicz, P., Carey, T., Arbiser, J., Nahta, R., Chen, Z., Tang Dong, J., et al. (2015). Evasion of anti-growth signaling: A key step in tumorigenesis and potential target for treatment and prophylaxis by natural compounds. *Seminars in Cancer Biology*. *35*, 55-77. <https://doi.org/10.1016/j.semcancer.2015.02.005>
- Russo, H. M., Rathkey, J., Boyd-Tressler, A., Katsnelson, M. A., Abbott, D. W., & Dubyak, G. R. (2016). Active Caspase-1 Induces Plasma Membrane Pores That Precede Pyroptotic Lysis and Are Blocked by Lanthanides. *Journal of immunology (Baltimore, Md.: 1950)*, *197*(4), 1353–1367. <https://doi.org/10.4049/jimmunol.1600699>
- Sabio, G., & Davis, R. J. (2014). TNF and MAP kinase signalling pathways. *Seminars in immunology*, *26*(3), 237–245. <https://doi.org/10.1016/j.smim.2014.02.009>
- Sage, J., & Burkhart, D. L. (2008). Cellular mechanisms of tumour suppression by the retinoblastoma gene. *Nature Reviews Cancer*, *8*(9), 671-682. <https://doi.org/10.1038/nrc2399>
- Saman, H., Raza, S. S., Uddin, S., & Rasul, K. (2020). Inducing Angiogenesis, a Key Step in Cancer Vascularization, and Treatment Approaches. *Cancers*, *12*(5), 1172. <https://doi.org/10.3390/cancers12051172>
- Saxena, Meera & Christofori, Gerhard. (2013). Rebuilding cancer metastasis in the mouse. *Molecular oncology*. *7*. 10.1016/j.molonc.2013.02.009.
- Schepisi, G., Cursano, M. C., Casadei, C., Menna, C., Altavilla, A., Lolli, C., Cerchione, C., Paganelli, G., Santini, D., Tonini, G., Martinelli, G., & De Giorgi, U. (2019). CAR-T cell therapy: a potential new strategy against prostate cancer. *Journal for immunotherapy of cancer*, *7*(1), 258. <https://doi.org/10.1186/s40425-019-0741-7>
- Schindler, C. K., Pearson, E. G., Bonner, H. P., So, N. K., Simon, R. P., Prehn, J. H.,

- & Henshall, D. C. (2006). Caspase-3 cleavage and nuclear localization of caspase-activated DNase in human temporal lobe epilepsy. *Journal of cerebral blood flow and metabolism: official journal of the International Society of Cerebral Blood Flow and Metabolism*, 26(4), 583–589. <https://doi.org/10.1038/sj.jcbfm.9600219>
- Shebawy W.N, Mroueh. M.A, Boukamp. P, Taleb. R.I, Bodman-Smith. K, El-Sibai. M, Daher. C.F. (2017). Wild carrot pentane-based fractions suppress proliferation of human HaCaT keratinocytes and protect against chemically-induced skin cancer, *BMC Complement. Altern. Med.* 17 (1) 36.
- Szaciłowski, K., Macyk, W., Drzewiecka-Matuszek, A., Brindell, M., & Stochel, G. (2005). Bioinorganic photochemistry: Frontiers and mechanisms. *Chemical Reviews*, 105(6), 2647-2694. <https://doi.org/10.1021/cr030707e>
- Sever, R., & Brugge, J. S. (2015). Signal Transduction in Cancer. *Cold Spring Harbor Perspectives in Medicine*, 5(4), a006098. <https://doi.org/10.1101/cshperspect.a006098>
- Segawa, K., Suzuki, J., & Nagata, S. (2011). Constitutive exposure of phosphatidylserine on viable cells. *Proceedings of the National Academy of Sciences of the United States of America*, 108(48), 19246–19251. <https://doi.org/10.1073/pnas.1114799108>
- Shamas-Din, A., Kale, J., Leber, B., & Andrews, D. W. (2013). Mechanisms of action of Bcl-2 family proteins. *Cold Spring Harbor perspectives in biology*, 5(4), a008714. <https://doi.org/10.1101/cshperspect.a008714>
- Sharma, A., Boise, L. H., & Shanmugam, M. (2019). Cancer Metabolism and the Evasion of Apoptotic Cell Death. *Cancers*, 11(8), 1144. <https://doi.org/10.3390/cancers11081144>
- Sherr, C. J., & McCormick, F. (2002). *The RB and p53 pathways in cancer*. United States: Elsevier Inc. [https://doi.org/10.1016/S1535-6108\(02\)00102-2](https://doi.org/10.1016/S1535-6108(02)00102-2)
- Shi, L., Mai, S., Israels, S., Browne, K., Trapani, J. A., & Greenberg, A. H. (1997). Granzyme B (GraB) autonomously crosses the cell membrane and perforin initiates apoptosis and GraB nuclear localization. *The Journal of experimental medicine*, 185(5), 855–866. <https://doi.org/10.1084/jem.185.5.855>
- Shi, D., & Gu, W. (2012). Dual Roles of MDM2 in the Regulation of p53: Ubiquitination Dependent and Ubiquitination Independent Mechanisms of MDM2 Repression of p53 Activity. *Genes & cancer*, 3(3-4), 240–248. <https://doi.org/10.1177/1947601912455199>
- Stadheim, T. A., & Kucera, G. L. (2002). c-Jun N-terminal kinase/stress-activated protein kinase (JNK/SAPK) is required for mitoxantrone- and anisomycin-induced apoptosis in HL-60 cells. *Leukemia research*, 26(1), 55–65. [https://doi.org/10.1016/s0145-2126\(01\)00099-6](https://doi.org/10.1016/s0145-2126(01)00099-6)
- Stanley M. (2017). Tumour virus vaccines: hepatitis B virus and human

papillomavirus. *Philosophical transactions of the Royal Society of London. Series B, Biological sciences*, 372(1732), 20160268.
<https://doi.org/10.1098/rstb.2016.0268>

Stennicke, H. R., Jürgensmeier, J. M., Shin, H., Deveraux, Q., Wolf, B. B., Yang, X., Zhou, Q., Ellerby, H. M., Ellerby, L. M., Bredesen, D., Green, D. R., Reed, J. C., Froelich, C. J., & Salvesen, G. S. (1998). Pro-caspase-3 is a major physiologic target of caspase-8. *The Journal of biological chemistry*, 273(42), 27084–27090.
<https://doi.org/10.1074/jbc.273.42.27084>

Stivala, S., Codilupi, T., Brkic, S., Baerenwaldt, A., Ghosh, N., Hao-Shen, H., Dirnhofer, S., Dettmer, M. S., Simillion, C., Kaufmann, B. A., Chiu, S., Keller, M., Kleppe, M., Hilpert, M., Buser, A. S., Passweg, J. R., Radimerski, T., Skoda, R. C., Levine, R. L., & Meyer, S. C. (2019). Targeting compensatory MEK/ERK activation increases JAK inhibitor efficacy in myeloproliferative neoplasms. *The Journal of clinical investigation*, 129(4), 1596–1611.
<https://doi.org/10.1172/JCI98785>

Subramaniam, S., Zirrgiebel, U., von Bohlen Und Halbach, O., Strelau, J., Laliberté, C., Kaplan, D. R., & Unsicker, K. (2004). ERK activation promotes neuronal degeneration predominantly through plasma membrane damage and independently of caspase-3. *The Journal of cell biology*, 165(3), 357–369.
<https://doi.org/10.1083/jcb.200403028>

Suvà, M. L., Riggi, N., & Bernstein, B. E. (2013). Epigenetic reprogramming in cancer. *Science (New York, N.Y.)*, 339(6127), 1567–1570.
<https://doi.org/10.1126/science.1230184>

Tanida, S., Mizoshita, T., Ozeki, K., Tsukamoto, H., Kamiya, T., Kataoka, H., Sakamuro, D., & Joh, T. (2012). Mechanisms of Cisplatin-Induced Apoptosis and of Cisplatin Sensitivity: Potential of BIN1 to Act as a Potent Predictor of Cisplatin Sensitivity in Gastric Cancer Treatment. *International journal of surgical oncology*, 2012, 862879. <https://doi.org/10.1155/2012/862879>

Tait, S. W. G., Ichim, G., & Green, D. R. (2014). Die another way – non-apoptotic mechanisms of cell death. *Journal of Cell Science*, 127(Pt 10), 2135–2144.
<https://doi.org/10.1242/jcs.093575>

Thomas, D. A., Du, C., Xu, M., Wang, X., & Ley, T. J. (2000). DFF45/ICAD can be directly processed by granzyme B during the induction of apoptosis. *Immunity*, 12(6), 621–632.

Tóvári, J., Futosi, K., Bartal, A., Tátrai, E., Gacs, A., Kenessey, I., & Paku, S. (2014). Boyden chamber-based method for characterizing the distribution of adhesions and cytoskeletal structure in HT1080 fibrosarcoma cells. *Cell adhesion & migration*, 8(5), 509–516. <https://doi.org/10.4161/cam.28734>

Tremmel, T., Holland-Cunz, S., & Günther, P. (2015). Metastasized pancreatic neuroendocrine tumor in a teenage girl: a case report. *Journal of medical case reports*, 9, 230. <https://doi.org/10.1186/s13256-015-0708-3>

- Twiddy, D., Brown, D. G., Adrain, C., Jukes, R., Martin, S. J., Cohen, G. M., MacFarlane, M., & Cain, K. (2004). Pro-apoptotic proteins released from the mitochondria regulate the protein composition and caspase-processing activity of the native Apaf-1/caspase-9 apoptosome complex. *The Journal of biological chemistry*, 279(19), 19665–19682. <https://doi.org/10.1074/jbc.M311388200>
- Verma, S., Petrella, T., Hamm, C., Bak, K., Charette, M., & Melanoma Disease Site Group of Cancer Care Ontario's Program in Evidence-based Care (2008). Biochemotherapy for the treatment of metastatic malignant melanoma: a clinical practice guideline. *Current oncology (Toronto, Ont.)*, 15(2), 85–89.
- Wallach, D., & Kovalenko, A. (2014). Keeping inflammation at bay. *eLife*, 3, e02583. <https://doi.org/10.7554/eLife.02583>
- Walsh, J. G., Cullen, S. P., Sheridan, C., Lüthi, A. U., Gerner, C., & Martin, S. J. (2008). Executioner caspase-3 and caspase-7 are functionally distinct proteases. *Proceedings of the National Academy of Sciences of the United States of America*, 105(35), 12815–12819. <https://doi.org/10.1073/pnas.0707715105>
- Walsh, C.J.; Luer, C.A.; Yordy, J.E.; Cantu, T.; Miedema, J.; Leggett, S.R.; Leigh, B.; Adams, P.; Ciesla, M.; Bennett, C.; Bodine, A.B. (2013). Epigonal Conditioned Media from Bonnethead Shark, *Sphyrna tiburo*, Induces Apoptosis in a T-Cell Leukemia Cell Line, Jurkat E6-1. *Marine Drugs*, 11, 3224-3257. <https://doi.org/10.3390/md11093224>
- Wang, C., Jin, H., Gao, D., Liefink, C., Evers, B., Jin, G., Xue, Z., Wang, L., Beijersbergen, R. L., Qin, W., & Bernards, R. (2018). Phospho-ERK is a biomarker of response to a synthetic lethal drug combination of sorafenib and MEK inhibition in liver cancer. *Journal of hepatology*, 69(5), 1057–1065. <https://doi.org/10.1016/j.jhep.2018.07.004>
- Wang, Z., Li, Y., Ahmad, A., Azmi, A. S., Kong, D., Banerjee, S., & Sarkar, F. H. (2010). Targeting miRNAs involved in cancer stem cell and EMT regulation: An emerging concept in overcoming drug resistance. *Drug resistance updates: reviews and commentaries in antimicrobial and anticancer chemotherapy*, 13(4-5), 109–118. <https://doi.org/10.1016/j.drug.2010.07.001>
- Warren, C. F. A., Wong-Brown, M. W., & Bowden, N. A. (2019). BCL-2 family isoforms in apoptosis and cancer. *Cell Death & Disease*, 10(3), 1-12. <https://doi.org/10.1038/s41419-019-1407-6>
- Wernitznig, D., Kiakos, K., Del Favero, G., Harrer, N., Machat, H., Osswald, A., Keppler, B. K. (2019). First-in-class ruthenium anticancer drug (KP1339/IT-139) induces an immunogenic cell death signature in colorectal spheroids in vitro. *Metallomics: Integrated Biometal Science*, 11(6), 1044-1048. <https://doi.org/10.1039/c9mt00051h>
- Wessling-Resnick M. (2018). Crossing the Iron Gate: Why and How Transferrin Receptors Mediate Viral Entry. *Annual review of nutrition*, 38, 431–458.

<https://doi.org/10.1146/annurev-nutr-082117-051749>

- Willis, S. N., & Adams, J. M. (2005). Life in the balance: How BH3-only proteins induce apoptosis. *Current Opinion in Cell Biology*, 17(6), 617-625. <https://doi.org/10.1016/j.cecb.2005.10.001>
- Wu, X. N., Yang, Z. H., Wang, X. K., Zhang, Y., Wan, H., Song, Y., Chen, X., Shao, J., & Han, J. (2014). Distinct roles of RIP1-RIP3 hetero- and RIP3-RIP3 homo-interaction in mediating necroptosis. *Cell death and differentiation*, 21(11), 1709–1720. <https://doi.org/10.1038/cdd.2014.77>
- Wu, M., Li, H., Liu, R., Gao, X., Zhang, M., Liu, P., Fu, Z., Yang, J., Zhang-Negrerie, D., & Gao, Q. (2016). Galactose conjugated platinum(II) complex targeting the Warburg effect for treatment of non-small cell lung cancer and colon cancer. *European Journal of Medicinal Chemistry*, 110(Supplement C), 32–42. <https://doi.org/10.1016/j.ejmech.2016.01.016>
- Xiaoning S., Rui L., Hailiang D., Ye L., Yanan C., Hua Z., Wenbing D., Bing H., Ying, Z., Xueqing, W., Qiang Z. (2018). Receptor mediated transcytosis in biological barrier: The influence of receptor character and their ligand density on the transmembrane pathway of active-targeting nanocarriers. *Biomaterials*. 180, 78-80 <https://doi.org/10.1016/j.biomaterials.2018.07.006>
- Xu, X., Lai, Y., & Hua, Z. (2019). Apoptosis and apoptotic body: Disease message and therapeutic target potentials. *Bioscience Reports*, 39(1) [doi:10.1042/BSR20180992](https://doi.org/10.1042/BSR20180992)
- Xu, X., Ho, W., Zhang, X., Bertrand, N., & Farokhzad, O. (2015). Cancer nanomedicine: from targeted delivery to combination therapy. *Trends in molecular medicine*, 21(4), 223–232. <https://doi.org/10.1016/j.molmed.2015.01.001>
- Yang, J. C., & Rosenberg, S. A. (2016). Adoptive T-Cell Therapy for Cancer. *Advances in immunology*, 130, 279–294. <https://doi.org/10.1016/bs.ai.2015.12.006>
- Yoshikawa, N., Yamabe, S., Sakaki, S., Kanehisa, N., Inoue, T., & Takashima, H. (2015). Transition states of the 3MLCT to 3MC conversion in Ru(bpy)₂(phen derivative)₂⁺ complexes. *Journal of Molecular Structure*, 1094, 98–108. <https://doi.org/10.1016/j.molstruc.2015.04.011>
- Yu, J., Zhang, Y., McIlroy, J., Rordorf-Nikolic, T., Orr, G. A., & Backer, J. M. (1998). Regulation of the p85/p110 phosphatidylinositol 3'-kinase: stabilization and inhibition of the p110alpha catalytic subunit by the p85 regulatory subunit. *Molecular and cellular biology*, 18(3), 1379–1387. <https://doi.org/10.1128/mcb.18.3.1379>
- Yuan, J., Lei, Z., Wang, X., Zhu, F., & Chen, D. (2015). Ruthenium complex Λ-WH0402 induces hepatocellular carcinoma LM6 (HCCLM6) cell death by triggering the Beclin-1-dependent autophagy pathway. *Metallomics: Integrated*

- Zembruski, N. C., Stache, V., Haefeli, W. E., & Weiss, J. (2012). 7-Aminoactinomycin D for apoptosis staining in flow cytometry. *Analytical biochemistry*, 429(1), 79–81. <https://doi.org/10.1016/j.ab.2012.07.005>
- Zeng, L., Gupta, P., Chen, Y., Wang, E., Ji, L., Chao, H., & Chen, Z. S. (2017). The development of anticancer ruthenium(ii) complexes: from single molecule compounds to nanomaterials. *Chemical Society reviews*, 46(19), 5771–5804. <https://doi.org/10.1039/c7cs00195a>
- Zerdane, S., Wilbraham, L., Cammarata, M., Iasco, O., Rivière, E., Boillot, M. L., Ciofini, I., & Collet, E. (2017). Comparison of structural dynamics and coherence of d-d and MLCT light-induced spin state trapping. *Chemical science*, 8(7), 4978–4986. <https://doi.org/10.1039/c6sc05624e>
- Zha, J., Harada, H., Osipov, K., Jockel, J., Waksman, G., & Korsmeyer, S. J. (1997). BH3 domain of BAD is required for heterodimerization with BCL-XL and pro-apoptotic activity. *The Journal of biological chemistry*, 272(39), 24101–24104. <https://doi.org/10.1074/jbc.272.39.24101>
- Zhang, J., Huang, Y., Li, X., Guo, Y., Zhao, Y., Xue, C., Hu, Z., Zhang, L., & Zhao, H. (2012). The impact of tumor size change after target therapy on survival: analysis of patients enrolled onto three clinical trials of advanced NSCLC from one institution. *OncoTargets and therapy*, 5, 349–355. <https://doi.org/10.2147/OTT.S38441>
- Zhao, J., Jitkaew, S., Cai, Z., Choksi, S., Li, Q., Luo, J., & Liu, Z. G. (2012). Mixed lineage kinase domain-like is a key receptor interacting protein 3 downstream component of TNF-induced necrosis. *Proceedings of the National Academy of Sciences of the United States of America*, 109(14), 5322–5327. <https://doi.org/10.1073/pnas.1200012109>
- Zhou, H., Ren, S., Han, Y., Zhang, Q., Qin, L., & Xing, Y. (2017). Identification and Analysis of Mitogen-Activated Protein Kinase (MAPK) Cascades in *Fragaria vesca*. *International journal of molecular sciences*, 18(8), 1766. <https://doi.org/10.3390/ijms18081766>
- Zhou, F., Wang, M., Luo, T., and Qu, J. (2020) Photo-activated chemo-immunotherapy for metastatic cancer using a synergistic graphene nanosystem. *Biomaterials*. 265. <https://doi.org/10.1016/j.biomaterials.2020.120421>
- Zijl, F., Krupitza, G., & Mikulits, W. (2011). Initial steps of metastasis: cell invasion and endothelial transmigration. *Mutation research*, 728(1-2), 23–34. <https://doi.org/10.1016/j.mrrev.2011.05.002>

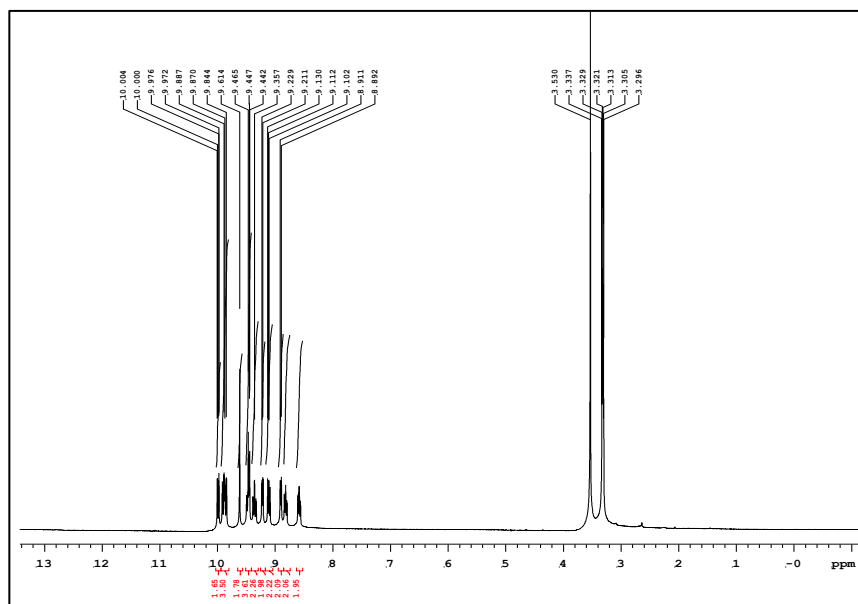
Appendix

Appendix A

A.1 Ru(bpy)₂Phen(PF₆)₂ ¹H NMR

Purity and synthesis of Ru(bpy)₂Phen(PF₆)₂, Ru(bpy)₂BC(PF₆)₂, Ru(bpy)₂Dpphen(PF₆)₂ and Ru(bpy)₂dpphen[H₂O](Cl₂) were ensured by ¹H NMR and peak characterization

(A)



(B)

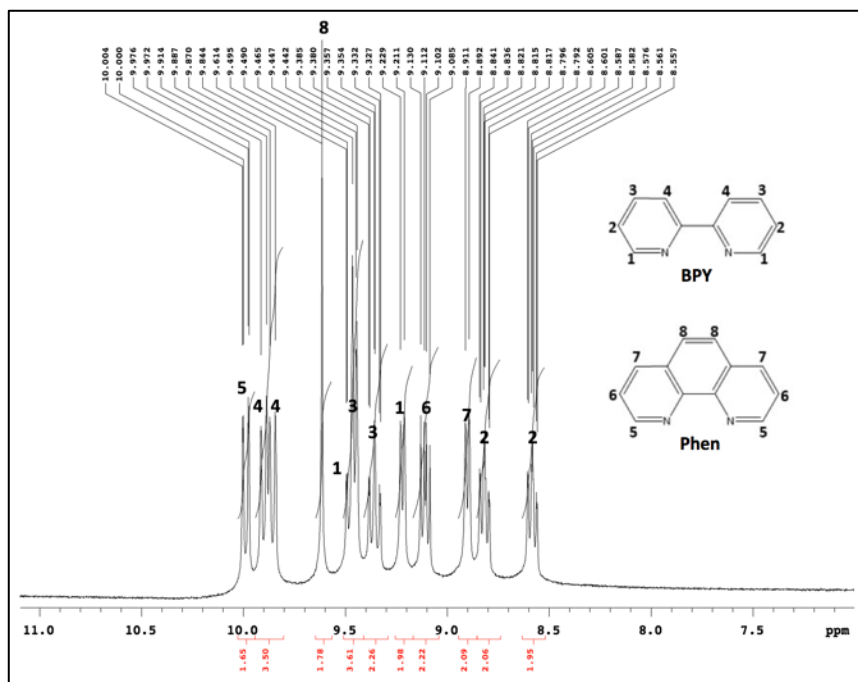
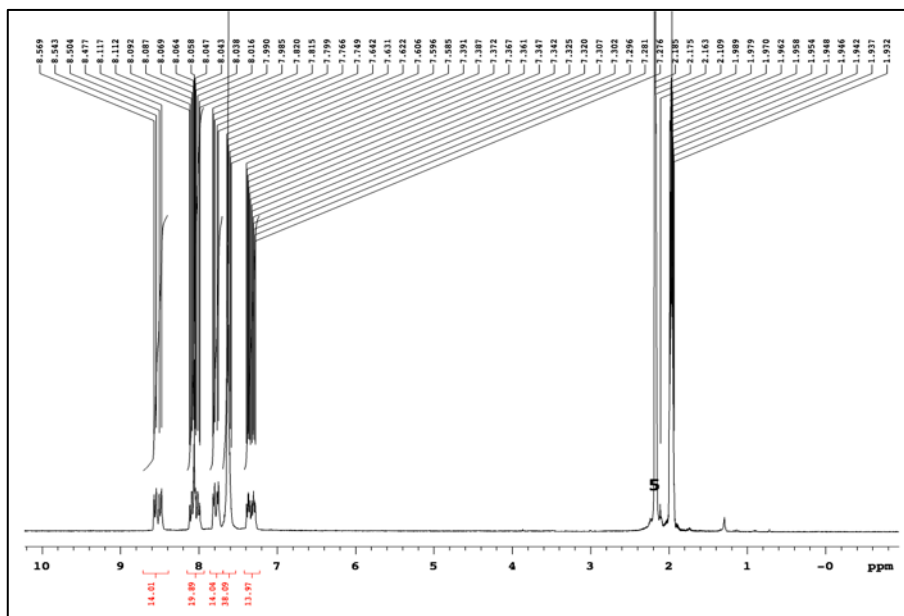


Figure 3.2. ¹H NMR spectra of Ru(bpy)₂Phen(PF₆)₂. The chemical shifts are expressed in ppm. The chemical structures represented belong to the coordinating ligands 2,2'-bipyridine (BPY) and 1,10'-phenanthroline (Phen). (A) Represents full

spectra, aromatic and aliphatic regions Solvent residual peaks are seen at 3-4 ppm. (B) Represents an expansion of the aromatic region of the spectrum. The hydrogens are labelled using numbers to assign to peaks on the NMR spectra. Ru(bpy)₂Phen.PF₆ was dissolved in deuterated CH₃CN.

A.2 Ru(bpy)₂BC(PF₆)₂ ¹H NMR

(A)



(B)

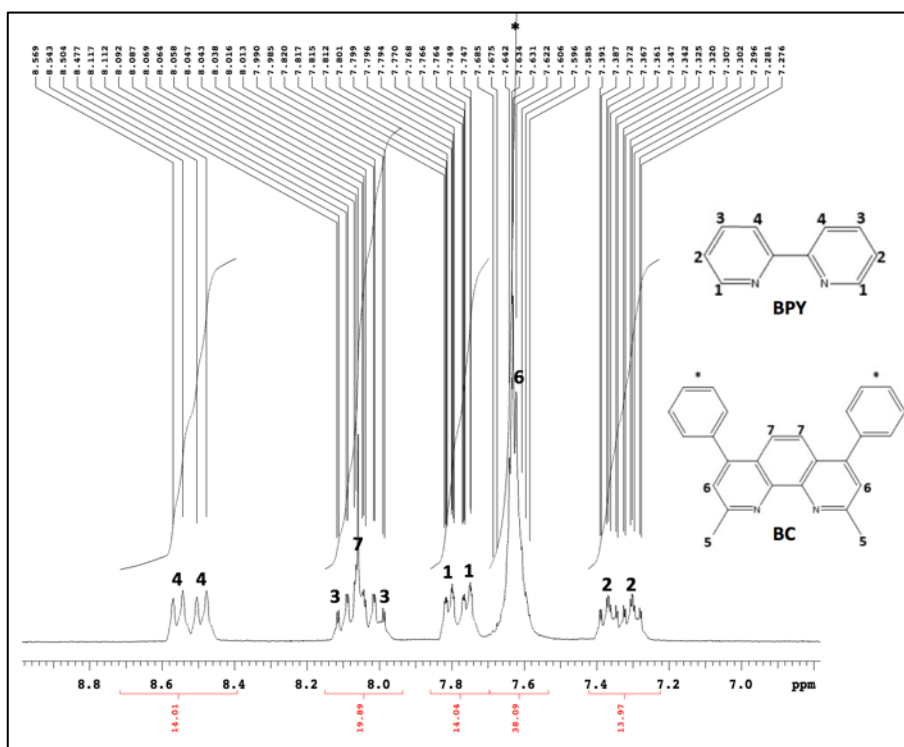


Figure 3.3. ¹H NMR spectra of Ru(bpy)₂BC(PF₆)₂. The chemical shifts are expressed in ppm. The chemical structures represented belong to the coordinating

ligands 2,2'-bipyridine (BPY) and Bathocuproine (BC). (A) Represents full spectra, aromatic and aliphatic regions Solvent residual peaks are seen at the upper left inset. (B) Represents an expansion of the aromatic region of the spectrum. The hydrogens are labelled using numbers to assign to peaks on the NMR spectra. The * represents the hydrogens on the phenyl groups which are detected as a multiplet on the spectrum. Ru(bpy)₂Phen.PF₆ was dissolved in deuterated CH₃CN.

A.3 Ru(bpy)₂Dpphen(PF₆)₂ ¹H NMR

The purity of Ru(bpy)₂dpphen(PF₆)₂ was done and confirmed via ¹H NMR spectra comparison to previously reported characterization of the compound (Mansour et al., 2018)

A.4 Ru(bpy)dpphen[H₂O](Cl₂) ¹H NMR

The characterization of Ru(bpy)dpphen[H₂O](Cl₂), is yet to be completed off-campus.

Appendix B

Table 3.2. Concentration of precursor vs. photoproduct

UV-vis	Peak	Absorbance	Concentration
Precursor	455.98nm	0.116688	2.77uM
Photoproduct	537.9898nm	0.092259	2.197uM

Appendix C

Table 3.10. Lethal dose and effect observed. M = balb/c mouse.

Dose	Effect
M1 → 5 mg/kg	No death
M2 → 10 mg/kg	Death within 30 mins → seizure like
M3 → 9 mg/kg	Death within 1-2 hrs
M4 → 7.5 mg/kg	Died ~ 5 hrs later
M5 → 6 mg/kg	No death
M6 → 7 mg/kg	Died overnight



Animal Care and Use Committee

NOTICE OF ACUC APPROVAL

To: Dr. Costantine Daher
Professor
School of Arts and Sciences

APPROVAL ISSUED: October 1 2020
EXPIRATION DATE: September 30 2023
REVIEW TYPE: FULL

Date: October 1 2020

RE: **IRB #:** LAU.ACUC.SAS.CD5. 1/October/2020

Protocol Title: Effect of the photoactivated complex [Ru(bpy)2BC]Cl2 on the DMBA induced skin cancer model

Your application for the above referenced research project has been reviewed and approved by the Animal Care and Use Committee.

This approval is limited to the activities described in the ACUC Application and all submitted documents listed on page 2 of this letter.

APPROVAL CONDITIONS FOR ALL ACUC APPROVED PROTOCOLS

MODIFICATIONS AND AMENDMENTS: All protocol modifications must be approved by the ACUC prior to implementation.

Protocol Expiration: The ACUC approval expiry date is listed above. The ACUC will send an email at least 45 days prior to protocol approval expiry - Request for Continuing Review - in order to avoid any temporary hold on the initial protocol approval. It is your responsibility to apply for continuing review and receive continuing approval for the duration of the research project. Failure to send Request for Continuation before the expiry date will result in suspension of the approval of this research project on the expiration date.

NOTIFICATION OF PROJECT COMPLETION: A notification of research project closure and a summary of findings must be sent to the ACUC upon completion. Study files must be retained for a period of 3 years from the date of notification of project completion.

IN THE EVENT OF NON-COMPLIANCE WITH ABOVE CONDITIONS, THE PRINCIPAL INVESTIGATOR SHOULD MEET WITH THE ACUC CHAIR IN ORDER TO RESOLVE SUCH CONDITIONS. ACUC APPROVAL CANNOT BE GRANTED UNTIL NON-COMPLIANT ISSUES HAVE BEEN RESOLVED.

If you have any questions concerning this information, please contact the ACUC office by email at acuc@lau.edu.lb

Dr. Sama Sleiman
Chair, Animal Care and Use Committee

BEIRUT CAMPUS	BYBLOS CAMPUS	NEW YORK OFFICE
P.O. Box: 13-5053 Chouran Beirut 1102 2801 Lebanon	P.O. Box: 36 Byblos Lebanon	475 Riverside Drive Suite 1846 New York, NY 10115
Tel: +961 1 78 64 56 +961 3 60 37 03 Fax: +961 1 86 70 98	Tel: +961 9 54 72 62 +961 3 79 13 14 Fax: +961 9 54 62 62	Tel: +1 212 870 2592 +1 212 870 2761 Fax: +1 212 870 2762
		www.lau.edu.lb



DOCUMENTS SUBMITTED:

ACUC Protocol Application	Received July 2020

